FORSCHUNGSZENTRUM ROSSENDORF
Mitglied der Wissenschaftsgemeinschaft Gottfried Wilhelm Leibniz

WISSENSCHAFTLICH-TECHNISCHE BERICHTE
FZR-338
März 2002

Annual Report 2001

Institut für Ionenstrahlphysik und

Materialforschung

Editors:

J. von Borany, M. Helm, H.-U. Jäger,

W. Möller, E. Wieser

Preface

The Forschungszentrum Rossendorf (FZR) represents the largest governmental research institution in the "new" states of the Federal Republic of Germany. Its presently about 600 employees, organized in five institutes, study problems of basic and applied science in the fields of materials science, biomedical and environmental research, and nuclear physics. The FZR is a member of the "Gottfried Wilhelm Leibniz Society" (WGL), with the federal government and the state of Saxony each contributing 50 % of the basic funding.

The Institute of Ion Beam Physics and Materials Research (IIM) employs more than 100 scientists, engineers, technicians and PhD and diploma students. The institute combines basic research and application-oriented studies in the fields of ion beam applications to materials and semiconductor research. The institute constitutes a national and international ion beam center, which, in addition to its own scientific activities, offers services and transfers know-how on ion beam techniques to universities, other research institutes, and industry.

For these purposes, a broad range of ion-related equipment is available, delivering ion energies from about 10 eV (plasma treatment) to several 10 MeV (electrostatic accelerators). In 2001 an unique double-implantation chamber in which two ion beams with different ion species can be scanned synchronously has been commissioned. For the diagnostics of ion-treated surfaces, standard analytical techniques are available such as transmission electron microscopy, X-ray diffraction, Auger and photoelectron spectroscopy, and a number of chemical, optical, electrical, and mechanical diagnostics. Sample preparation in a dedicated clean room is available for a large number of different materials including standard silicon processing. Optical techniques, in particular for semiconductor research, play a more important role since the recent establishment of a semiconductor spectroscopy group. In the future, this group will also be a prime user of the infrared radiation from the free-electron laser at the superconducting electron accelerator ELBE at the FZR, which is presently under construction. The group has equipped the new labs with various spectrometers and a femto-second laser system and has started experimental work.

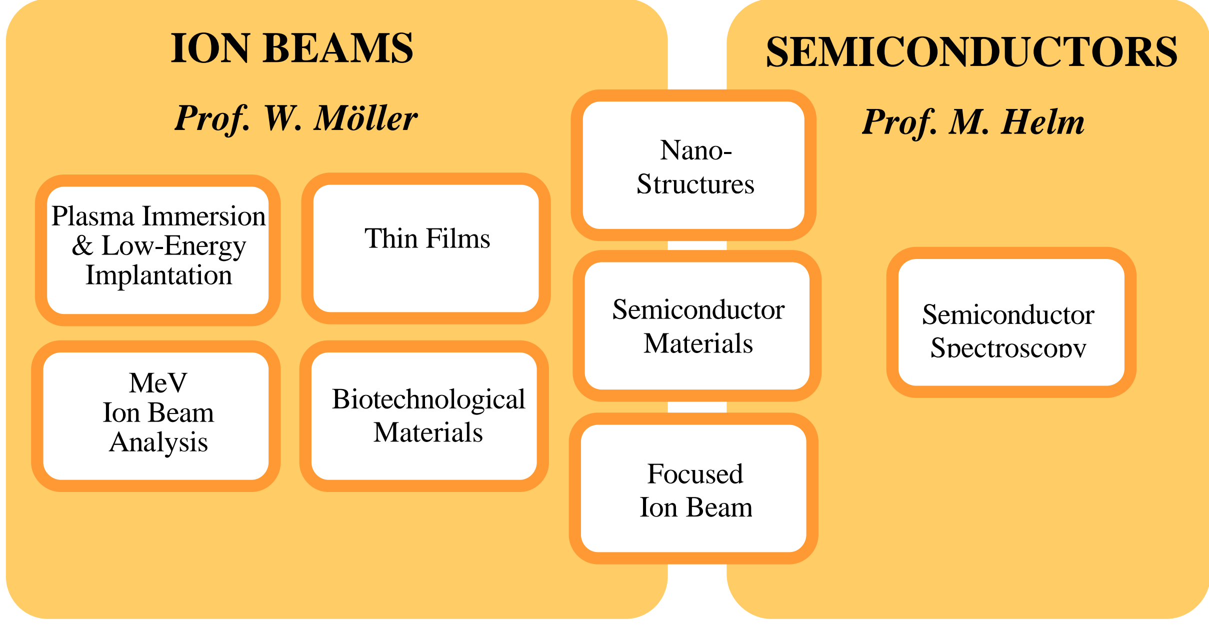

The diagram on page 3 displays the main R&D activities of the institute. It is the purpose of the present Annual Report to document its scientific progress in 2001 by a few selected extended contributions, numerous short contributions, and a statistical overview on publications, conference contributions and lectures given by members of the institute. It also reports on the training of young scientists and on external and collaborative actions.

In addition to the European Large Scale Facility "Center for Application of Ion Beams in Materials Research" ("AIM"), under which more than 30 different groups from all over Europe were hosted, the "Synchrotron Radiation Beamline for Radiochemistry and Materials Research (ROBL)" at the ESRF in Grenoble is operated as a European Large Scale Facility. The dedicated research capacity of both installations was fully booked with nearly 30 different user groups in materials research. In addition, the institute has been selected as "Marie-Curie Training Site" of the European Union, named "Development of Functional Layers Using Ion Beam Techniques". By its support, four foreign PhD students performed part of their work at Rossendorf.

In 2001, one diploma student and three PhD students finished their theses at the institute and their examinations at the Technical University of Dresden. The institute (co-)organized workshops on the topics “Infrared and THz Radiation: Generation and Applications” and “Slow Positron Beam Techniques for Solids and Surfaces”, both held at the FZR and summer schools on ”Vacuum, Electron, and Ion Technologies“ in Varna, Bulgaria, and on ”Nuclear Probes and Ion Beams“ in Bad Blankenburg, Thuringia.

The number of activities related to technology transfer and ion-beam service were again quite high in 2001. These collaborations include process simulation for microelectronics, the development of new non-volatile semiconductor memories, the improvement of diffusion barriers for copper metallization in integrated circuits, the surface treatment of mechanical tools, and the enhancement of corrosion resistance of high-temperature metallic alloys. Services for universities, other research institutes and industry cover numerous applications of ion-beam analysis, the enhancement of ceramic coating adhesion on dental implants, the surface hardening of cutting, forming and engraving tools, and the ion-beam tailoring of high-power semiconductor device properties. With *“nanoparc GmbH”* (www.nanaoparc.de) and *“APT – Angewandte Pulstechnik GmbH”* (www.apt-dresden.de) two start-up companies, led by former institute members, grew out of the research activities.

The institute would like to thank all partners and friends, and the organizations who supported its progress in 2001. Special thanks are due to the Executive Board of the Forschungszentrum Rossendorf, the Minister of Science and Arts of the Free State of Saxony, and the Minister of Education and Research of the Federal Government of Germany. Our partners from universities, industry and research institutes all around the world contribute essentially to the success of the institute, and play a crucial role for its further development. Last but not least, the directors would like to thank all members and guests of the institute for their active and excellent contributions in 2001.

Prof. Wolfhard Möller Prof. Manfred Helm

Contents

Selected Reports

Page

N. Schell, J. Bøttiger, W. Matz, J. Chevallier and A. Mücklich 9
Growth Mode and Texture Development in TiN Films during Magnetron Sputtering – an *in situ* Synchrotron Radiation Study

M. Posselt, L. Bischoff and J. Teichert 13
Influence of Dose Rate and Temperature on Ion-Beam-Induced Defect Evolution in Si Investigated by Channeling Implantation at Different Doses

K.H. Heinig, B. Schmidt and H. Bernas 17
Inverse Ostwald Ripening of Nanocrystals under Ion Irradiation

B. Schmidt, K.H. Heinig, D. Grambole and F. Herrmann 21
Impact of Ambient Atmosphere on As-Implanted SiO_2 Layers

L. Rebohle, J. von Borany, G. Franzò, T. Gebel, M. Helm, D. Pacifici, F. Priolo and W. Skorupa 25
Transient Behavior of the Strong Violet Electroluminescence of Ge-Implanted SiO_2 Layers

T. Gebel, M. Voelskow, W. Skorupa, G. Mannino, V. Privitera, F. Priolo, E. Napolitani and A. Carnera 29
Flash Lamp Annealing with Millisecond Pulses for Ultra-Shallow Boron Profiles in Silicon

J. von Borany, V. Beyer, D. Beyer, B. Schmidt and B. Schnabel 32
A Novel Silicon Detector for Energetic Electrons with Improved Linearity Characteristics

Short Contributions

Thin Films 39

Low Energy Implantation / Plasma Based Ion Implantation 43

Biotechnological Materials 45

Ion Beam Analysis 48

Semiconductor Materials 52

Semiconductor Spectroscopy 58

Nanostructures 61

Focused Ion Beam 66

Equipment 68

Others 70

Glossary 71

Statistics

Publications 75

Invited Talks 86

Conference Contributions 88

Lectures 99

Reports 103

Patents 104

PhD Theses 104

Awards 104

Laboratory Visits 104

Guests 107

European Large Scale Facility Visitors 110

Marie Curie Trainig Site 112

Seminar of the Institute 113

Other Seminars 113

Meetings organized by the Institute 116

Project based on External Funds 117

Experimental Equipment 120

Organigram 122

List of Personnel 123

Selected Reports

Growth Mode and Texture Development in TiN Films during Magnetron Sputtering – an *in situ* Synchrotron Radiation Study

N. Schell, J. Bøttiger[1], W. Matz, J. Chevallier[1] and A. Mücklich

[1]*Institute of Physics and Astronomy, University of Aarhus, 8000 Aarhus C, Denmark*

The technological importance of thin films has stimulated increasing interest in the detailed characterisation of structure and morphology of thin films and their interfaces and in the underlying growth mechanisms. TiN and other transition metal nitrides, e.g., find widespread use as hard wear-resistant coatings on cutting tools and as corrosion- and abrasion-resistant layers on optical and mechanical components [1]. They are deposited by plasma-assisted chemical vapor deposition and by magnetron sputtering. Because of the lack of well established surface analysis techniques that can be used in an environment of gases with pressures in the range 10^{-2} to 100 Pa and of magnetic stray fields, there are only few published *in situ* measurements of surface structures on the atomic scale during deposition with those techniques – contrary to vacuum processes such as molecular-beam epitaxy [2,3]. X-rays are in that case a powerful probe.

To follow the growth mode and the micro-structural development during sputter deposition, we developed a miniature chamber [4] which distinguishes itself from other equipment described in the literature [5-7] by using a maximum number of different modes of synchrotron radiation scattering and by fitting into a standard HUBER six-circle diffractometer which is used as a multi-purpose instrument at the Rossendorf beamline ROBL in Grenoble [8].

To get as much information as possible on the growth process, the sputter deposition chamber allows: (1) symmetric x-ray diffraction (Bragg-Brentano geometry) for measuring out-of-plane lattice constants and texture, (2) vertical grazing incidence diffraction for enhancing the signal of very thin films and suppressing substrate scattering, (3) reflectometry for determining film thickness and interface roughness, (4) in-plane grazing incidence/exit diffraction (GIXS) for the determination of lattice constants, stress and preferred orientation in the surface plane, (5) crystal truncation rod (CTR) scattering to determine the growth mode (*step flow, layer-by-layer* or *island formation*).

The deposition chamber, shown in Fig. 1, is described in detail in Ref. 4. The magnetron sources, running at a dc power of 80 W, are placed at a distance of 100 mm from the substrate and tilted 30 degrees away from the substrate normal. To avoid cross contamination of the two targets (diameters 1 inch), chimneys are mounted on the magnetrons. Air-pressure-controlled shutters are placed in front of the chimneys. The base pressure is ≈ $2x10^{-5}$ Pa. The targets were 99.98% pure Ti. The reactive sputter gas was a mixture of Ar (99.9996%) and N_2 (99.99990%) with the ratio 4:1, at a total gas pressure of 0.3 Pa. A resistive heater was mounted below the substrate, so the temperature, measured by a chromel-alumel thermocouple, could be varied from room temperature up to 700 °C. A negative bias voltage could be applied to the sample.

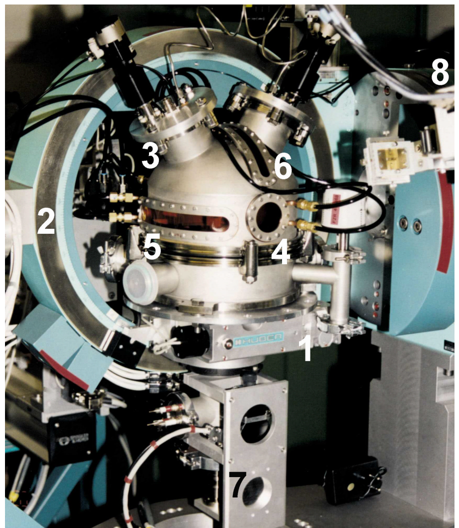

Fig. 1: Photo of the deposition chamber mounted into the HUBER six-circle goniometer. 1: φ-circle, 2: χ-circle of Eulerian cradle, 3: magnetrons, 4: beam exit x-ray window, 5,6: semi-circular large x-ray windows for the diffracted beam in horizontal and vertical planes, 7: drive for sample height adjustment, 8: detector unit with slits (power supply, gas inlets and pumps are not connected).

The substrates were 1.5 x 1.5 cm^2 silicon wafers with a 1000 Å amorphous oxide layer on top and MgO(001) single crystals with a thickness of 1 mm (cleaned before deposition by heating to 600 °C for 1 hour). The incident x-rays were monochromatized to 12.651 keV and 11.696 keV, respectively.

Several TiN films were grown under systematically varied conditions (temperature, bias voltage, substrate) in order to gain information about the growth mechanism. In all cases the experimental procedure was the same: cleaning of the magnetron targets by pre-sputtering, sputter deposition for a certain time, interruption of the growth process to characterise the sample by specular reflectivity (giving density, thickness and roughness of the surface and the interface), vertical Bragg-Brentano scattering and in-plane (horizontal) GIXS (incidence/exit angles = $0.2^o/0.4^o$, i.e. the x-rays penetrated only ≈ 100 Å). The whole process was repeated many times. Several identical scans were also taken to elucidate the time behaviour (annealing at the deposition temperatures). Sometimes, after film completion, high temperature *in situ* annealing has been performed.

The films were also characterized *ex situ* by x-ray diffraction (on a powder diffractometer in Bragg-Brentano geometry with CuK_α radiation), by Rutherford backscattering spectrometry (RBS) (with 2.0 MeV He^+ and a scattering angle of 161^0) to obtain the composition, and by transmission electron microscopy (TEM) to obtain cross-sectional electron micrographs.

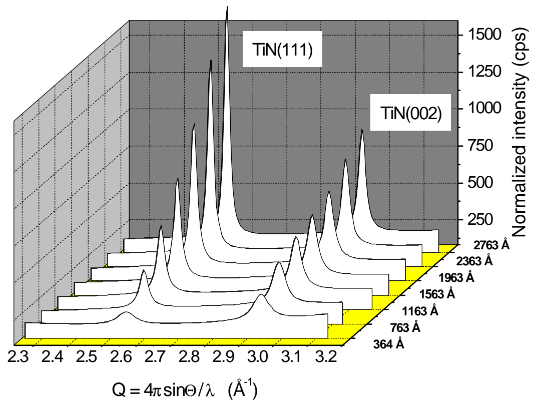

Fig. 2: Three-dimensional representation of a series of vertical Bragg-Brentano diffractograms as a function of film thickness for a film grown at 450 °C with a bias of -30 V. A crossover is clearly seen, where grains with (002) planes parallel to the film surface dominate in the beginning, while (111) grains take over at a larger film thickness.

Specular reflectivity reveals a linear growth rate of ≈ 0.9–1.4 Å/s on SiO_2 and ≈ 0.4–0.7 Å/s on MgO. The lower growth rates correspond to higher deposition temperatures which may be connected with a decrease in sticking coefficients.

Fig. 2 shows representative results for the deposition of TiN on SiO_2. For all chosen deposition parameters, the film growth is characterised by a crossover of the crystallographic orientation of the surface as also seen in other investigations [9,10]. At small film thickness, the (002) grains (the (002) planes of the grains parallel with the surface) dominate the vertical diffraction scans while (111) grains take over at larger thickness. As such scans probe the whole film thickness, they indicate the change of texture with increasing thickness. Cross sectional TEM micrographs of the TiN films (not shown) reveal a columnar structure where the individual columns are composed of grains with low-angle grain boundaries. There is no indication of "competitive growth" [10] in the micrographs.

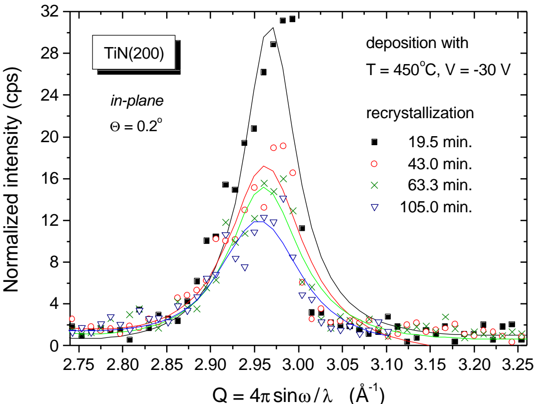

Fig. 3: TiN(200) horizontal-scan diffraction peaks obtained from a 1963 Å thick TiN film (grown at 450 °C with a bias of –30 V), measured 19.5 min., 43 min., 63.3 min. and 105 min., respectively, after the deposition was stopped. The substrate temperature was held constant at 450 °C. The lines are the results of a peak fit procedure.

As demonstrated in Fig. 3, where only the upper 100 Å of the film contribute to the intensity, for the first time the underlying mechanism for this texture change could be observed by repeated GIXS scans. It directly reveals recrystallisation (change of crystallographic orientation) of the topmost layer immediately after deposition. Another proof is the comparison of integrated peak intensities in vertical Bragg-Brentano geometry with those taken by horizontal GIXS scans as demonstrated in Fig. 4: the volume of the (111) grains steadily increases with thickness, while the volume of the (002) grains levels off and stays then nearly constant. This saturation of the volume of the (002) grains is in contrast to the summed (002) intensity of GIXS scans (where only the surface is probed) that steadily increases with film thickness, i.e. with each new deposition step. Without recrystallisation of the (002) grains after deposition, the (002) Bragg-Brentano signal should be proportional to the summed (002) GIXS signal, since it reflects the amount of all primarily grown (002) grains. The saturation of the (002) signal, therefore, indicates recrystallisation of the (002) grains in the film. Other mechanisms that

also influence the texture reorientation – the cross-over – cannot be completely excluded. However, mechanisms like the "tilted-(002) surface" [6] and "competitive growth" [10] cannot play a significant role under the present deposition conditions. They should especially lead to a levelling-off or even decreasing intensity for horizontal-scan (002) diffraction which, however, is in contrast to the actual observations.

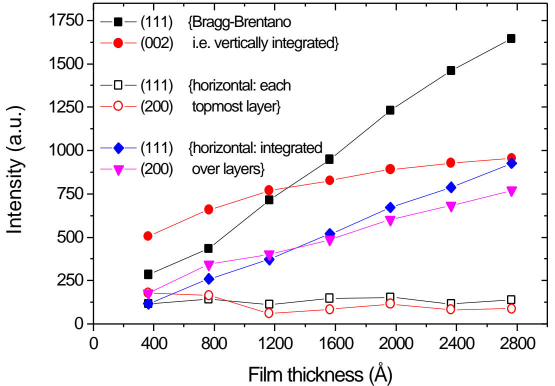

Fig. 4: Intensity data of the same film as in Figs. 2 and 3 (450 °C, –30 V) shown as a function of its thickness. Upper two curves: intensities of the (111) (filled squares) and the (002) (filled circles) Bragg-Brentano diffraction peaks. Lower two curves: intensities of the (111) (open squares) and the (200) (open circles) horizontal-scan diffraction peaks taken under grazing incidence/exit, i.e. with probing depth 100 Å. The two curves in the middle represent the added GIXS intensities – summed up to the corresponding total thickness in question: (111) as filled diamonds and (200) as filled triangles.

During growth, enhancement in the grain size is observed (by TEM micrographs and by a diminishing FWHM of the Bragg peaks with increasing film thickness) which cannot be explained as normal grain growth [11]. Otherwise grain growth/defect annihilation should be observable also during post-annealing. Rather than being thermodynamically driven, the increasing grain size with film thickness is probably controlled by kinetics. As the in-plane lattice constant is found to be smaller than that one out-of-plane, it is concluded that the films are stressed in compression.

During the very first sputter deposition steps of TiN on amorphous SiO_2 we observed once a weak oscillatory behaviour of the specular reflectivity for a fixed detector position. Such features, CTR intensity *versus* time, are measured to observe changes on an atomic scale in the surface morphology during growth [12–14], and can be used to identify the growth mode of the deposited film [15]. The latter is determined, among other things, by a competition between the deposition rate and the surface diffusion rate (dependent on temperature and the bombardment with atomic species). At low temperatures, the CTR intensity typically drops rapidly to a constant value, indicating that the surface immediately roughens, i.e. 3D islands are formed. At higher temperatures, the CTR intensity oscillates with time. This shows that the film grows layer-by-layer, i.e. 2D islands alternately nucleate and coalesce on the surface.

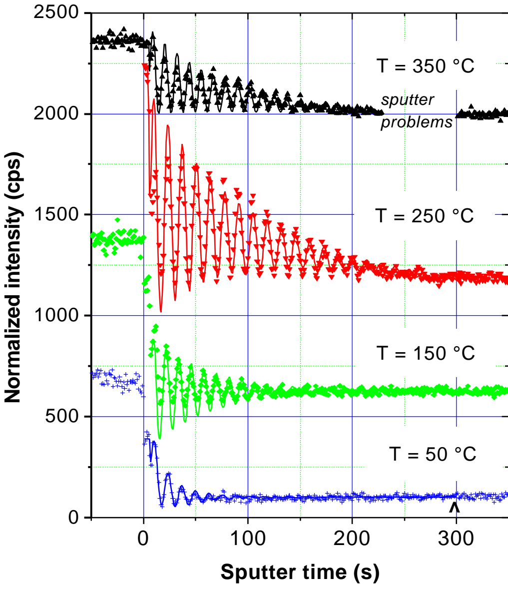

Fig. 5: Oscillations in the CTR intensity as a function of time for TiN films on MgO(100). The films were deposited at different temperatures as indicated in the graphs (shifted for better view) The sputtering starts at t = 0 s and ends at t = 300 s (as marked by ^). The lines are fits from which oscillation periods and decay times can be determined.

Real-time oscillations in the CTR intensity of TiN growing on MgO (this substrate was chosen because of the nearly equal lattice constants of film and substrate in order to obtain hetero-epitaxial growth) are shown in Fig. 5 for various growth temperatures. The experimental points were fitted by functions composed of exponentials and cosines (lines in the figure). In all cases the reflected intensity begins to drop after the shutter opening and the start of the deposition process. The oscillations are superimposed with a general drop. As discussed, the oscillations thus reveal layer-by-layer growth while decreasing oscillation amplitude indicates surface roughening with time. At later times the oscillations die out which is understood as a transition to an uncorrelated growing mode (island growth). The oscillation periods increase only slightly with increasing deposition temperature. Converted to film thickness using the measured growth rates, the oscillation lengths varied from 7.9 Å to 8.7 Å for the various films. In contrast, the decay time is found to increase strongly with temperature, i.e. during growth the surface roughens faster at lower

temperatures. These x-ray data revealing that the TiN films grow heteroepitaxially in registry with the substrate are confirmed by HRTEM. A high resolution cross-sectional electron micrograph from a 360 Å TiN film grown at 250 °C on Mg(001) is shown in Fig. 6. A detailed evaluation will be published elsewhere [16].

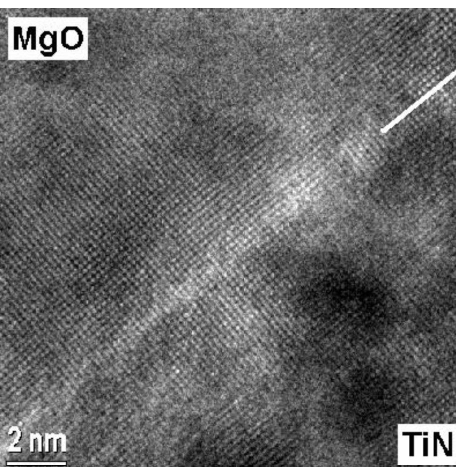

Fig. 6: High resolution electron micrograph in cross-section from a TiN film grown at 250 °C. Crossing (100) lattice planes are visible on both sides of the TiN–MgO boundary, indicated by a line marker. It is seen that the TiN film grew pseudomorphic to the MgO substrate.

In conclusion, TiN films were grown on amorphous SiO_2 and single crystal MgO substrates by reactive magnetron sputtering from a Ti target in a dedicated chamber which allowed *in situ* observation of the film growth by synchrotron x-ray reflectivity and diffraction in vertical and horizontal scattering geometries. During growth, the microstructural development, especially the change in texture with film thickness, was studied in dependence on the deposition temperature and the bias voltage on SiO_2 substrate. Grains with (002) planes parallel to the film surface, observed in vertical diffraction scans, dominate at small film thickness, while (111) grains take over at larger thickness. The crossover thickness increases with growing deposition temperature. Recrystallization was identified for the first time as the mechanism controlling the development of the texture. During growth, the grain size increases with film thickness. This increase is not due to normal grain growth but was probably controlled by kinetics. As concluded from the measured lattice constants, the films experience compressive stress which is slightly reduced with increasing thickness.

TiN films heteroepitaxially grown on MgO show oscillations in their CTR intensity *versus* time which reveal that the films grow in the layer-by-layer mode. The surface roughens faster during growth at lower temperatures.

References

[1] K. Holmberg, A. Mattews, Coatings Tribology, Elsevier, Amsterdam, 1994

[2] J.J. de Miguel, A. Sánchez, A. Cebollada, J.M. Gallego, J. Ferrón, S. Ferrer, Surf. Sci. **189/190** (1987) 1062

[3] N. Grandjean, J. Massies, P. Vennegues, M. Leroux, F. Demangeot, M. Renucci, J. Frandon, J. Appl. Phys. **83** (1998) 1379

[4] W. Matz, N. Schell, W. Neumann, J. Bøttiger, J. Chevallier, Rev. Sci. Instrum. **72** (2001) 3344

[5] Hsin-Yi Lee, K.S. Liang, Chih-Hao Lee, Tai-Bos Wu, J. Mater. Res. **15** (2000) 2606

[6] J.H. Je, D.Y. Noh, H.K. Kim, K.S. Liang, J. Appl. Phys. **81** (1997) 6126

[7] S. Williams, J.Q. Zheng, M.C. Shih, X.K. Wang, S.J. Lee, E.D. Rippert, *et al.*, J. Appl. Phys. **72** (1992) 4798

[8] W. Matz, N. Schell, G. Bernhard, F. Prokert, T. Reich, J. Claußner, *et al.*, J. Synchr. Rad. **6** (1999) 1076

[9] U.C. Oh, J.H. Je, J. Appl. Phys. **74** (1993) 1692

[10] F. Adibi, I. Petrov, J.E. Greene, L. Hultman, J.-E. Sundgren, J. Appl. Phys. **73** (1993) 8580

[11] N. Schell, W. Matz, J. Bøttiger, J. Chevallier, P. Kringhøj, J. Appl. Phys. **91** (2002) 2037

[12] P.H. Fuoss, S. Brennan, Annu. Rev. Mater. Sci. **20** (1990) 365

[13] I.K. Robinson, D.J. Tweet, Rep. Prog. Phys. **55** (1992) 599

[14] H.A. van der Vegt, H.M. van Pixteren, M. Lohmeier, E. Vlieg, J.M.C. Thorton, Phys. Rev. Lett. **68** (1992) 3335

[15] E. Weschke, C. Schüssler-Langeheine, R. Meier, G. Kaindl, C. Sutter, D. Abernathy, G. Grübel, Phys. Rev. Lett. **79** (1997) 3954

[16] J. Bøttiger, J. Chevallier, J.H. Petersen, N. Schell, W. Matz, A. Mücklich, J. Appl. Phys. (2002), in press

Influence of Dose Rate and Temperature on Ion-Beam-Induced Defect Evolution in Si Investigated by Channeling Implantation at Different Doses

M. Posselt, L. Bischoff and J. Teichert

The shape of ion range profiles obtained by channeling implantation changes with increasing implantation dose. This behavior is caused by the enhanced dechanneling of the incident ions due to the buildup of ion-beam-induced damage. The effect was extensively studied [1-4] for room temperature (RT) implants using conventional implanters with typical dose rates of 10^{12}-10^{14} cm^{-2} s^{-1}. It was shown that the dose dependence of the profile shape occurs already at doses below the amorphization threshold.

In this work the competing influence of dose rate and implantation temperature on the alteration of the shape of ion range distributions is investigated. The use of a focused ion beam (FIB) system enables the application of a dose rate which is four to six orders of magnitude higher than in conventional implanters. Based on the discussion of the experimental results the dose rate and temperature effects are modeled, and the ion range profiles measured are reproduced using atomistic computer simulations.

The implantations were performed using the FIB system IMSA-100 [5] with a $Au_{77}Ge_{14}Si_9$ liquid metal ion source [6]. Ge^{2+} ions were implanted into a n-type (100) Si substrate at 70 keV. The direction of the ion beam was 0^0 with respect to the surface normal of the target holder, i.e. it was nearly identical to the [100] axial channel direction of the Si sample. The FIB spot size was 300 nm, the ion beam current was (80 ± 2) pA. Averaged over the inhomogeneity of the beam spot, this corresponds to a dose rate of about 10^{18} cm^{-2} s^{-1}. Due to the small beam spot and the high thermal conductivity of Si, the temperature rise by FIB implantation can be neglected [7]. In the FIB implantations the beam was scanned meanderlike [8] over an area of 300 µm x 300 µm which was divided into discrete pixels. The scan was performed step by step with a certain pixel dwell time (PDT). Since the beam diameter was 300 nm but the distance between the pixel centers 80 nm, the average pixel irradiation time is 3-4 times higher than the PDT.

The FIB implantations were performed at 250 °C and RT. Two different cases were studied at both temperatures: (i) Each pixel was irradiated only once at the nominal dose rate of 10^{18} cm^{-2} s^{-1}. The desired dose was achieved by the variation of the PDT. (ii) A constant PDT of 1 µs was applied. Many repetitions of the beam scan yielded the desired dose. In the first case the ion-beam-induced defect formation is determined by the nominal dose rate. In order to obtain the effective dose rate in the second case, for a single ion impact the average three-dimensional distribution of primary atomic displacements per target atom was calculated using the Crystal-TRIM code [9,10]. It was found that the lateral cross-section of the region in which the number of displacements is above 10% of its maximum value, i.e. above 0.05 displacements per atom, is about 5 nm^2. Therefore at the nominal dose rate of 10^{18} cm^{-2} s^{-1} the time between subsequent implantations into this region is about 10 µs, i.e. at the PDT of 1 µs an overlap of regions with significant atomic displacements produced by different ions can be excluded. Thus the effective dose rate can be estimated by the division of 10^{18} cm^{-2} s^{-1} by the total number of pixels irradiated, leading to a value of about 10^{11} cm^{-2} s^{-1}.

The depth profiles of Ge were determined by Secondary Ion Mass Spectroscopy (SIMS) at Evans East using a PHI Quadrupole SIMS instrument. The continuous lines in Figs. 1(a) and 1(b) depict the measured data for the two widely different effective dose rates and for the implantation temperature of 250 °C. The dose dependence of the shape of the Ge profiles is strongly influenced by the dose rate. The weak dependence shown in Fig. 1(a) is obviously due to the fact that at 250 °C the defects created by a previous ion impact have almost disappeared before a subsequently implanted ion hits the same region of the target. The relatively high temperature and the low dose rate favor defect annealing so that the enhanced dechanneling is not very pronounced if the dose increases. The use of the lateral cross section of 5 nm^2 mentioned above as a characteristic area of a damaged region allows a rough estimation of the time scale for the annealing of defects relevant for the dechanneling, leading to about 100 s. At the high dose rate (Fig. 1(b)) a

stronger dependence of the profile shape on the dose is observed. This indicates pronounced dechanneling of the incident ions due to the buildup of radiation damage. As discussed above, at the dose rate of 10^{18} cm^{-2} s^{-1} the time between subsequent ion impacts producing significant primary atomic displacements in the same region of the target is about 10 µs. At the implantation temperature of 250 °C this time is obviously too short in order to prevent the accumulation of radiation defects.

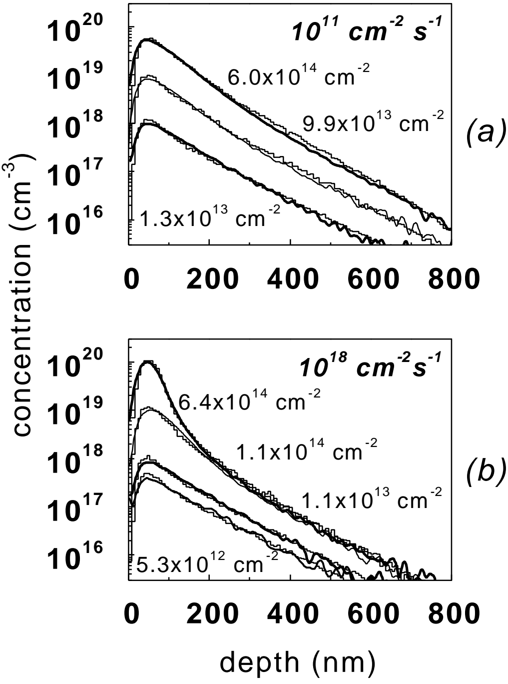

Fig. 1: Depth profiles of Ge obtained by 70 keV implantation into the [100] channel direction of (100) Si, at 250 °C. A very low (a) and a very high (b) dose rate were used. The continuous lines and the histograms show the SIMS data and the results of Crystal-TRIM simulations, respectively.

For the RT implant at the high and the low dose rate a strong dose dependence of the shape of Ge depth distributions is found. Fig. 2(a) illustrates this for the dose rate of 10^{11} cm^{-2} s^{-1}. The profiles obtained at 10^{18} cm^{-2} s^{-1} are nearly identical, with the exception of the highest implantation dose as shown in Fig. 2(b). Due to the high degree of reproducibility of the SIMS data, the difference between both profiles is considered as significant. Therefore the dechanneling of the incident ions slightly depends on the time between subsequent ion impacts into the same target region. Due to the above estimations, this time is about 10 µs at the high dose rate, and about 100 s at the low dose rate. The dose rate dependence demonstrated in Fig. 2(b) indicates that at RT some defect relaxation occurs within this time interval.

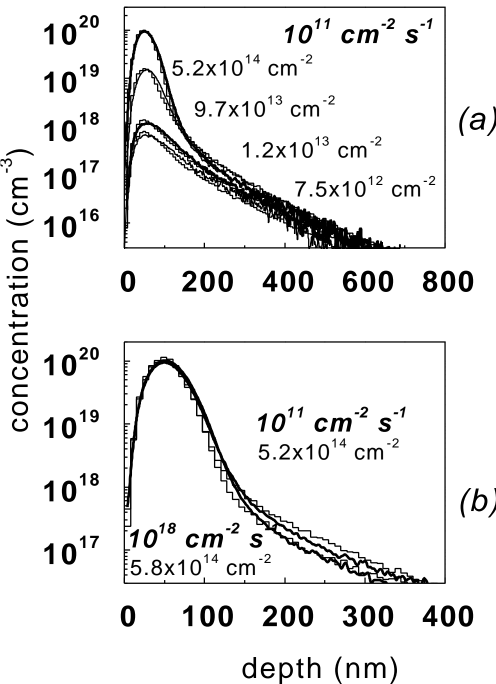

Fig. 2: Ge depth distributions for 70 keV channeling implantation at RT, at the low dose rate (a). The profiles determined for the case of the high dose rate are nearly identical, with the exception of the highest dose, as shown in the bottom figure (b). The experimental and theoretical results are given by continuous lines and histograms, respectively.

It should be mentioned that Tian *et al.* [11] found also an influence of dose rate on the shape of channeling implantation profiles obtained at RT. They used conventional medium and high current implanters with effective dose rates between 10^{13} and $5x10^{14}$ cm^{-2} s^{-1}. Their results clearly show that an accurate control of effective dose rate and substrate temperature is required in the application of channeling implantation in silicon technology.

The Crystal-TRIM code was applied to simulate the measured Ge depth distributions. Based on previous investigations [3,4] and the discussion of the present experimental results, a modified phenomenological model for damage buildup was developed which allows a quantitative description of dose rate and temperature effects. The introduction of such a model is necessary, since the Crystal-TRIM program *per se* can only treat ballistic processes during ion bombardment, but not subsequent relaxation processes. Due to their size, extended defects like amorphous pockets are considered to be most relevant for the dechanneling of incident ions. The probability p_d that in a certain volume element the ion collides with a target atom of a damaged region is the fundamental quantity of the model. It is assumed to be a function of the nuclear energy deposition by all ions previously implanted into this volume

element. Fig. 3 illustrates the dependence of p_d on the nuclear energy deposition per target atom E_n^A.

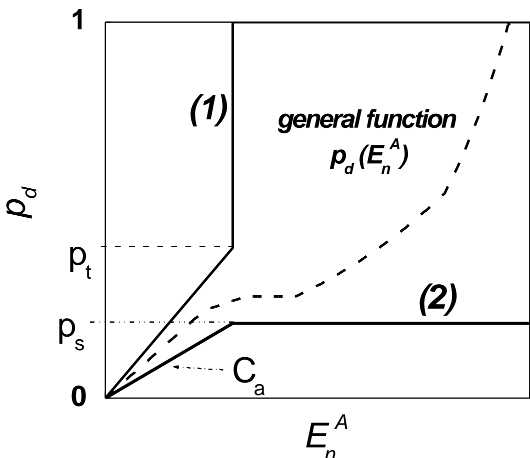

Fig. 3: Schematic representation of the probability p_d that in a certain volume element the ion collides with a target atom of a damaged region versus the nuclear energy deposition per atom E_n^A. The two extreme cases of the general function $p_d(E_n^A)$ which are given in Eqs. (1) and (2) are also shown.

In general $p_d(E_n^A)$ should increase monotonically with growing E_n^A. For small and high E_n^A one should expect a linear and a nonlinear behavior, respectively. As shown schematically, there are two extreme cases of nonlinear behavior:

(i) Above a threshold p_t an abrupt increase of p_d to 1 models the total amorphization.

$$p_d = \begin{cases} C_a E_n^A & C_a E_n^A \leq p_t \\ 1 & C_a E_n^A > p_t \end{cases} \quad (1)$$

This approximation is applied if the dose rate is sufficiently high and if the implantation temperature is relatively low. It was successfully used to model the dose dependence of the shape of range profiles in conventional ion implantation [3,4]. The parameter C_a is a measure for the size and the amount of relevant defects remaining in a cascade region after the relaxation processes. The value of C_a grows with ion mass. It depends on dose rate and temperature: The lower the temperature the smaller is the reduction of amount and size of defects. The higher the dose rate the shorter is the time available for the relaxation processes before the next ion is implanted into the same region. Therefore, the parameter C_a should grow if the temperature decreases and/or the dose rate increases. Due to the accumulation of the surviving defects, during the continuous irradiation, the target is amorphized above the threshold p_t which depends only on the ion mass [3,4].

(ii) The probability p_d cannot exceed a saturation value p_s.

$$p_d = \begin{cases} C_a E_n^A & C_a E_n^A \leq p_s \\ p_s & C_a E_n^A > p_s \end{cases} \quad (2)$$

This case should be observed at sufficiently high temperatures and small dose rates. Here the lifetime of defects created in a certain cascade region has the same order of magnitude as the time interval between subsequent implantations into such a region. Despite the continuous ion irradiation the defect concentration cannot be higher than a certain saturation value. The value of p_s should decrease with growing temperature and/or decreasing dose rate. The qualitative dependence of C_a on dose rate and temperature should be the same as discussed above.

The histograms in Figs. 1 and 2 depict the results of Crystal-TRIM simulations. In the case of Fig. 1(a) an excellent agreement with experimental data is obtained if Eq. (2) with $C_a = 5.33 \times 10^{-4}$ eV^{-1} and $p_s = 3 \times 10^{-3}$ is employed. Application of Eq. (1) allows a nearly perfect simulation of the Ge profiles in the case of Fig. 1(b) ($C_a = 1.87 \times 10^{-3}$ eV^{-1}, $p_t = 5 \times 10^{-2}$) and Fig. 2 ($C_a = 8 \times 10^{-3}$ eV^{-1} for the low dose rate, $C_a = 1.33 \times 10^{-2}$ eV^{-1} for the high dose rate; $p_t = 5 \times 10^{-2}$). A better description of the difference between the two profiles of Fig. 2(b) is beyond the capability of the simple model used. In this work a more detailed microscopic interpretation of the phenomenological damage buildup model is avoided due to the complexity of the as-implanted defect structure and the variety of defect interaction processes. The reader is referred to a recent attempt to explain the model used for RT implants by results of a combined atomistic simulation method [12].

Acknowledgements

The authors are grateful to Evans East for the SIMS analysis. In particular they thank Dr. C.W. Magee and Dr. S.W. Novak for valuable comments.

References

[1] K.M. Klein, C. Park, A.F. Tasch, Nucl. Instr. Meth. B **59-60** (1991) 60

[2] G. Hobler, A. Simionescu, L. Palmetshofer, C. Tian, G. Stingeder, J. Appl. Phys. **77** (1995) 3697

[3] M. Posselt, B. Schmidt, C.S. Murthy, T. Feudel, K. Suzuki, J. Electrochem. Soc. **144** (1997) 1495

[4] M. Posselt, B. Schmidt, T. Feudel, N. Strecker, Materials Science and Engineering B **71** (2000) 128

[5] L. Bischoff, E. Hesse, D. Janssen, F.K. Naehring, F. Nötzold, G. Schmidt, J. Teichert, Microelectron. Eng. **13** (1991) 367

[6] L. Bischoff, J. Teichert, S. Hausmann, T. Ganetsos, G.L.R. Mair, Nucl. Instr. Meth. B **161-163** (2000) 1128

[7] J. Melngailis, J. Vac. Sci. Technol. B **5** (1987) 469

[8] S. Hausmann, L. Bischoff, J. Teichert, M. Voelskow, W. Möller, J. Appl. Phys. **87** (2000) 57

[9] M. Posselt, Radiation Effects and Defects in Solids **130-131** (1994) 87

[10] C.S. Murthy, M. Posselt, T. Frei, J. Vac. Sci. Technol. B **14** (1996) 278

[11] S. Tian, S.H. Yang, S. Morris, K. Parab, A. F. Tasch, D. Kamenitsa, R. Reece, B. Freer, R.B. Simonton, C. Magee, J. Electrochem. Soc. **142** (1995) 3215

[12] M. Posselt, in: Process Physics and Modeling in Semiconductor Technology (Editors: C.S. Murthy, G.R. Srinivasan, and S.T. Dunham), Proc. Vol. **99-2**, The Electrochemical Society, Pennington NJ, USA, 1999, p. 58

Inverse Ostwald Ripening of Nanocrystals under Ion Irradiation

K.H. Heinig, B. Schmidt and H. Bernas[1]

[1] *CSNSM, CNRS-IN2P3, Orsay, France*

Novel applications of nanoclusters (NCs) are often based on size-dependent physical properties. When the dimensions of NCs approach the atomic scale, significant changes can occur in the electronic [1,2], optical [3,4], magnetic, or thermodynamic properties compared with those of bulk material. For instance, there is a strong increase of the band gap of semiconductor NCs with decreasing size. The dielectric constants and the light absorption by surface plasmons is NC size-dependent, and also the voltage which is needed to charge NCs with electrons.

As ion beam synthesis (IBS) of NCs is compatible with CMOS technology, a great effort is currently devoted to its application in micro- and optoelectronics. However, the fabrication of NCs by IBS requires usually a thermal treatment for phase separation of implanted impurity atoms and for damage annealing. This annealing leads inevitably to a broad NC size distribution of the Lifshitz-Slyosov-Wagner type which is typical for conventional Ostwald ripening (COR). Due to the broad size distribution of NCs fabricated by IBS, their size-dependent characteristics can be obscured. Thus, the potential for tailoring of size and size distribution of NCs by IBS is rather limited [5]. Here it will be shown that size and size distribution can be tailored by high-energy ion irradiation through the layer of NCs [6-9].

An analytical treatment of the steady state of a NC under ion irradiation requires a combined study of ion beam mixing at the interfaces and impurity diffusion in the host matrix. Fig. 1 illustrates the situation for NCs of phase B (Au) embedded in a matrix of phase A (SiO_2) under 4 MeV Au^+ ion irradiation. The trajectories of Au ions as well as O and Si recoils were calculated with TRIM. The recoils move approximately isotropically. This is in agreement with Sigmunds assumption in his theories of sputtering and mixing.

In thermal equilibrium (without ion irradiation), for an NC of radius R the steady-state concentration of NC atoms dissolved in the SiO_2 matrix is given by the Gibbs-Thomson relation

$$C(R) = C_\infty \times \left(1 + R_c / R\right), \qquad (1)$$

where C_∞ is the solubility at a flat interface and $R_C = 2\sigma V_a/kT$ is the capillary length with the surface tension σ and the atomic volume V_a.

The starting point of the analytical treatment of NCs under ion irradiation is the spatial probability distribution $f(r)$ of displaced atoms as illustrated in Fig. 2(a). $f(r)$ is given in a good approximation by $f(r) \propto \exp[-r/\lambda]$, where r is the distance of the displaced atom from its original position, and λ is the mean displacement distance. The spatial probability distribution $W_R(r)$ of atoms displaced out of a NC is obtained by a superposition of the displacement probabilities of all atoms in a NC (see Fig. 2(b)). To take full advantage of the symmetry of the problem, the origin of the coordinate system is now assumed to

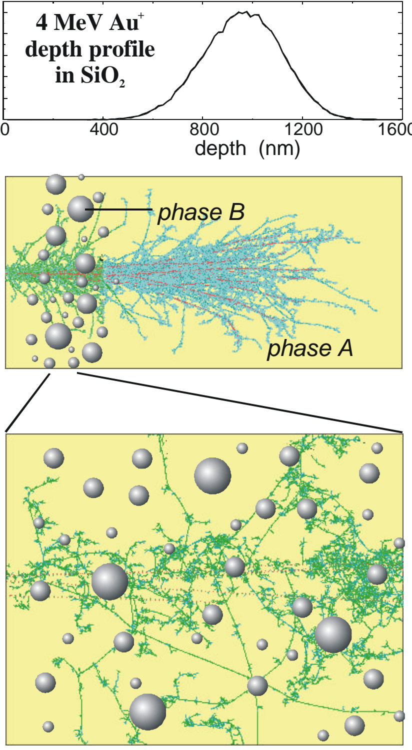

Fig. 1: Scheme of ion beam mixing between phases A and B. A situation is considered where ions come to rest far behind a layer of NCs (phase B) in a host matrix (phase A). The example shows a TRIM calculation of 4 MeV Au^+ trajectories in SiO_2 as well as the trajectories of O and Si recoils. In the NC region ion beam mixing occurs nearly isotropically.

be the NC center. For $r>R$, i.e. atoms mixed out of a NC of radius R, $W_R(r)$ is given by

$$W_R(r) = \frac{qe^{-r}}{2r}\begin{bmatrix}(rR+3R)\cosh(R)\\ -\left(R+3+R^2\right)\sinh(R)\end{bmatrix} \tag{2}$$

In Eq. (2) the distances are measured in units of ***l***. Introducing a new coordinate ***d*** = r - R and considering the limit R ® ¥, one obtains $W_{¥}(r)$ of atoms displaced from a flat interface into the neighboring half-space.

$$W_\infty(\delta) = \frac{q}{2}\left(1+\frac{\delta}{2}\right)\exp[-\delta]. \tag{3}$$

Formula (3) can be used to determine the parameters q and ***l*** by a fit of $W_{¥}(r)$ to a TRIM simulation [10] (***l*** is a hidden parameter, it is taken as the unit of length).

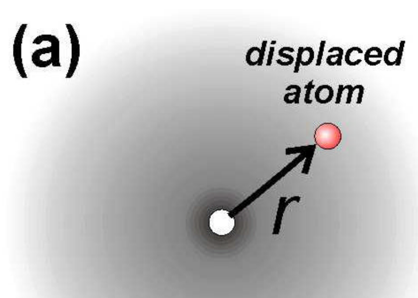

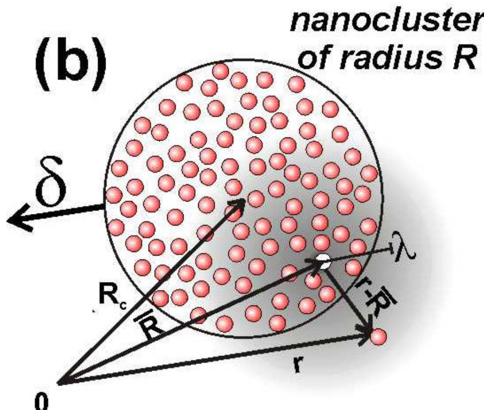

Fig. 2: (a) An atom, originally located at r=0, is displaced isotropically in a collision with a recoil and comes to rest at r. The grey area is the displacement probability f(r) ∝ exp[-r/λ]. (b) The number of atoms displaced out of a NC into the host matrix is obtained by an integration over the f(r) of the single atoms in a NC.

The steady-state solute concentration around a NC is obtained from the diffusion equation

$$D\frac{1}{r^2}\frac{\P}{\P r}\left(r^2\frac{\P}{\P r}C(r)\right) = \Phi\, W_R(r) \tag{4}$$

where $W_R(r)$ is given by Eq. (2), Φ is the ion current density, and D is the diffusion coefficient of NC atoms dissolved in the host matrix. The boundary conditions for $C(r)$ at $r = R$ and r ® ¥ are given by the Gibbs-Thomson relation and mass conservation of phase B atoms, respectively. Eq. (4) was solved analytically. The exact result looks rather complicated. However, taking into account that for the present study the profile of dissolved atoms $C(r)$ is meaningless very close to the NC surface (***d***<***1***), the analytical solution can be simplified substantially by the restriction to the asymptotic behavior:

$$\begin{aligned} C^I(R) &= C^I{}_\infty \times\left(1+R^I{}_c/R\right),\\ C^I{}_\infty &= C_\infty\left(1+\Delta\right), \\ \textit{with}\quad R^I{}_c &= \left(R_c - 5\lambda\Delta/4\right)/\left(1+\Delta\right),\\ \Delta &= q\Phi\lambda^2/DC_\infty. \end{aligned} \tag{5}$$

Thus, Δ is proportional to the damage rate.

Eq. (5) proves that for both thermal treatment with and without ion irradiation the impurity concentration around a nanocluster obeys the same law, the Gibbs-Thomson relation Eqs. (1) and (5).

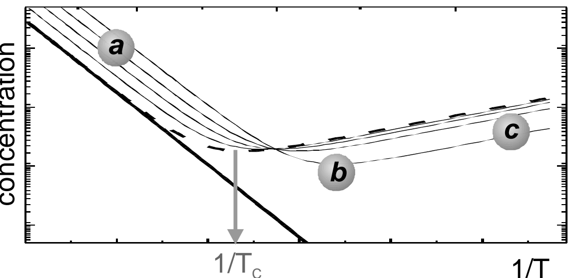

Fig. 3: Dependence of the steady-state solute concentration $C^I(R,T)$ around a NC on the sample temperature T during ion irradiation, as predicted by Eq. (5). The thick solid line shows the equilibrium solubility (solidus). The thick dashed curve denotes the steady-state solute concentration at a flat interface under ion irradiation. The thin solid curves denote the steady-state solute concentrations of ion irradiated NCs of 1.5, 2, 4 and 10 nm size, where the curves are the more distant from the dashed curve the smaller the NCs. The curves are calculated for $CoSi_2$ NCs in Si. To underline the general behavior, numbers have been omitted. It should be noted that for a given $T>T_c$ smaller NCs have a higher steady-state solute concentration than larger ones (normal behavior), whereas the situation becomes inverse for $T<T_c$.

Under ion irradiation the only difference comes from the modified solubility C^I_∞ and capillary length R^I_C.

It should be emphasized that under ion irradiation the system can be far from equilibrium. It could not be expected that a law found for the solute concentration of a NC in thermodynamic equilibrium holds also for the NC under nonequilibrium conditions. However, despite of the conserved formula (5), under ion irradiation the NC evolution can be completely different from equilibrium physics. The most striking feature of Eq. (5) is the change of the capillary length R^I_c. It becomes negative for high damage rates $q\Phi$, large displacement distances λ or low irradiation temperatures T (i.e. small values of $D(T)$ and $C_\infty(T)$). The behavior of a NC described by Eq. (5) can also be seen in Fig. 3. The dependence of $C^I(R,T)$ on T has been plotted for different R. The thick solid line shows the Arrhenius-like behavior of the steady-state solute concentration at a flat interface without ion irradiation, whereas the thick dashed curve is the plot of $C^I(R\to\infty,T)$ of Eq. (5).

The thin solid curves denote $C^I(R,T)$ with R = 1.5, 2, 4 and 10 nm as calculated for $CoSi_2$ NCs in Si, where the curves are the more distant from the dashed curve the smaller the NCs are. Under ion irradiation a high-temperature and a low-temperature behavior can be distinguished. With increasing irradiation temperature T the parameter Δ approaches exponentially zero, i.e. in regime *a* of Fig. 3 the Eq. (5) approaches to Eq. (1), the conventional Gibbs-Thomson relation. The NC behavior in regime *a* is characterized by an increasing solute concentration with decreasing NC size. The growth competition of NCs by diffusional interaction is known as (diffusion controlled) conventional Ostwald ripening.

Below a critical temperature T_c

$$T_c = \frac{E_A + E_S}{k_B \ln\left(\frac{C_0 D_0 E_S}{q\lambda^2 E_A}\right)} \qquad (6)$$

the capillary length R^I_C becomes negative for a flat interface. The surface tension of small NCs becomes negative at somewhat lower T (see Fig. 3). Here C_0, D_0 and E_S, E_A are the pre-exponentials and activation energies, respectively, of the equilibrium solubility $C_\infty = C_0 \exp[-E_S / kT]$ and the diffusion coefficient $D = D_0 \exp[-E_A / kT]$.

In Fig. 3 the critical temperature T_c separates the regime *a* ($R^I_c > 0$; conventional behavior of NCs) from regimes *b* and *c* ($R^I_c < 0$; nonequilibrium behavior). The new feature in regimes *b* and *c* is the inverse sequence of the thin solid lines, which is a consequence of the negative capillary length R^I_c (or *negative interface energy*). Here, small NCs grow at the expense of large ones. Therefore, the growth competition of NCs by diffusional interaction leads for $R^I_c < 0$ to a monodisperse size distribution of NCs, a phenomenon which is called inverse Ostwald ripening.

The theoretical prediction of Eq. (5) has been checked by kinetic lattice Monte-Carlo simulations taking into account collisional mixing with a displacement probability distribution $f(r) \propto \exp(-r/\lambda)$. An excellent agreement between analytical predictions and atomistic simulations was found. Additionally, atomistic simulations predict for very high mixing rates or low irradiation temperatures another regime were new NCs may nucleate, i.e. the mean NC size decreases even with time.

A first experiment was performed in order to prove the predictions of Eq. (5) and of the kinetic lattice MC simulations. 480 nm SiO_2 layers were grown on (100)Si substrates (n-type, 5-10 Ωcm) by thermal oxidation in wet O_2 at 1100 °C. The oxide was implanted with $2x10^{16}$ Au^+cm^{-2} at E = 330 keV. The projected range of the Au ions in SiO_2 was R_p = 102 nm. The Au^+ implanted samples were annealed at 1000 °C for 1 h in dry O_2 to form Au NCs in the SiO_2 matrix. The evaluation of high-resolution XTEM images showed that the mean NC diameter d_{NC} in the region ($R_p \pm 15$ nm) was 4.2 nm with a FWHM of 2.7 nm. (see Fig. 4(a)). 4.5 MeV Au^+ ion irradiation at 200 °C with a flux density of $3.9x10^{11}$ $Au^+cm^{-2}s^{-1}$ was used for the study of the evolution of the initial NC size distribution under ion irradiation. The high-energy Au^+ ions have a projected range of R_p = 1.06 µm and a longitudinal straggling of ΔR_p = 0.11 µm, i.e. they come to rest in the (001)Si substrate. The NCs in the SiO_2 layer are influenced by the collision cascade of the 4.5 MeV Au^+ ions only, not by deposition of Au^+ ions. In this first, preliminary experiment, the mean size of Au NCs decreases with increasing doses of $5x10^{15}$ Au^+cm^{-2} and $10x10^{15}$ Au^+cm^{-2} (see Figs. 4(b) and 4(c), respectively). Additionally, an increase of NC density and decrease of the width of the size distribution with increasing ion dose were found. This experimental result is in good qualitative agreement with the theoretical predictions. A quantitative comparison fails due to the lack of reliable values of the diffusivity and solubility of Au in SiO_2.

It appears that the ion irradiation of the Au NCs has been performed in regime *c* of Fig. 3. Thus, for Au NCs in SiO_2, an irradiation temperature of 200 °C is too low in order to prevent nucleation of additional NCs. For that reason, the mean NC size decreases during irradiation. Ion

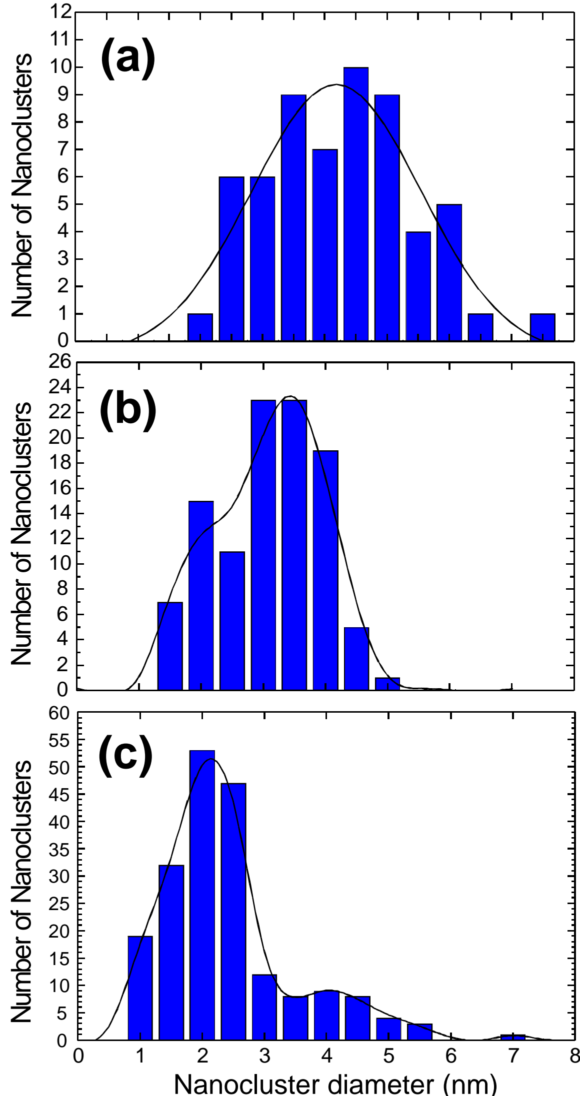

Fig. 4: Evolution of the size distribution of NCs under ion irradiation. The initial size distribution of NCs formed by 330keV, $2x10^{16}Au^{+}cm^{-2}$ implantation and annealing at 1000°C for 1h in dry O_2 is shown in (a). (b) and (c) show the NC size distribution after 4.5 MeV irradiation with $5x10^{15}$ $Au^{+}cm^{-2}$ and $10x10^{15}$ $Au^{+}cm^{-2}$, respectively.

irradiation at higher temperatures will be performed in order to explore regime *b* of Fig. 3. Furthermore, according to Fig. 4, a steady state of the NC size distribution has not yet been reached by the maximum ion fluence used in the present experiment.

Acknowledgements

The authors greatly acknowledge the kind assistance of Arndt Mücklich and Alexander Schmidt for cross-section TEM investigations and for quantitative evaluation of TEM micrographs, respectively.

References

[1] Y. Inoue, A. Tanaka, M. Fujii, S. Hayashi, K. Yamamoto, J. Appl. Phys. **86** (1999) 3199

[2] W. Chen, H. Ahmed, K. Nakazoto, Appl. Phys. Lett. **66** (1995) 3383

[3] L. Rebohle, J. von Borany, H. Fröb, W. Sko rupa, Appl. Phys. **B71** (2000) 131

[4] S. Okamoto, Y. Kanemitsu, K.S. Min, H.A. Atwater, Appl. Phys. Lett. **73** (1998) 1829

[5] K.-H. Heinig, B. Schmidt, A. Markwitz, R. Grötzschel, M. Strobel, S. Oswald, Nucl. Instr. Meth. **B 148** (1999) 969

[6] K.-H. Heinig, B. Schmidt, M. Strobel, H. Bernas, Mater. Res. Soc. Symp. Proc. **650** (2001) R9.6; *ibid.* **647** (2001) O14.6

[7] G. Rizza, M. Strobel, K.-H. Heinig, H. Bernas, Nucl. Instr. Meth. **B 178** (2001) 78

[8] M. Strobel, K.-H. Heinig, W. Möller, Phys. Rev. **B 64** (2001) 245422

[9] B. Schmidt, K.-H. Heinig, A. Mücklich, Mater. Res. Soc. Symp. Proc. **650** (2001) O11.20

[10] J.F. Ziegler, SRIM: The Stopping and Range of Ions in Matter, Program Manual, IBM Research, Yorktown, NY (1996)

Impact of Ambient Atmosphere on As-Implanted SiO_2 Layers

B. Schmidt, K.H. Heinig, D. Grambole and F. Herrmann

Nanocrystals are produced by a variety of methods, most of which fabricate the nanocrystals in a glass (SiO_2) matrix. One of the widely applied techniques is the ion implantation of Si, Ge or Sn ions into thermally grown SiO_2 on a silicon substrate, followed by high-temperature processsing to induce phase separation and defect annealing.

Ion-beam synthesis (IBS) of nanoclusters in SiO_2 layers requires high dose ion implantation ($1x10^{15}$ - $1*10^{17}$ cm^2) leading to a high degree of destruction of the amorphous network. In the case of low energy ion implantation (E < 30 keV) into SiO_2, the damaged layer will be located very near the SiO_2 surface. The large number of broken bonds in the SiO_4-tetrahedra due to displaced Si and O atoms results in rearrangements of the fundamental ring structure within the glassy network [1] in which moisture from the ambient can be absorbed. Water molecules adsorb at the surface, and damage-enhanced inward diffusion can take place. Therefore, chemical reactions of the implanted impurities with hydrogen and oxygen must be expected during subsequent annealing. This can interfere with precipitation and Ostwald-ripening of nanocrystals. In recent publications [2-3] was reported that a hydrogen-containing annealing atmosphere drastically increases the solubility and diffusivity of Ge by forming GeH_x complexes, leading to fast precipitation and Ostwald ripening of unusually large Ge nanocrystals and even to Ge loss from the implanted SiO_2 by outward diffusion of GeH_x. Also, partial oxidation of implanted Ge in the near surface region of implanted SiO_2 by small amounts of oxygen in the annealing atmosphere has been reported [4-6].

On nondamaged SiO_2, the water absorption from the ambient and interaction with disiloxane groups have been intensively investigated for different glasses [7] and are explained by a 3-step process: (i) adsorption of H_2O molecules at the SiO_2 surface, (ii) activated complex formation, and (iii) hydrolysis of H_2O [8]. These steps lead to a SiO_2 network breakage in the near surface layer or to the so-called “leached layer” [7]. As far as we know, the water absorption process has been not investigated for heavy ion-damaged SiO_2-layers. On the other hand radiation defects, induced in amorphous SiO_2 by VUV, X- and (-ray, electron, proton and neutron irradiation, have been extensively studied to date [9-11]. Defect generation in SiO_2 by these kinds of radiation is mainly caused by electronic energy loss (ionization). During ionizing irradiation of SiO_2 the production of E'_1-centers and interstitial oxygen atoms represents the basic radiation-induced events. In general, centers relevant to this Frenkel-defect are oxygen hole centers (OHC), such as nonbridging oxygen hole centers (NBOHCs, /Si-O@) and peroxy radicals (PORs, /Si-O-O@), as well as Si-Si bonds and interstitial O_2 molecules. Furthermore, it is well known that water is frequently present in non-irradiated glasses in the form of OH^- groups [7]. There are few data for incorporation of water into heavy ion-damaged amorphous SiO_2, where the ion energy loss is dominated by nuclear energy loss in displacements of silicon and oxygen atoms in the matrix [12-13].

The samples were SiO_2 films, 100 nm thick and grown on Si(100) wafers by oxidation at 1000 °C in dry oxygen. The SiO_2 films were implanted with Si^+, Ge^+ and Sn^+ ions in the dose range 10^{13}-10^{16} ions/cm^2 at room temperature. The ion energies were chosen in such a way that the projected ion range R_p was 20 nm in all cases. After removing the samples from the implantation chamber, they were stored in a clean-room at 40 % rel. hum for some days. Additionally, one part of the samples was wet- chemically cleaned by a sulfuric acid/ hydrogenperoxide mixture (H_2SO_4: H_2O_2 = 1:1 at 130 °C for 15 min), after that rinsed in deionized water, and dried in a usual way. One part of the wet- cleaned samples was annealed at 600 °C for 10 min in dry N_2 to study the reduction of the H (H_2O) content by outward diffusion or inward diffusion into deeper regions of SiO_2.

The total hydrogen concentration in SiO_2 was measured by Nuclear Reaction Analysis (NRA) using the following reaction: $^{15}N + {}^1H \rightarrow {}^{12}C + {}^4He + \gamma$ (4.43 MeV). This reaction has a narrow resonance at the energy E_{res} = 6.385 MeV. By increasing the energy of the ^{15}N ions above E_{res}, the ions reach the resonance energy at a certain depth of the sample due to energy loss in the material. Measuring the yield of the γ-rays with an energy of 4.43 MeV as function of the beam energy, the hydrogen depth profiles were obtained. The γ-rays were detected by a 10cm x 10cm NaI(TI) scintillation detector. Typically a ^{15}N ion beam current of 15-20 nA and a beam spot of

5 x 5 mm^2 were used. Because hydrogen loss of the samples was observed during $^{15}N^+$ ion irradiation, the measured γ-ray yield versus the $^{15}N^+$ dose had to be extrapolated to dose zero. Consequently, every measurement for a certain depth was done on a virgin area of the sample.

The results of H depth profiling after storage are shown in Fig. 1 for ions of different mass, implanted into SiO_2. The ion dose was $5x10^{15}$ cm^{-2} for all ions. As can be seen, the H concentration C_H increases with increasing ion mass and has the highest level for the imlantation of Sn^+ ions. For Ge and Sn, the H content at 5nm depth reaches (10"1) at%. The H profiles are extended to a SiO_2 layer depth of (40-50) nm. The measured values C_H at the surface are not shown in this and in all following figures, because the surface adsorption of water cannot be controlled during all experimental steps.

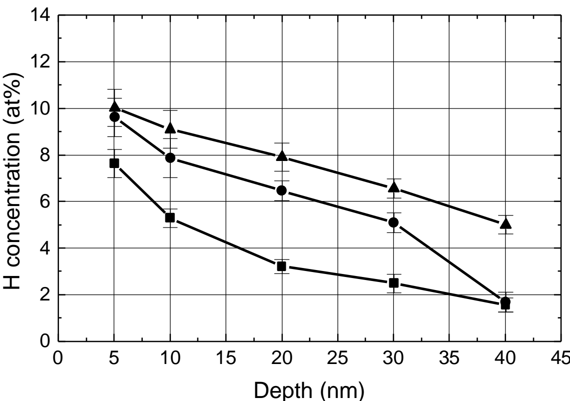

Fig. 1: Hydrogen depth profiles of Si^+-, Ge^+ and Sn^+-implanted SiO_2 after storage. The ion dose was $5x10^{15}$ cm^{-2} for all ions (• - Si^+, E = 13 keV; Ž - Ge^+, E = 22 keV; • - Sn^+, E = 26 keV).

In Fig. 2 the results of hydrogen depth profiling after different preparation steps (storage, wet chemical cleaning and 600 °C annealing for 10 min in dry N_2) after Ge^+ implantation are shown. For comparison, in Fig. 2 the H concentration in the unimplanted as-grown oxide and in an oxide that was only wet-chemically treated is included. The measured H concentration in the non-implanted samples is smaller than 0.5 at%, which is near the sensitivity limit deriving from the uncertainty of the extrapolation procedure for the measured data (normally the sensitivity limit is -0.05 at%). Wet chemical cleaning of the as-implanted samples increases the H content in SiO_2 by only 1-2 at% compared to the as-implanted sample. Therefore, we can conclude that the hydrogen concentration up to a SiO_2 depth of (40-50) nm is caused by water absorption from the air humidity and defect-enhanced inward diffusion at room temperature.

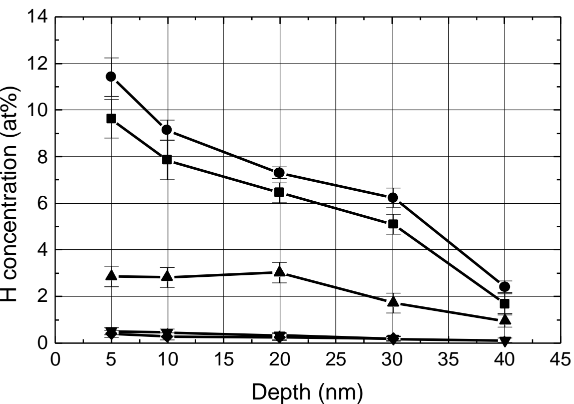

Fig. 2: Hydrogen depth profiles in Ge^+-implanted SiO_2 after different preparation steps (• - storage after implantation, Ž - wet chemical cleaning (SPM) and • - 600 °C annealing for 10 min in dry N_2). For comparison, the H concentration profiles in the unimplanted, as-grown, oxide (–) and in an oxide, which was only wet-chemically treated (SPM) (–), are included.

Annealing reduces C_H approximately by a factor of two in the depth of R_p = 20 nm. The reduction of the H content near the SiO_2 surface is more pronounced due to possible outward diffusion of H and OH^- and/or H_2O molecules during thermal treatment. To investigate the dose dependence of water absorption, SiO_2 was implanted with Ge^+ ions at different doses, ranging from $1x10^{13}$ cm^{-2} up to $1x10^{16}$ cm^{-2}. The corresponding H depth profiles are shown in Fig. 3. A dose of $1x10^{14}$ Ge^+/cm^2 was established as a threshold dose for significant water inward diffusion. At doses higher than $1x10^{15}$ Ge^+/cm^2, the H concentration versus depth decreases again, which can be explained by densification of the SiO_2 matrix due to an increasing Ge concentration in the SiO_2 up to 20 at% in the maximum of the implantation profile.

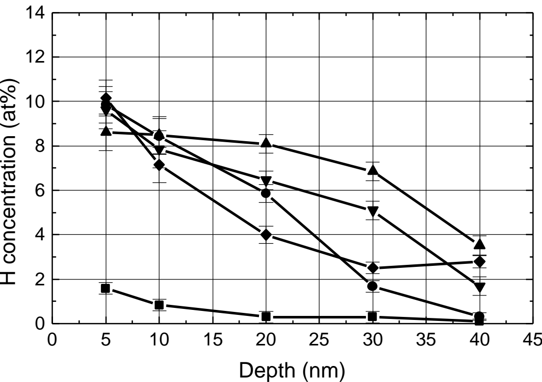

Fig. 3: Ion dose dependence of H depth profiles in as-implanted SiO_2 after storage. The implantation was done with 22 keV Ge^+-ions at different doses: • - $1x10^{13}$ cm^{-2}, Ž - $1x10^{14}$ cm^{-2}, • - $1x10^{15}$ cm^{-2}, – - $5x10^{15}$ cm^{-2}, – - $1x10^{16}$ cm^{-2}.

The absorption of water from the ambient into ion irradiated SiO_2, is initiated by the Si-O bond cleavage occurring as a result mainly of nuclear energy loss of the ions in the SiO_2 matrix (energy deposited by electronic processes displaces atoms about 1000 times less efficient [1]). Fig. 4 shows the displacements per atom (dpa) calculated by TRIM [14].

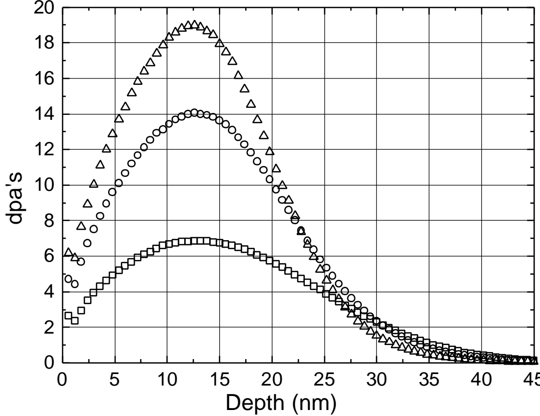

Fig. 4: Depth distribution of displacements per atom (dpa) calculated by TRIM [11] for 13 keV Si^+- (9), 22 keV Ge^+- (O) and Sn^+ (Δ) ions at D = $5x10^{15}$ cm^{-2} for all ions.

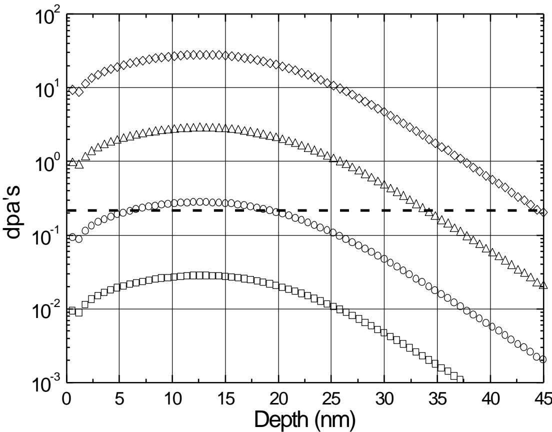

Fig. 5: Dose dependence of displacements per atom (dpa) over depth in SiO_2 implanted with 22 keV Ge^+ ions at $1x10^{13}$ cm^{-2} (9), $1x10^{14}$ cm^{-2} (O), $1x10^{15}$ cm^{-2} (Δ) and $1x10^{16}$ cm^{-2} (").

As can be seen from Fig. 4 for an implantation dose of $5x10^{15}$ cm^{-2} of Si, Ge and Sn, every matrix atom is displaced more than once up to a SiO_2 depth of 30 nm. The number of displacement per atom increases with increasing ion mass. Therefore, the ion-induced damage in the depth up to 30 nm is the highest one for Sn implantation. This corresponds to the highest H content in the case of Sn implantation (see Fig 1). At deeper regions, from 30 nm to 40 nm, only every third or fourth matrix atom is displaced. Taking into account the structure of the SiO_4-tetrahedra, most probably one O-atom will be displaced. This can explain also the threshold dose of $1x10^{14}$ Ge^+/cm^2 for significant water inward diffusion. In Fig. 5, where the depth dependence of dpa for 22 keV Ge^+ implantation is shown, it can be seen that for the dose of $1x10^{14}$ Ge^+/cm^2 nearly every fourth matrix atom in the depth up to 20 nm will be displaced (see dashed line in Fig. 5). Taking into account that at depths up to 30 nm still approximately every tenth atom will be displaced we conclude that in deeper SiO_2 regions a sufficiently high number of displaced target atoms are present. Additional defects in deeper regions, like E´-centers, interstitial oxygen atoms, nonbridging oxygen hole centers and other defects, might be induced by ionization processes. This may explain the penetration of moisture into the depth of 40-50 nm.

For the adsorption and room temperature inward diffusion of water molecules into ion damaged SiO_2 there are two possible mechanism: i) the water molecules diffuse into the more or less open SiO_2 network directly because H_2O is a "point-like" molecule with a small diameter of < 0.3 nm or ii) the H_2O molecule dissociates at the SiO_2 surface and H^+ and OH^- diffuse into the silicon dioxide. In either case, an internal source of hydrogen and oxygen will be present during thermal treatment, and the following chemical reaction of the implanted impurities M (Si, Ge, Sn) should be take place: $H^+ + OH^- + M$ Y $MH_x + MO_x$. The hydrides MH_x have a high solubility and are mobile in SiO_2 (fast mass transport), while the oxides MO_x are miscible with SiO_2 (except SnO and SnO_2) and will be incorporated into the amorphous matrix at the place of formation. The formation of MH_x is recognized as a fast reaction still at temperatures < 900°C, whereas the oxidation process for the impurities M is slower at lower temperatures. From the measured H depth profiles, we can conclude that an oxygen concentration of 3-4 at% exists at R_p, corresponding to about 50% of the H concentration (most probably OH-groups are present). This is of the same order as the impurity concentration in the maximum of the implanted profile for an implanted dose of $5x10^{15}$ cm^{-2}. Therefore, we must expect in the initial state of post-implantation annealing (sample heating up) a very fast redistribution of the implanted profile due to the rapid formation of MH_x-compounds, leading to fast precipitation and even H-stimulated outward diffusion of the implanted atoms. With increasing temperature and time, oxidation (like wet oxidation of Si) of the implanted atoms M or of their precipitates and nanocrystals takes place [4-6].

Assuming the chemical reactions described, unexpected nanocrystal distributions, experimen-

tally observed especially in very shallow implanted SiO_2-layers, can in many cases be explained. The observed water incorporation is very important in IBS, especially for the case of Si, Ge and Sn nanocrystals in ultrathin gate oxides (10-30 nm thick) that are currently investigated because of their application in nanocrystal-based nonvolatile memory devices.

Acknowledgements

The authors thank W. Möller and T. Müller for helpful discussions and support in TRIM-calculations. This work was sponsored by the European Community under the auspices of the GROWTH Project. GRD1-2000-25619.

References

[1] R.A.B. Devine, Nucl. Instr. Meth. **B 91** (1994) 378

[2] A. Markwitz, B. Schmidt, W. Matz, R. Grötzschel, A. Mücklich, Nucl. Instr. Meth. **B 142** (1998) 338

[3] A. Markwitz, W. Matz, B. Schmidt, R. Groetzschel, Surf. Interface Anal. **26** (1998) 359

[4] K.-H. Heinig, B. Schmidt, A. Markwitz, R. Grötzschel, M. Strobel, S. Oswald, Nucl. Instr. Meth. **B 148** (1999) 969

[5] V.A. Borodin, K.-H. Heinig, B. Schmidt, Nucl. Instr. Meth. **B 147** (1999) 286

[6] S. Oswald, B. Schmidt, K.-H. Heinig, Surf. Interface Anal., **29** (2000) 249

[7] H. Scholz, Glas – Natur, Struktur und Eigenschaften, Springer Verlag, Berlin, 1988, pp. 305

[8] A.C. Lasaga, G. V. Gibbs, Am. J. Sci. **290** (1990) 263

[9] D.L. Griscom, J. Ceram. Soc. Jpn. **99** (1991) 923

[10] H. Hosono, H. Kawazoe, N. Matsunami, Phys. Rev. Lett. **80** (1998) 317

[11] H. Akazawa, J. Vac. Sci. Technol. **B 19** (2001) 649

[12] G.W. Arnold, Nucl. Instr. Meth. **B 32** (1988) 268

[13] G.W. Arnold, G. Battaglin, G. Mattei, P. Mazzoldi, S. Zandolin, Nucl. Instr. Meth.**B 166-167** (2000) 440

[14] J.F. Ziegler, SRIM: The Stopping and Range of Ions in Matter, Program Manual, 1996, IBM Research,

Transient Behavior of the Strong Violet Electroluminescence of Ge-Implanted SiO_2 Layers

L. Rebohle, J. von Borany, G. Franzò[1], T. Gebel, M. Helm, D. Pacifici[1], F. Priolo[1] and W. Skorupa

[1]*INFM and Dipartimento di Fisica e Astronomia, Università di Catania, 95129 Catania, Italy*

Because of the enormous development of communication technology there is a high need for optoelectronic devices. Unfortunately, silicon is unsuitable to operate as a light emitter due to its indirect band gap. Although compound semiconductors are used today for discrete light emitting devices, the problems to combine these materials with Si-based integrated circuits have not been overcome so far. This has initiated an extensive search for alternative, Si-based light emitting materials. Among the different approaches ion implantation into thin SiO_2 films is one of the most suitable fabrication methods because of the robustness of the matrix, the very good control over the fabrication process and its full compatibility with current Si technology.

Strong blue-violet photoluminescence (PL) of Si- and Ge-implanted SiO_2 layers in the blue or violet spectral region has already been demonstrated [1-4]. This PL is generally believed to be caused by an oxygen deficiency center, but there is no agreement about the specific microstructure of this center. Current explanations for the blue-violet PL of doped glasses prefer either the twofold coordinated atoms of Si (Si_2^0) and Ge (Ge_2^0) [5] or neutral oxygen vacancies [6] whose both formation is favored by the presence of excess Si or Ge atoms. However, it is more difficult to excite this strong luminescence electrically, and therefore the number of studies reporting on successfully achieved blue-violet electroluminescence (EL) from these layers is very limited. Recently, blue EL from Si-implanted SiO_2 layers [3,7,8] and violet EL from Ge-implanted SiO_2 layers [3,9,10] were observed. In the latter case a power efficiency of 0.5 % has been achieved, and the first successfully integrated optocoupler was demonstrated [10].

Whereas models about the optical excitation of the oxygen deficiency centers in implanted SiO_2 films were recently developed [4], the specific excitation mechanism of the EL is still unclear. In this paper the excitation mechanism of Ge-implanted SiO_2 layers is investigated by means of electrical and EL transient measurements. Starting from the existing knowledge about electron injection and transport in pure oxides a qualitative transport model in Ge-implanted oxides is developed. Based on this model and in combination with the results of the EL transient measurements, the impact excitation of the luminescence centers (LCs) by hot electrons is regarded to be the most probable excitation mechanism.

Thin 200 nm thick SiO_2 layers were thermally grown on [100]-oriented, n-type Si substrates at 1000 °C. The oxide films were implanted with 100 keV Ge^+ ions resulting in a Gaussian implant profile with a peak Ge concentration ranging between 0.3 and 3 at. %. After implantation, rapid thermal annealing (RTA) at 1000 °C was applied with an annealing time of 30 s. For electrical and EL studies, circular metal-oxide-semiconductor (MOS) device structures were prepared using sputtered 80 nm thick layers made of indium tin oxide (ITO) and Al as top and bottom electrodes, respectively. The device matrix with a dot diameter of 0.5 mm was fabricated by photolithographic patterning. EL and PL measurements were performed at room temperature in a Spex Fluoromax spectrometer with an R298 Hamamatsu photomultiplier and a Keithley 237 Source Measure Unit.

For the EL, the voltage and the current transient measurements a voltage pulse with an amplitude of 30 V and a width of 9 ms was added to a constant voltage of about 150 V. A RC element was used to smooth the edges of the voltage pulse to 3 μs, and a second capacitor was used to bridge the constant voltage generator for AC pulses. The voltage and current transients were measured by an oscilloscope directly or via a 10 kΩ resistance, respectively. The EL transient measurements were performed by detecting the intensity yield at 390 nm (3.18 eV) with a water cooled C4877 Hamamatsu photomultiplier tube and by analyzing it with a photon counting multi-channel scaler (SR430, Stanford Research Systems) triggered by the pulse generator. The time response of the detecting system was about 30 ns.

Fig. 1a displays the normalized EL and PL spectrum of a 200 nm thick Ge-implanted SiO_2-film containing 3 at.% Ge. Whereas the PL was recorded using an excitation wavelength of 240 nm

(5.17 eV), the EL was observed by applying an external electric field of 7.15 $MVcm^{-1}$.

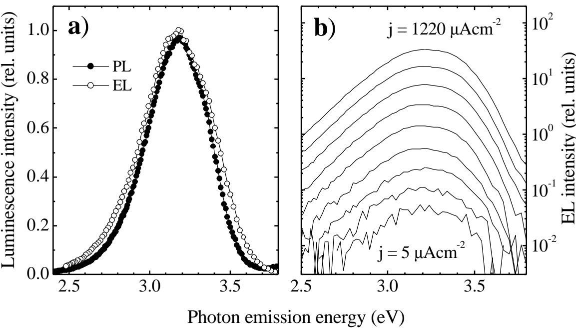

Fig. 1: The PL and EL spectrum of a 200 nm thick Ge-implanted oxide layer containing 3 % Ge, annealed at 1000 °C for 30s (a). Both spectra are nearly identical. Whereas the shape of the EL spectrum does not change with the injection current density, the EL intensity shows a linear dependence on it (b).

Both spectra are nearly identical and show a luminescence peak in the violet spectral region at 3.18 eV (390 nm). This implies that the luminescence for both, PL and EL, is caused by the same type of LCs, and that the emission mechanism is identical. Fig. 1b shows the EL spectrum of the same device for different injection current densities on a logarithmic scale. Obviously the shape of the spectrum does not change at all with the injection current. Furthermore, the EL intensity exhibits a linear dependence on the injection current over 3 orders of magnitude.

Fig. 2 shows the applied voltage composed of a 150 V constant voltage and a 9 ms long voltage pulse with an amplitude of 30 V (upper curve). The rise and decay time of the pulse is about 3 μs. The capacity of the MOS device differentiates the edges of the voltage pulse and causes a current spike with a time constant of again 3 μs (middle curve). Apart from these spikes the tunnel resistance of the MOS device leads to a rectangular current pulse with an amplitude of 6-7 μA which really crosses the oxide layer. This current flow causes the EL whose rising and falling edge is shown in the lower curve. For both the rise and decay time of EL a value of about 100 μs was estimated which does not depend on the Ge concentration or the annealing procedure.

First it should be reviewed very briefly what is known about the LCs causing the PL of Ge-implanted SiO_2 layers. In previous investigations [3,4,9] we found that the violet PL of Ge-implanted SiO_2 films is caused by a Ge-related oxygen deficiency center. The energy level scheme of such a LC consists of a ground singlet state S_0, a first excited singlet state S_1 and a first excited triplet state T_1 (Fig. 3). The PL can be understood as a radiative excitation from S_0 to S_1 followed by relaxation and intersystem crossing to T_1 and a radiative transition back to S_0. The radiative transition $T_1 \rightarrow S_0$ is optically forbidden by first order and occurs only because of the spin orbit coupling. The observed high intensity of this transition is explained by the heavy atom effect [4] which increases the spin orbit coupling if one Si atom of the LC is substituted by a heavier but isoelectronic Ge atom. Furthermore, intersystem crossing is a very efficient process leading to a much higher population of the T_1 state in comparison with the S_1 state. As the radiative transition $T_1 \rightarrow S_0$ is optically forbidden, the PL decay time is rather long and was estimated to be 100 μs [4].

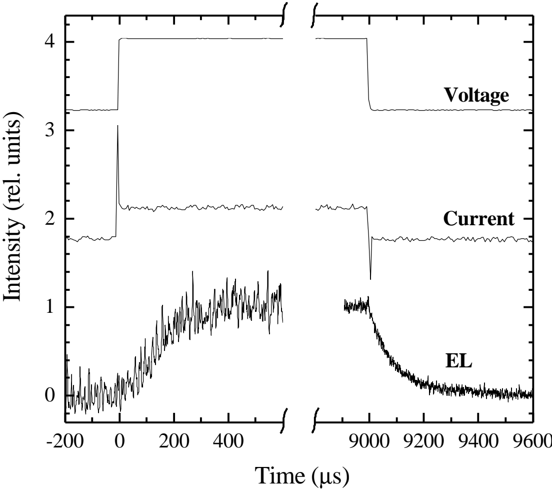

Fig. 2: The voltage, current and EL transient of a 200 nm thick Ge-implanted oxide layer with 3 % Ge in comparison.

As already stated the good correspondence between the PL and EL spectra implies that in both cases the luminescence is caused by the same LC, and that the radiative deexcitation is identical. However, in the case of EL the excitation of the LC to the T_1 state is more complex and can be divided into three different parts: interface electron injection, bulk electron transport and the excitation of the LC itself. In the case of unimplanted SiO_2 electrons are injected by Fowler-Nordheim tunneling. If the oxide is implanted, defects are created in the oxide layer which appear as electron traps in the band gap of SiO_2. Traps located close to the injecting interface can support the injection by trap assisted tunneling of electrons from the conduction band of the Si substrate to the traps.

If there is a considerable amount of traps within the oxide, the electrons can be transported between the traps by hopping or Poole-Frenkel conduction. Another possibility is the quasi-free movement of the electrons in the conduction band of SiO_2. In the case of unimplanted thermally grown SiO_2 the electrons will be accelerated by the high electric field, but lose energy by phonon scattering and impact ionization. Whereas phonon

scattering is efficient for low kinetic energies, impact ionization occurs only for kinetic energies above the band gap energy of SiO_2 of approximately 9 eV. In the case of equilibrium the electrons can be characterized by a distinct energy distribution depending on the position in the oxide and the electric field. After a mean path length depending on the electric field the energy distribution will saturate. As a result the mean kinetic energy of the electrons in the conduction band of pure SiO_2 is rather high for high electric fields and amounts to 2-4 eV for electric fields higher than 7 $MVcm^{-1}$ [11,12]. Also the number of electrons having energies higher than 9 eV becomes non-negligible at 7 $MVcm^{-1}$ and grows rapidly with increasing electric field.

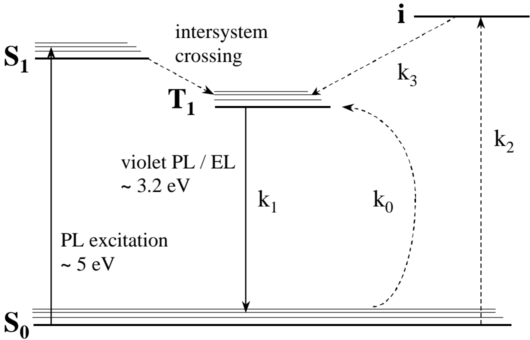

Fig. 3: Energy level scheme of an oxygen deficiency center consisting of a ground singlet state S_0, a first excited singlet state S_1 and a first excited triplet state T_1. In addition, an intermediate state i is drawn. Radiative transitions are marked by solid, non-radiative with dashed arrows.

In the case of implanted oxides this model must be modified. Both the trapping of electrons and the scattering of electrons at LCs are efficient processes to decelerate electrons. Furthermore it may be possible that the ionization of LCs requires an energy less than 9 eV, and finally trap assisted ionization can occur. All these processes will lead to a reduction of the mean kinetic energy of electrons moving in the SiO_2 conduction band. Indeed, the trapping of electrons will cause additional effects, namely the buildup of a negative space charge counteracting the further injection of electrons. The negative potential of the space charge will lift the SiO_2 conduction band which lowers the local electric field at the SiO_2-Si interface. In contrast to this the local electric field at the metal gate is increased. Corresponding to the increase and decrease of the local electric field the mean kinetic energy of the electrons increases and decreases, respectively.

Due to the two general transport mechanisms there are two possible models to excite the LCs. If the electrons are moving in the SiO_2 conduction band they can be scattered inelastically at the LCs and transfer the energy which is required to excite a LC to the T_1 state. If the electrons are transported via traps, the LCs can be ionized due to the high electric field. The now positively charged LCs can easily trap another electron and can relax – with a certain probability – to the T_1 state.

Now the decay and rise time measurement will give additional information about the excitation mechanism which allows one to favor one of the two possible excitation mechanisms. Let us start with the consideration of a general 3-level-system as shown on the right side of Fig. 3. Hereby the specific nature of the intermediate state i - whether it is an ionized state, the S_1 state or whatever – is out of interest. In the general case the decay will be biexponential with k_1 and k_3 as exponential rate coefficients. As only a monoexponential decay with a decay constant of 100 µs – which is identical to the PL decay time – was measured, we find $1/k_1 \approx 100$ µs and k_3 has to be very large. This means that a LC being in the intermediate state i relaxes in a very short time to the T_1 state, and that the physical behavior is very similar to that of a 2-level-system. Also from the mathematical point of view, the asymptotic limit for $k_3 \to \infty$ is a 2-level-system consisting of the states S_0 and T_1 only. In this case k_2 and k_3 can be combined to k_0, and the rate equation is given in the simple form

$$\dot{N}_T = -k_1 N_T + k_0 N_S = k_0 N_0 - (k_0 + k_1) N_T$$
$$\text{with} \quad N_T + N_S = N_0$$

with N_0, N_S and N_T being the total number of LC, the number of LC in the S_0 state and the number of LC in the T_1 state, respectively. For the rising edge (switch on) the time dependence of N_T will be

$$N_T(t) = N_0 \frac{k_0}{k_0 + k_1} \{1 - \exp[-(k_0 + k_1)t]\}.$$

As a rise time of 100 µs was measured, k_0 must be small compared to k_1 and thus also $k_2 \ll k_1$. At this point the different physical meaning of k_0 and k_1 has to be emphasized. Whereas k_1 gives an information of the internal time scale of deexcitation, k_0 is only related to the mean interaction cross section σ between an electron and a given ensemble of LCs and the injection current density j. As the absolute EL intensity increases linearly with j, k_0 should be also proportional to j and can be expressed as

$$k_0 = \frac{1}{|q|} \sigma\, j$$

with q being the electron charge. With the experimental values it is now possible to assess an upper limit for the excitation cross section. If $k_0 \leq 0.1$, $k_1 \approx 10\ s^{-1}$ and $j \approx 10^{-3}\ Acm^{-2}$ are assumed, a maxi-

mal value of $\sigma \approx 1.6x10^{-13}$ cm^2 is obtained. Finally, it should be noted that, in spite of the use of a 2-level-system for modeling, it cannot be distinguished, whether the LCs are excited directly or via an intermediate state with a fast transition rate to T_1. The EL transient measurements only exclude the case of a 3-level-system with a slow k_3 value.

Based on these results we slightly favor the inelastic scattering of electrons at LC as the dominant excitation process because of the following reasons: If the LC is ionized the internal structure of the LC will be rearranged, and the recapture of an electron could result in a structure different from the initial one. So the probability can be low that the ionization of a LC followed by electron recapture is resulting in the same structure. A similar phenomenon is known from silica, where the ionization of the neutral oxygen vacancy is regarded to be an irreversible (and destructive) process [13]. Due to the decay time measurement the electron recapture would have to be a fast process. However, the recapture of electrons depends on the capture cross section and the injection current density, and for low injection currents a small transition rate to T_1 is expected. Finally the energy to ionize a LC will be higher than the energy to excite it, and therefore a smaller fraction of electrons will have sufficient energies to ionize a LC than to excite it. Based on these considerations we find it unrealistic that the process of impact ionization followed by electron recapture fulfils all conditions to fit the experimental results.

If the LC is excited by inelastic scattering of electrons, the excitation cross section will be linked to the specific energy distribution of the electrons. As already mentioned, the buildup of space charges causes local deviations of the electric field. The excitation cross section will vary in the same manner leading to an inhomogeneous excitation of the LCs depending on their position in the oxide layer. More specifically, most of the EL will come from LCs located closer to the gate due to the higher local electric field. Furthermore, after injection the electrons need a certain acceleration distance to approach the saturated energy distribution. According to this there should be a dark zone close to the Si-SiO_2 interface where the kinetic energy of the electrons is not high enough to excite a LC.

In summary, we have investigated the excitation mechanism of the strong violet EL of Ge-implanted SiO_2 layers. The rise and decay time of the EL was measured and in both cases a value of about 100 μs was estimated. The electrons are injected by trap assisted tunneling and transported via traps or by the quasi-free movement within the SiO_2 conduction band. Based on the electrical and the EL transient measurements the excitation of the LC by inelastic scattering of hot electrons moving in the SiO_2 conduction band is favored. Finally, an upper limit for the excitation cross section of about $1.6x10^{-13}$ cm^2 was estimated.

Acknowledgements

We would like to thank H. Fröb as well as N. Marino and R. Kliemann for their assistance regarding the PL and EL measurements and the electronic instrumentation, respectively. The work in Catania has been supported by INFM through the project RAMSES.

This contribution has been published as L. Rebohle *et al.*, Appl. Phys. B 74, 53 (2002).

References

[1] L.S. Liao, X.M. Bao, N.S. Li, X.Q. Zheng, N.B. Min, Solid State Comm. **97** (1996), 1039

[2] X.M. Bao, T. Gao, F. Yan, S. Tong, Mat. Res. Soc. Symp. Proc. **438** (1997) 477

[3] L. Rebohle, J. von Borany, R.A. Yankov, W. Skorupa, I.E. Tyschenko, H. Fröb, K. Leo, Appl. Phys. Lett. **71** (1997) 2809

[4] L. Rebohle, J. von Borany, W. Skorupa, H. Fröb, S. Niedermeier, Appl. Phys. Lett. **77** (2000) 969

[5] L. Skuja, J. Non-Cryst. Solids **149** (1992) 77

[6] R. Tohmon, Y. Shimogaichi, H. Mizuno, Y. Ohki, K. Nagasawa, Y. Hama, Phys. Rev. Lett. **62** (1989) 1388

[7] P. Knàpek, B. Rezek, D. Muller, J.J. Grob, R. Lèvy, K. Luterovà, J. Kocka, I. Pelant: phys. stat. sol. (a) **167** (1998) R5

[8] F. Kozlowski, H.E. Porteanu, V. Petrova-Koch, F. Koch, Mat. Res. Soc. Symp. Proc. **452** (1997) 657

[9] L. Rebohle, J. von Borany, H. Fröb, W. Skorupa, Appl. Phys. B **71** (2000) 131

[10] L. Rebohle, J. von Borany, D. Borchert, H. Fröb, T. Gebel, M. Helm, W. Möller, W. Skorupa, J. Electrochem. Soc.: Electrochem. and Solid State Lett. **7** (2001) G57

[11] D. Arnold, E. Cartier, D.J. DiMaria, Phys. Rev B **49** (1994) 10278

[12] M.V. Fischetti, D.J. DiMaria, S.D. Brorson, T.N. Theis, J.R. Kirtley, Phys. Rev B **31**, (1985) 8124

[13] T. Hori, Gate Dielectrics and MOS ULSIs, Springer, Berlin (1997) p.165

Flash Lamp Annealing with Millisecond Pulses for Ultra-Shallow Boron Profiles in Silicon

T. Gebel, M. Voelskow, W. Skorupa, G. Mannino[1], V. Privitera[1], F. Priolo[2], E. Napolitani[3] and A. Carnera[3]

[1]*CNR-IMETEM, Catania, Italy*
[2]*INFM and University of Catania, Catania, Italy*
[3]*INFM and University of Padova, Padova, Italy*

Higher integration in semiconductor technology with the continuing downscaling of device dimensions into the sub-hundred nanometer range causes the need for ultra-shallow junctions [1]. Novel techniques are necessary to achieve abrupt and sharp profiles of dopants at high activation levels without significant diffusion of dopants. Two processes, low energy ion implantation and rapid thermal annealing (RTA), are currently the key processing steps for the formation of such ultra-shallow junctions [2,3].

Since boron diffuses by an interstitial mechanism, the presence of excess interstitials leads to an enhanced diffusion of boron. This transient enhanced diffusion (TED) of boron is the main problem for the formation of ultra-shallow junctions. It has been demonstrated that the coupling between silicon self-interstitials and B decreases with increasing annealing temperature, thereby reducing the driving force for TED [4]. This implies that RTA processes with high ramping rates are necessary for the formation of electrically active ultra-shallow junctions. As a result "spike annealing" procedures have been developed with ramp rates in the range of several hundred degrees per second. Although processing at high heating ramp rates can reduce TED, a very large increase in the ramp rate is required to fully minimize TED [5]. At the same time a high peak temperature is needed in order to activate the dopant. For this reason alternative methods for ultra-short time annealing are of great interest. The laser annealing has recently attracted lot of attention as it allows the melting and recrystallization of ultrathin layers leading to ultra-shallow and abrupt junctions. However, process integration is still an issue for this technique and possible solutions have to be pursued. An alternative approach for the formation of future ultra-shallow junctions is flash lamp annealing (FLA) as a technique which was developed in the beginning of the eighties [6]. Using an array of flash lamps which are ignited by a high voltage pulse it allows annealing for times in the range of 100 µs – 500 ms by using light flashes.

In this paper we report on a comparison between FLA and RTA treatment of samples implanted with boron at an energy of 500 eV using seconddary ion mass spectroscopy (SIMS) and spreading resistance profiling (SRP) analysis. Si (100) wafers were implanted at ultra-low energy (500 eV) with boron to a fluence of 10^{15} ions/cm^2. For the FLA a self-made setup was used. The apparatus consists of a system containing two heating stages, one consisting of halogen lamps for preheating of the samples from the rearside and a second one for FLA with xenon flash lamps for heating from the front side. The flash lamps are operated by means of a network of capacitors and solenoids (LC-network). A bank of 120 capacitors (200 µF each) is used for energy storage allowing to store an energy up to 0.3 MJ. By discharging of the capacitors the flash lamps are ignited. Due to the parameters of the LC-network the duration of the pulse can be tailored. In the measurements described here a pulse time of 20 ms was used. The optical spectrum of the flash lamps shows a maximum at a wavelength of about 500 nm. This is distinctly shorter than that of commonly used halogen lamps applied for RTA showing maximum light intensities at about 900-1100 nm. The maximum temperature which can be obtained with this system is 2000 °C, the maximum energy density is about 120 Jcm^{-2}. Preheating of the samples was performed at 250 °C under Argon atmosphere. FLA was carried out at temperatures in the range 1100-1300 °C in Argon. Since the temperature cannot be measured directly during the FLA process, the system was calibrated before. With FLA the final temperature is reached within 20 ms. To achieve effective soak times up to 100 ms a multiple pulse regime (up to 5 pulses, each 20 ms) was carried out. After each single pulse the preheating was switched off for 5 min and then turned on for 5 min again at a temperature of 250 °C to obtain clearly defined conditions before the next pulse. For comparison conventional RTA was performed at 1100°C and 1200°C for the shortest reliable time of 1s and longer times up to 80 s.

Following the thermal treatment the samples were investigated by SIMS and SRP. SIMS analysis was performed using a CAMECA IMS-4f. A primary low-energy O_2^+ ion beam of 1.5 keV at glancing incidence was used in order to improve the depth resolution and to reduce the equilibrium depth. SRP was carried out using an SSM-150 spreading resistance probe. In order to obtain the exact location of the starting point of the spreading resistance profiles an oxide was deposited on top of the samples. This allows the determination of the starting point of the profile due to the possible discrimination between the surface of the original sample and the bevel. Furthermore this process prevents the rounding of the bevel edge during preparation.

Fig. 1 shows the SIMS and SRP profiles after FLA at 1100 °C for 1, 2 and 5 pulses with a duration of 20 ms. After one pulse no significant enhanced diffusion of the implantation profile can be observed in the SIMS profile (Fig. 1) while after two and five pulses the dopant diffuses. In comparison the SIMS profile after RTA treatment for 1 s is much broader reaching a depth of 63 nm at a concentration of $1x10^{18}$ atoms/cm^3. The SRP profiles after FLA are comparable in depth but show with an increasing number of pulses an increase in the activated dose. For 1, 2 and 5 pulses the active dose was 3.0, 3.4 and $6.3x10^{13}$ atoms/cm^2, respectively. The RTA samples show an active dose of $1.9x10^{14}$ atoms/cm^2 but a much broader profile leading to a junction depth of 52 nm.

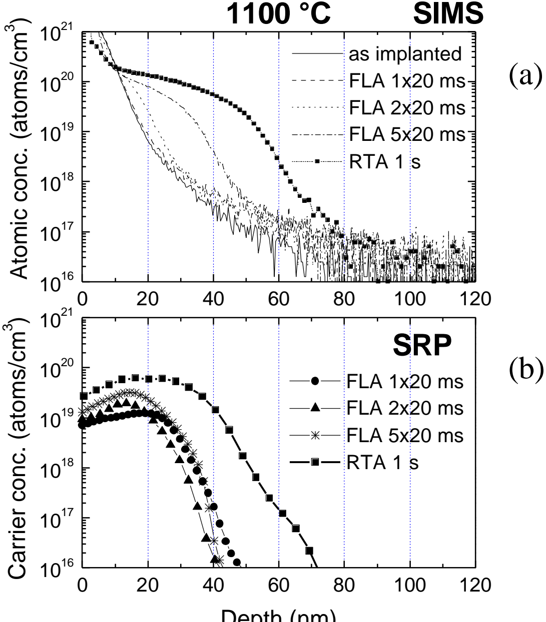

Fig. 1: The SIMS and SRP profiles of B^+ implanted ($1x10^{15}$ cm^{-2}, 500 eV) samples after FLA and RTA at 1100 °C.

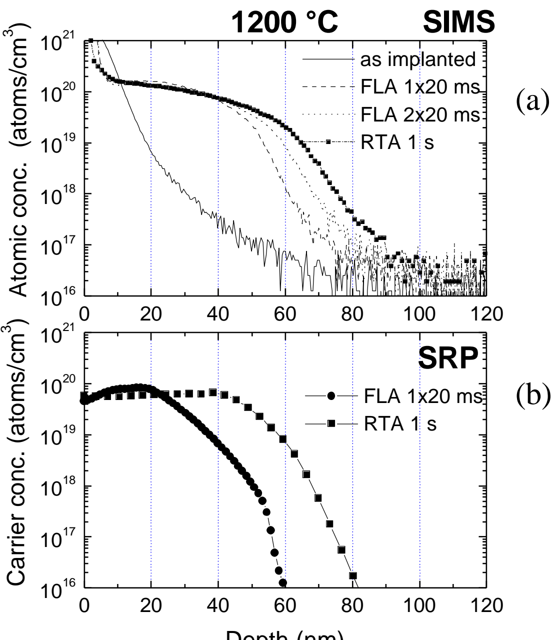

Fig. 2: The SIMS and SRP profiles of B^+ implanted ($1x10^{15}$ cm^{-2}, 500 eV) samples after FLA and RTA at 1200 °C.

In order to increase the amount of active dopant, annealing at a higher peak temperature was investigated. Fig. 2 shows the profiles after annealing at 1200 °C. The SIMS results after FLA and RTA are nearly indistinguishable up to a depth of 35 nm. However the dopant distribution in the tail region increases in depth for the longer annealing times. In comparison to the 1100 °C anneal the difference between the boron profiles following FLA and RTA becomes smaller at 1200 °C. However, the results obtained from SRP measurements suggest significant differences in the active boron between FLA and RTA: the junction depth defined at $1x10^{18}$ atoms/cm^3 is at 50 nm for FLA (20 ms) compared to 70 nm for RTA (1 s). The activated doses are $2.1x10^{14}$ atoms/cm^2 for FLA and $3.1x10^{14}$ atoms/cm^2 for RTA. This implies that FLA at such a high temperature is advantageous to RTA regarding the formation of shallow junctions.

In Fig. 3 the active dose is plotted versus the annealing time on a logarithmic scale. The data for longer annealing times (> 1 s) were obtained using RTA and furnace annealing (FA). It can be seen that all data for the different temperatures can be fitted linearly, indicating that the activation mechanism is identical [7] regardless of temperature and the annealing process. The plot for 1100 °C shows on the left hand side additional data from FLA. In good agreement with the RTA results the linear fit can be extended to these ultra short times. This result suggests that also the FLA technique shows a similar activation behavior. It has to be mentioned that for temperatures >1000 °C and

long annealing times a remarkable evaporation of B was observed (data not plotted in the graph).

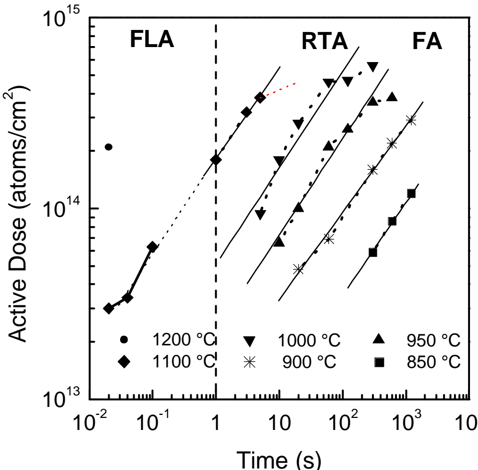

Fig. 3: The active boron dose plotted as a function of annealing time for different temperatures.

One of the most important parameters for device applications is the sheet resistance which has to be minimized. In Fig. 4 the sheet resistance is plotted vs. junction depth. The plot contains the results of the FLA and RTA experiments described in this work and also data from different spike anneals [8] for the purpose of comparison.

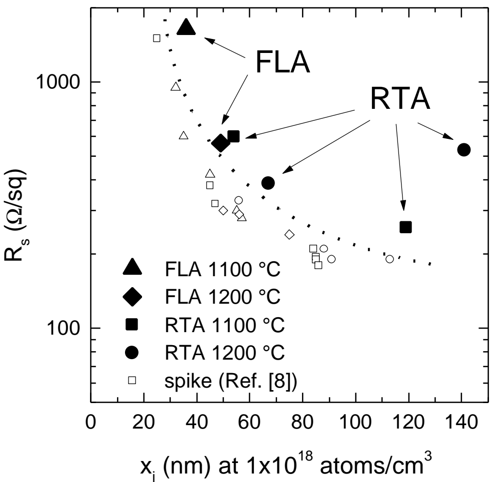

Fig. 4: The sheet resistance R_s plotted as a function of the junction depth x_j.

The dotted line is given as a guide to the eye. It can be seen that the junction depth after FLA treatment can reach values below 50 nm with sheet resistances of 1639 Ω/sq (1100 °C, 5x20 ms pulses) and 565 Ω/sq (1200 °C, 1x20 ms pulse). This suggests that a further improvement of the FLA method is required in order to increase the activated dose. Therefore new approaches by optimizing the annealing temperature and the regime for multiple flashes have to be tried. A first hint for possible improvements is given by the increasing activation with the number of flashes at 1100 °C and the strong increase at 1200 °C. In particular, the observation that active doses are similar after annealing at 1200 °C, 20 ms and 1100 °C, 1 s suggests that even shorter pulses might be of interest in this temperature regime.

In summary, the SIMS and SRP investigations of FLA treated, low energy boron implanted Si show the formation of shallow junctions at depths of 31-50 nm. The activated dose for a 1200 °C, 20 ms FLA can be up to 20 % of the implanted dose corresponding to a sheet resistance of 565 Ω/sq. These values appear promising for a method which allows a one-shot-one-wafer treatment. Further work is necessary to obtain a higher activation of the implanted boron. For future applications investigations related to the homogeneity are necessary. These investigations are strongly related to the main problem of FLA: the scaling of the apparatus for the treatment of common wafer sizes (=8”). One of the crucial problems which has to be solved is the setup of a more sophisticated highly compact energy storage system which meets the requirements for operation at pulse powers in the 10 MW range.

Acknowledgements

We wish to thank Applied Materials for providing the ultra-low energy B implants. This work has been supported in part by the Project COFIN2000, the Project MADESS II funded by CNR and the DAAD - VIGONI program.

This contribution has been published as T. Gebel *et al.*, Nucl. Instr. Meth. **B 186** (2002) 287.

References

[1] SIA International Technology Roadmap for Semiconductors, Austin, TX, 2000

[2] A.T. Fiory, K.K. Bourdelle, Appl. Phys. Lett. **74** (1999) 2658

[3] V. Privitera, E. Schroer, F. Priolo, E. Napolitani, A. Carnera, J. Appl. Phys. **88** (2000) 1299

[4] A.E. Michel, W. Rausch, P.A. Ronsheim, R.H. Kastl, Appl. Phys. Lett. **50** (1987) 416

[5] G. Mannino *et al.*, Appl. Phys. Lett. **78** (2001) 889

[6] K.K. Ushio Denki, German Patent, DE 3136105 (1981)

[7] G. Mannino, Nucl. Instr. Meth. **B 186**, (2002) 246

[8] A. Agarwal *et al.*, Mat. Res. Symp. Proc. **568** (1999) 19

A Novel Silicon Detector for Energetic Electrons with Improved Linearity Characteristics

J. von Borany, V. Beyer, D. Beyer[1], B. Schmidt and B. Schnabel[1]

[1] *LEICA Microsystems Lithography GmbH, Göschwitzer Str. 25, 07745 Jena, Germany*

Si pn-junction detectors are widely used for the detection and spectrometry of ionizing radiation, in particular of charged particles. Recently, such detectors have been also developed for the detection of electrons in modern lithography tools. To this end, a conventional pn-junction diode is covered with an additional patterned heavy metal layer which possesses well-defined windows of various dimensions in the micrometer and nanometer range (see Fig. 1) [1]. The heavy metal layer on top of the detector acts as an absorber allowing the electrons to penetrate the sensitive detector region only through these windows. From the evaluation of the detector signal arising from a scanned beam one can derive information about the properties of the incoming beam [2].

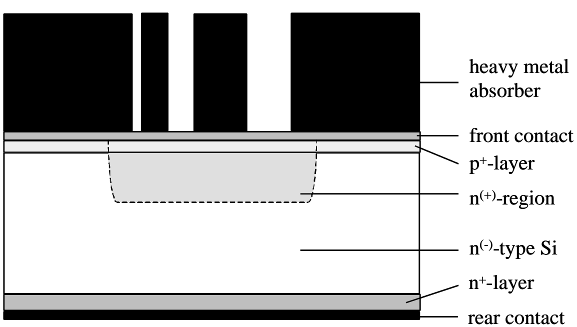

Fig. 1: Sketch of the principle structure of an electron detector used in lithography tools [1].

The requirements to lithography tools, in particular e-beam writers, are closely related to the development of the microelectronic integrated circuit technology characterized by a continuous decrease of the structure dimension and a simultaneous increase of the wafer size. Therefore, both the use of higher energies (to maintain better pattern fidelity), higher current densities (to increase the throughput) and, even more critical, tighter beam specifications become more and more important.

One main problem of Si pn-junction diodes applied for the diagnostics of intense electron beams is the nonlinearity between the incoming electron current and the detector response measured as an output voltage after external signal processing. From the physical point of view this problem is caused by the plasma effect: For electron currents of several A/cm^2 ionization leads to the formation of a nearly spherical volume with a high electron/hole (eh) concentration of 10^{17} to10^{18} eh-pairs/cm^3 (often called plasma cloud). During the characteristic plasma time (some ns) this cloud screens the external field and eh-recombination is favored. The dissolution of the plasma cloud proceeds via ambipolar diffusion leading to a reduction of the eh-density and a subsequent carrier separation by the electric field starting at the outer shell of the plasma cloud. It has been shown that a standard Si detector made from high resistivity Si (~ kΩcm) which is characterized by a triangular field distribution with a maximum field strength of 2-3 kV/cm does not enable complete eh-separation without any charge loss for the diagnostics of intense electron beams (or heavy ion detection). As in first approximation the plasma time is inverse proportional to the electric field strength an increase of the electric field is necessary to lower plasma based charge loss.

For this purpose detectors with enhanced electric field strength of about 10-20 kV/cm near the surface have been developed. By this means the linearity of the detector response considerably improves. Such a local increase of the electric field can be realized by a near-surface $n^{(+)}$-doped layer (N ~ 10^{15} cm^{-3}) formed by phosphorous ion implantation and subsequent high temperature drive-in diffusion. However, due to the small diffusion coefficient of P in Si the high field region is limited to a depth of # 3 µm which does not fulfill the requirements for the detection of electrons with E $ 30 keV. The present contribution describes a new diode design for an electron detector with high field region suitable for electron energies up to 50 keV and high current densities.

The starting consideration is derived from the ionization distribution shown in Fig. 2. The stopping power peak shifts from 1 µm to about 5.5 µm by increasing the electron energy from 20 keV to 50 keV. Furthermore, for higher energies the distribution is characterized by a larger width and a lower value of the stopping power. For E $ 30 keV the maximum of the ionization is behind the high field region of the “classical” electron detector configuration with a diffused $n^{(+)}$-layer (Fig. 1).

Thus, the electric field does not support the carrier separation in the region of high eh-density.

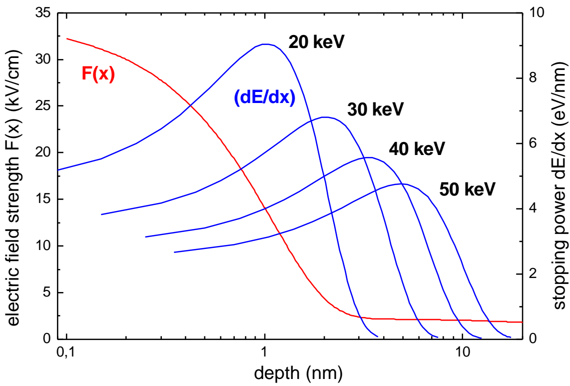

Fig. 2: Stopping power due to ionization for electrons (E = 20-50 keV) in Si. The graph also contains the electric field distribution characteristic for the present technology of pn-junction detectors with diffused $n^{(+)}$-region (implantation: ^{31}P, 50 keV, $2x10^{11}$ cm^{-2}, diffusion 1150 °C, 11 h). The high field region is limited to a depth of about 2 µm followed by a broad region with *F* # 3 kV/cm.

The new design is based on the application of a buried $n^{(+)}$-layer formed by ion implantation of ^{31}P with energies in the MeV range [3]. Assuming a depth of the high field region of 10 µm and taking into account a projected range of

$$R_p\,[\mu m] = 0.23 + \ln(E[MeV]-2.30)\,, \qquad (1)$$

(valid for E = 1-40 MeV) an energy of about 30 MeV is necessary to form a buried $n^{(+)}$-layer with a Gaussian like dopant profile in a depth of about 10 µm. With the knowledge of the dopant distribution the electric field distribution can be determined from the solution of Poisson's equation according to

$$F(N,w,x) = \frac{e}{\varepsilon\cdot\varepsilon_0}\left(\int_0^w N(x)\cdot dx - \int_0^x N(x)\cdot dx\right), \qquad (2)$$

with $N(x) = N_{Sub} + N_{II}(x)$,

where N_{Sub} and $N_{II}(x)$ denote the dopant concentration of the bulk and the implantation profile, respectively. e, ε, ε_0 are the elemental charge, the relative and absolute dielectric constant of Si, and w is the depletion depth, which can be derived in an implicit way from

$$U(w,N) = \frac{e}{\varepsilon\cdot\varepsilon_0}\left(\int_0^w x\cdot N(x)\cdot dx\right). \qquad (3)$$

Here U is the sum of the applied bias and the diffusion voltage.

As an example the field distributions of electron detectors with a buried implanted $n^{(+)}$-layer (^{31}P, 27 MeV) are shown in Fig. 3. For comparison this graph contains also the dopant distribution. From that calculation one can conclude that

(i) the extension of the high field region corresponds to the depth of the buried $n^{(+)}$-layer,

(ii) the field strength is nearly constant over that region which is significantly different to the case of high field regions resulting from diffused dopant profiles (see Fig. 2),

(iii) the electric field strength can be easily varied by choosing a proper implantation fluence. Values between 20-30 kV/cm can be realized already for an implantation fluence of about $2x10^{11}cm^{-2}$. Increasing the fluence it is possible to cover the field strength range between 30 and 60 kV/cm which is interesting for very high beam currents. It should be noted that for standard operation conditions the field strength should be limited to values < 70 kV/cm to avoid avalanche multiplication.

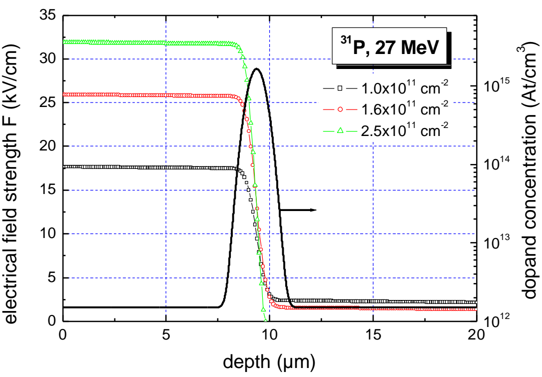

Fig. 3: Electric field distribution of pn-junction detectors with buried implanted $n^{(+)}$ layer (^{31}P, 27 MeV) determined for an constant operating voltage of 30 V which represents different values of w (115 µm, 80 µm, 9.8 µm) for implantation fluences of 1.0, 1.6 or $2.5x10^{11}$ cm^{-2}, respectively. For comparison the dopant concentration is shown on the right axis for a bulk donor concentration of 1.5x1012 cm^{-3} and an implantation fluence of $1.6x10^{11}$ cm^{-2} (annealing: 1100 °C, 30 s). For the field strength calculation complete electrical activation of the implanted dopants has been assumed.

Based on these considerations electron detectors using the novel technology have been fabricated. As the high field region is formed only at a small part of the pn-junction area implantation masks suitable for MeV ion implantation are required. The low implantation fluence allows to use thick film photoresist masks of 20 to 25 µm thickness. The fabrication of the p^+- and n^+- layers (see Fig. 1) was carried out in a conventional procedure using ion implantation of B^+ and P^+ at 50 keV with fluences of $5x10^{14}$ cm^{-2}, respectively. For annealing a combination of RTA processing at 1100 °C, 30 s and furnace annealing at 900 °C for 30 min was used. The patterned metal absorber was fabricated via sputtering, electron beam lithography and reactive ion etching in a collaboration

with the Technical University in Chemnitz and Leica Microsystems Lithography Jena.

The capacitance-voltage (*CV*) characteristics of different electron detectors and test diodes are shown in Fig. 4. In the test diodes the buried $n^{(+)}$-layer was formed across the full pn-junction area. The *CV*-characteristics of the test diodes clearly show a sharp drop in the capacitance at a certain voltage U_K which is mainly determined by the implantation fluence. This drop corresponds to the point where the space charge region (SCR) becomes larger than the depth of the buried implanted layer. Afterwards, the SCR extends very quickly with increasing voltage due to the low dopant concentration of the Si bulk material [~ 10^{12} cm^{-3}). For $U < U_K$ the SCR is limited to the depth of the buried $n^{(+)}$-layer and the electric field increases nearly linearly with the applied bias. The same behaviour is observed also for the electron detectors (see Fig. 4, lines), but as the high field region comprises only a small part of the total detector area (~ 3.5 %) this effect is much less pronounced. The evaluation of the *CV*-characteristics of the test diodes allows to determine the charge carrier concentration *N(x)* according to the well-known relations [4]

$$N(x) = -\frac{C^3(V)}{e\,\varepsilon_0\,\varepsilon_{rel}\{dC(V)/dV\}}\ , \qquad (4)$$

$$\text{and} \quad x(V) = (\varepsilon_0\,\varepsilon_{rel}\,A)/C(V)\ ,$$

where A is the pn-junction area. The corresponding field distribution can be calculated after Eq. (2).

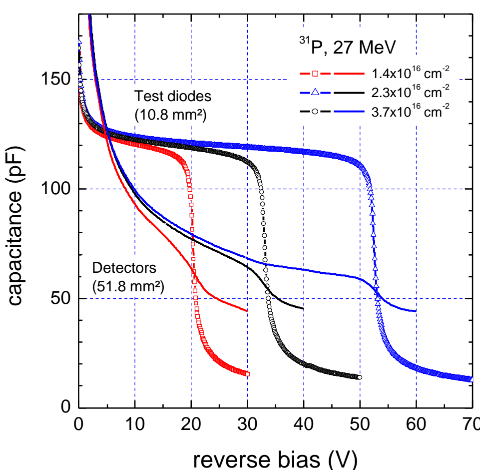

Fig. 4: Capacitance-voltage-*(CV)*-characteristics of pn-junction diodes with buried implanted $n^{(+)}$-layer (^{31}P, 27 MeV, various fluences) both for test diodes (symbols) and electron detectors (lines).

In addition, combining *CV*- and *IV* (current-voltage) characteristics the distribution of the minority carrier lifetime ***t****(x)* can be determined according to

$$\tau(x) = \frac{e\,n_i\,\varepsilon_0\,\varepsilon_{rel}\ A^2}{2}\,\frac{[\,d(1/C)/dV\,]}{(dI/dV)}\ , \qquad (5)$$

where n_i denotes the Si intrinsic carrier concentration. The evaluation of the data reveals that the minority carrier lifetime distribution follows the dopant profile with values of 10 to 50 µs and ~ 1000 µs for the implantation peak position and the Si bulk material, respectively. These relatively large values are a clear indication for a good annealing of the damage due to the MeV implant. This is important to note, as electron ionization also occurs also in the depth of the MeV implant (see Fig. 2) and the probability for eh-recombination is directly related to the minority carrier lifetime. Typical reverse currents I_r of 5-10 nA for the preferred operating bias of 30 V were measured which is one order of magnitude lower than the current level of detectors with high-field regions based on diffused $n^{(+)}$-layers. This is attributed to r the considerable decrease of the thermal budget which keeps ***t*** of the Si bulk material nearly unchanged (***t*** ~ 1 ms and I_r ~ 1/***t***).

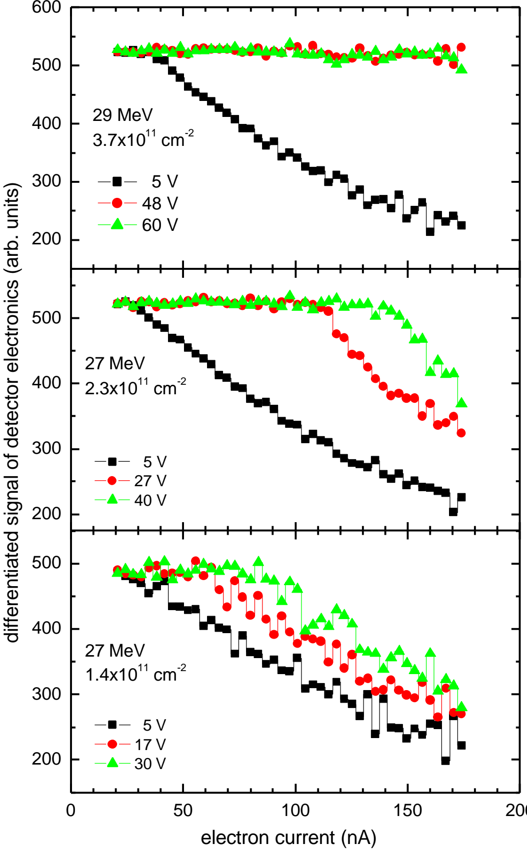

Fig. 5: Linearity behaviour of electron detectors with buried implanted $n^{(+)}$-layer. For a better clarity the differentiated output voltage (dU_{Out}/dI_e) is plotted. A constant value stands for a linear relation between output voltage and electron current; a decrease indicates carrier recombination inside the plasma cloud.

Fig. 5 shows the results of the investigation to the linearity range of the detectors. The measurements were performed with electrons of 50 keV energy using different incident electron currents. It is important to note that in any case the beam spot area (A # 2 µm^2) is small in comparison to the extension of the nearly spherical ionization region which corresponds to the size of the eh-plasma cloud. The graphs reveal a clear dependence of the linearity range on the implantation fluence and the applied voltage. Both parameters determine the electric field strength in the high field region as can be derived from Eqs. (2),(3). The linearity range extends with the implantation fluence and with increasing detector bias. For the highest fluence of 3.5x10^{11} cm^{-2} investigated in our experiments a linearity range up to 200 nA has been achieved. If the linearity range is plotted versus the electric field strength a linear correlation is obtained (Fig. 6). This behaviour agrees with the assumption that deviations from the linearity are caused by charge loss due to plasma related recombination which is in first order inversely proportional to the electric field strength [5, 6].

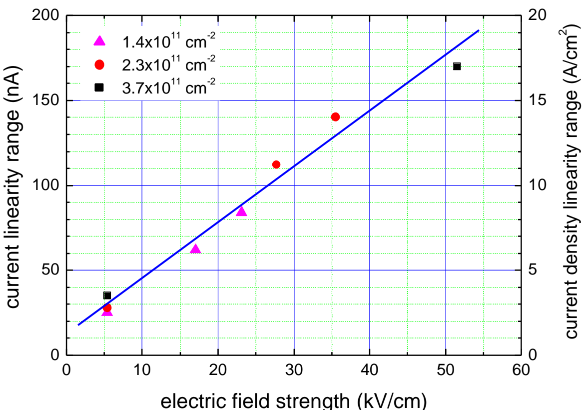

Fig. 6: Dependence of the linearity range of the electron detectors on the electric field strength in the high field region. The different points for each implantation fluence represent different detector bias values. The estimated linearity range for the current density (right axis) is only valid, if the electron spot size is small in comparison to the diameter of the ionization volume.

In summary, it has been shown that pn-junction detectors with a high electric field strength of 10 to 50 kV/cm and a constant electric field distribution up to a depth of about 10 µm can be realized via MeV ion implantation which creates a buried n$^{(+)}$-doped layer. Based on this technology detectors with considerably improved linearity for electrons of 50 keV and current densities up to 20 A/cm^2 have been fabricated.

Acknowledgements

The authors wish to thank I. Beatus, H. Felsmann, B. Scheumann (FZR) and Dr. A. Bertz (TU Chemnitz) involved in the preparation of the electron detectors. The high-energy implantation was performed at the 5 MV Tandem accelerator of the FZR. The support of the accelerator operating group leaded by Dr. M. Friedrich is gratefully acknowledged. The work was supported by the Bundesministerium für Forschung und Bildung.

References

[1] H.J. Döring, M. Deutscher, H. Elsner; Halbleitersperrschichtdetektor, Patent DD 225 824

[2] M. Deutscher, Ein Justierdetektor für Elektronenformstrahlen, Habilitationsschrift, Teil D, AdW der DDR, 1989

[3] J. von Borany, B. Schmidt, R. Grötzschel, Nucl. Instr. Meth. **A 377** (1996) 514

[4] P. Blood, J.W. Orton, The Electrical Characterization of Semiconductors, Academic Press 1992, ISBN 0-12-528627-9, pp. 220 ff.

[5] W. Seibt, K.E. Lundström, P.A. Tove, Nucl. Instr. Meth. **113** (1973) 317

[6] E.C. Finch, M. Ashger, M. Forte, Nucl. Instr. Meth. **163** (1979) 467

Short Contributions

Thin Films

B. Fritsche
T. Chevolleau
J. Kourtev[1]
A. Kolitsch

Plasma diagnostic of an RF magnetron Ar/N_2 discharge

For the characterization of an unbalanced RF magnetron Ar/N_2 discharge used for cBN thin film deposition, Langmuir probe measurement and energy selective mass spectrometry were carried out at the sample position. RF power and total pressure were varied from 50 to 300 W and from 0.1 to 0.5 Pa, respectively, for different Ar/N_2 mixtures. The main neutral species are Ar and N_2. Concerning contamination, only water from the wall of the chamber is detected, whereas other contamination species are below the detection limit of the mass spectrometer. Main ionic species are found to be Ar^+ and N_2^+ with a very low fraction of N^+. The ion density increases with RF power, pressure and Ar content. The magnetic confinement of the plasma becomes visible in the decrease of the measured ion density when the Langmuir probe is removed stepwise from the center of the discharge. The ion energy distribution consists of one single narrow peak with full width at half maximum of a few eV.

Supported by DFG

Collaboration: [1]Bulgarian Academy of Science, Institute of Electronics

B. Fritsche
U. Kreissig

Growth rate and stoichiometry of rf magnetron sputtered boron nitride layers

Magnetron sputtering from a hBN target was employed to deposit boron nitride layers. To determine the arrival rate of the film forming atoms, layers have been deposited in pure Ar atmosphere without substrate bias. Different rf powers were applied, all other conditions were kept constant. The growth rate was monitored by in-situ ellipsometry and the films were investigated with ERDA. From the area density of boron and nitrogen atoms the atom arrival rate was calculated assuming a sticking coefficient of 1. Using the film thickness, obtained by ellipsometry the density of the films could be calculated. Under the given deposition conditions, the films are boron rich (B/N = 1.5) and have a lower density than bulk material (≅ 1.8 g/cm^3). Energy resolved mass spectrometry measurements showed that some part of the nitrogen from the BN sputter target is lost to the plasma by recombination of N. Therefore, films deposited without additional nitrogen in the source gas are boron rich. Together with ion density measurement by Langmuir probe, the ion/atom arrival rate at the growing film surface can be calculated (I/A ≅ 1). ERDA revealed high H and O contents in the films (> 5 at% O).

Supported by DFG

V. Linß[1]
U. Kreissig

Study of compositional, structural and mechanical properties of BCN layers produced by reactive dc magnetron sputtering

Within the triangle B-C-N some materials with exceptional mechanical, electrical and optical properties were found, like e.g. diamond, c-BN, DLC or B_4C. Recently efforts were made to combine all of these elements to produce thin layers with superior properties. Layers of the full ternary system B-C-N with thicknesses in the range of 800 – 2000 nm were deposited on silicon by reactive dc magnetron sputtering. In order to vary the B/C ratio different sputter targets like BC_4, BC and B_4C as well as pure boron and carbon targets were used. To add on nitrogen the sputtering process occured in a reactive atmosphere consisting of a N_2/Ar mixture with a total pressure of 0.46 Pa. The substrate potential was floating or fixed between 100 and 400 V to study the influence of ion energy on the layer growth. The elemental compositions of the layers were determined by ERDA using 35 MeV Cl^{7+} ions. The mechanical properties of the layers were characterized by determination of hardness and Young´s modulus and their bonding characteristics by FTIR measurements. For substrate temperatures up to 100 °C the B/C ratio of the sputter target is reproduced in the layer and the N-content increases linearly with the N_2/Ar

ratio. At higher temperatures the formation of volatile CN-compounds obviously leads to boron rich layers. By adjusting the composition of the layers their mechanical properties can be varied by a factor of three, whereas the ion bombardment leads to a variation by a factor of two.

Supported by BMBF

Collaboration: [1]Institut für Physik, Technische Universität Chemnitz

R. Gago
U. Kreissig
I. Jimenez[1]
J.M. Albella[1]

Studies of carbon incorporation in ternary boron-carbon-nitrogen thin films by ERDA and XANES

By means of ERDA the incorporation of carbon in ternary cubic and hexagonal boron-carbon-nitrogen (BCN) layers was studied. The films were prepared by IBAD, combining e-beam evaporation of B_4C and ion assistance with N_2/Ar. The carbon content was increased by adding small amount of CH_4 (< 10 %) to the gas mixture. The bonding structure of the resulting BCN films was determined by X-Ray Absorption Near Edge Spectroscopy (XANES) at the SSRL synchrotron facility. The results show that without the use of CH_4 the carbon content is limited to ~15 at% and ~5 at% for the hexagonal and cubic BCN arrangements, respectively. Despite the use of CH_4, the hydrogen content is always below 5 at% since the substrate temperature during deposition was 500 °C. Regarding the hexagonal arrangement, the carbon content can be increased above 30 at% while keeping the bonding structure. However, the cubic structure is disrupted with a small increase on the carbon content above ~5 at%, evolving towards a hexagonal structure. In order to introduce more carbon atoms in the cubic arrangement, the key condition seems to rely on being able to keep constant the B/N ratio in the composition as the carbon content is increased.

Collaboration: [1]Material Science Institute of Madrid (CSIC), Madrid (Spanien)

S. Mukherjee
F. Prokert
H. Reuther
E. Richter
W. Möller

Compressive stress, preferred orientation and film composition in Ti based coatings deposited by PIIIAD

Plasma immersion ion implantation assisted deposition (PIIIAD from a filtered cathodic arc plasma has been employed to develop Ti based coatings in the presence or absence of a reactive nitrogen environment. For TiN coatings on Al alloys it has been observed that a large compressive stress develops in the coating which can be reduced by increasing the negative substrate bias (up to 4 kV), keeping the deposition temperature constant. Simultaneously the preferred orientation of TiN planes parallel to the substrate surface changes from (111) to (200) and also the hardness reduces. The formation of stress is attributed to the atomic peening effect which densifies a coating, whereas thermal spikes generated at high substrate bias reduces the stress. At higher substrate bias (200) preferred orientation results from minimum surface energy conditions. The results indicate that there is an effective bias which determines the stress when the film is grown under pulsed substrate bias conditions. Using a TiAl cathode,the Al content in the coating decreases as the negative substrate bias increases (up to 2 kV). This result is reproduced by TRIDYN computer simulations confirming the effect of preferential sputtering of Al when sputtering becomes significant at higher ion energy. Therefore, the substrate bias can be used as an additional tool to control the film composition.

Supported by AvH

J. Neidhardt[1]
B. Fritsche
R. Gago

CN-compounds in a dc magnetron Ar/N_2 discharge sputtering from a carbon target

A dc magnetron Ar/N_2 discharge for the deposition of fullerene-like CN_x films has been investigated by means of energy resolved mass spectrometry. A carbon sputter target was used, the source gas composition was varied from pure Ar to pure nitrogen over some intermediate compositions. Major contributions to the ionic composition are Ar^+, N_2^+ and N^+ coming from the source gases. Beside these, a variety of ionic species is found including C^+, C^{2+}, CN^+,

C_2N^+ but also CNO^+ and especially $C_2N_2^+$. The presence of $C_2N_2^+$ is observed even at very low nitrogen concentration. It is shown that $C_2N_2^+$ forms at the surface of the sputter target whereas the CN^+ appears to form in the gas phase. $C_2N_2^+$ may play an important role in the growth of fullerene-like structures by providing nucleation sites.

Supported by EU

Collaboration: [1]University of Linköping

M. Peikert
R.P. Bhandari
E. Wieser
Ch. Wenzel[1]
A. Mücklich
H. Reuther

Modification of thin Ta layers by Si^+ ion implantation

To improve their barrier properties against Cu diffusion, 40 nm Ta layers deposited on oxidized Si were amorphized by implantation of 25 keV Si^+. Fluences of $5 \cdot 10^{16}$ and $8 \cdot 10^{16}$ Si/cm^2, respectively, result in a Si content in the Ta films of about 20 and 30 at%, respectively, with a weak depth dependence. The obtained amorphous structure is stable against annealing up to 950 °C while the non-implanted layer reacts strongly already at 900 °C with the SiO_2 substrate and residual oxygen in the ambient. 50 nm Ta films deposited on (100) Si were implanted with 120 keV Si^+ in order to study the influence of interface mixing on the contact resistivity. For $1 \cdot 10^{16}$ Si/cm^2 18 nm of the Ta layer adjacent to the interface as well as the interface region of the Si substrate become amorphous. Si recrystallization is observed after annealing at 600 °C / 1h. From the amorphous Ta only a 10 nm layer in contact with Si becomes nanocrystalline.

Supported by Sächsische Aufbau-bank GmbH

Collaboration: [1]TU Dresden, Institut für Halbleiter- und Mikrosystemtechnik

T. Ujvari[1]
A. Kolitsch
A. Toth[1]
M. Mohai[1]
I. Bertoti[1]

XPS characterisation of the composition and bonding states of elements in CN_x layers prepared by IBAD

CN_x layers were grown on polished Si(100) wafers by ion beam assisted deposition at temperatures varying between 200 and 600 °C. A Kaufman type ion source fed by Ar and N_2 was applied together with an e-beam heated evaporation source of graphite for the deposition of the CN_x layers. The composition and chemical bonding state of elements were studied by XPS. The N-content varied in the range of 8-16 at% and decreases with increasing deposition temperature. The broad C1s and N1s XPS lines manifest several bonding states. The relative intensities of the component peaks vary with the preparation conditions. The two main components of the N1s peak situated at binding energies of 398.2 eV and 400.6 eV are assigned to sp^2 (C-N = C) and sp^3 (N-C) type bonding states, respectively. The stability of the sp^3 states was higher than that of the sp^2 ones, because the intensity of the 398.2 eV component decreases preferentially with increasing deposition temperature. A post-deposition treatment with low energy N_2^+ ion bombardment resulted in a significant increase in the overall N-content on the surface, with a preferential increase in the concentration of sp^2 type nitrogen.

Supported by EU

Collaboration: [1]Hungarian Academy of Sciences Budapest, Research Laboratory of Materials and Environmental Chemistry, Hungary

E. Wieser
E. S. Vlakhov[1]
K. A. Nenkov[2]
R. Grötzschel
K. Doerr[2]

Effect of ^{56}Fe- and ^{58}Ni-ion implantation on the magnetoresistance of $La_{0.7}Sr_{0.3}MnO_3$ thin films

$La_{0.7}Sr_{0.3}MnO_3$ is of high interest because of its extremly large negative magnetoresitivity (MR) near the Curie temperature where also a transition from semiconducting to metallic conductivity occurs. Implantation of Fe and Ni with increasing fluence leads to an increase of resistivity and a decrease of the temperature corresponding to the maximum MR. Whereas this maximum occurs at about 360 K for the as-deposited films, the MR at 300 K, as a parameter important for potential applications, can be enhanced by implantation. The transition to insulator- or semiconductor-like behaviour observed at low temperatures for medium and higher fluences, respectively, is strongly indicative for the coexistence of ferromagnetic metallic and antiferromagnetic

or spin-canted insulating regions where the current is realized by percolative transport between ferromagnetic metallic clusters.

Supported by DFG

Collaboration: [1]Institute of Solid State Physics, Bulgarian Academy of Sciences, Sofia, Bulgaria, [2]Institut für Festkörper- und Werkstoffforschung Dresden

A. Belov

Atomic scale calculations of elastic constants in amorphous carbon

Atomic calculations, based on empirical potentials and the method of homogeneous deformation, were performed to study the effect of intrinsic stresses on the elastic properties of as-deposited amorphous carbon at 0 K. The method employed takes into account anharmonicity of all orders. Several structural models of amorphous carbon generated by a realistic molecular-dynamics simulation of ion-beam deposition were investigated. The models are shown to yield intrinsic compressive stresses of approximately 10 GPa, typical of as-deposited (not annealed) tetrahedral amorphous carbon films. The dependence of the second-order elastic constants of amorphous carbon on the intrinsic stress as well as on hydrostatic pressure was examined. Different sets of elastic constants describing the behavior of a solid under stress were considered. The nonlinear effects are shown to become appreciable at a pressure of 10 GPa, whereas the difference between the elastic constants measured by acoustic methods and the Lagrangian elastic constants is not large.

Supported by DFG

H.U. Jäger

Understanding of ta-C film deposition by means of atomistic simulations

Ion beam deposition of carbon films was studied by molecular-dynamics simulations. Using an analytic hydrocarbon potential of Brenner with an increased C-C interaction cutoff value, deposition of films with a thickness of up to 10 nm was computed for ion energies E_{ion} = 10 - 80 eV, and for substrate temperatures ranging from 100 to 900 K. The following properties of the calculated films were analyzed: (i) sp^3 content versus mass density in inner film regions, (ii) binding energies of 3- and 4-fold coordinated carbon atoms in films of different mass densities, (iii) probability distributions for the number of sp^3-bonded atoms generated (or annihilated) per deposited ion, and (iv) structure and width of the graphite-like surface regions. As a result, an atomistic picture is provided which shows how the formation of tetrahedral amorphous carbon (ta-C) films is influenced by both ion energy and substrate temperature.

Supported by DFG

P. Neumaier[1]
G. Dollinger[1]
A. Bergmaier[1]
C. Ronning[2]
H. Hofsäss[2]
H.U. Jäger

Range distributions of low energy carbon ions in tetrahedral amorphous carbon

Range distributions of C^+ ions which are of relevance to the deposition process of tetrahedral amorphous carbon (ta-C) films were studied experimentally and theoretically. The ta-C samples that have been specially designed for this analysis, were grown by mass-selected ion-beam deposition. Initially about 12 nm ^{12}C were deposited with a defined ion energy E_{ion} ranging from 12 to 92 eV. In a subsequent step, about $5 \cdot 10^{14}$ at/cm^2 ^{13}C were deposited with the same energy. The ^{13}C depth profiles of the resultant films were measured by high-resolution ERDA with single monolayer depth resolution, using the Q3Dmagnetic spectrograph of the Munich tandem accelerator. For the same deposition conditions, theoretical ^{13}C depth profiles were calculated, using classical molecular dynamics and a slightly modified hydrocarbon potential of Brenner. Excellent agreement is obtained.

Supported by DFG

Collaboration: [1]Technische Universität München, Physik Department E12, Germany; [2]Universität Göttingen, II. Physikalisches Institut, Germany

Low Energy Implantation / PIII

U. Hornauer
G. Laudien
R. Günzel
E. Richter
E. Wieser
A. Donchev
M. Schütze[1]

Improvement of the high temperature oxidation behavior of TiAl alloys by Cl -PIII

Extensive improvements of the PIII set-up were carried out to enable the use of PIII of chlorine for the improvement of the high temperature oxidation of titanium aluminides. The gas supply system was changed to a corrosion resistant one. A pulsing system was installed in order to get a better pulse rise time of the high voltage pulse above 10 kV. The maximum current in the pulse was extended from 4 A to 32 A to increase the area which can be treated. Different plasma sources were tested and optimized. A quartz insulated transformer coupled antenna with two coils was installed. Using this antenna a plasma density up to $3x10^{10}$ cm^{-3} was achieved. By systematic studies of plasma density, plasma potential and the contribution of Cl^- ions in dependence on gas composition (Ar:Cl) and RF power, respectively, the process conditions were optimized. Following successful experiments with conventional low energy implantation into the technically important alloys γ-Met and γ-Tab, a significantly reduced oxidation rate at 900 °C in air was obtained by PIII of Cl into γ-Met, too.

Supported by AiF

Collaboration: [1]Karl-Winnacker-Institut der DECHEMA e.V., Frankfurt a.M.

A. Rogozin
E. Richter
V.T. Astrelin[1]

Integrated high voltage modulator for plasma immersion ion implantation (PIII) with an RF plasma

The high voltage plasma based modulator for PIII was further developed for us with a RF plasma. The modulator is placed into the vacuum chamber of the PIII device and produces high voltage pulses using grid controlled extraction of electrons from the same plasma, which is also used for the implantation. The operation features of the modulator in application with an RF-plasma were investigated. The modulator was applied to nitrogen implantation of stainless steel. The results indicate significant hardness improvements which confirm the practical use of high voltage modulator.

Collaboration: [1]Institute of Nuclear Physics Novosibirsk, Siberian Academy of Sciences, Russia

A. Rogozin
V.T. Astrelin[1]

Focusing of an electron beam extracted from the plasma to a metallic anode

Focusing of an electron beam extracted from the plasma to a metallic anode in axi-symmetric triode geometry was investigated experimentally. The electron beam was extracted through a controlling grid arranged on a cylindrical focusing electrode. The pulsed beam extraction was controlled by the bias voltage applied to the grid. After extraction the focused beam enters the anode. If the duration of the beam pulse exceeds a limit which is determined by the anode material, a considerable increase of the extracted beam current and improved beam focusing were observed. A physical model of this phenomenon was developed assuming an influence of the anode plasma on the extraction and focusing of the electron beam. Numerical simulation based on this model qualitatively confirms the experimental results.

Collaboration: [1]Institute of Nuclear Physics Novosibirsk, Siberian Academy of Sciences, Russia

T. Telbizova
F. Prokert
E. Richter
W. Möller

Characterization of nitride layers obtained by ion nitriding of Al

Ion nitriding of pure Al was performed by a hot filament ion source (Kaufman type) at an ion energy of 1.6 keV, a current density of 0.2 mA/cm^2, and a substrate temperature of 400 °C for nitriding times increasing from 5 min to 60 min. The obtained nitride layers were characterized in terms of composition, phase formation, structure and atomic density. Analytical methods as NRA,

ERDA, SEM and XRD at grazing incidence were applied. The obtained results show that the layers have a composition close to stoichiometric AlN, with very low contamination of oxygen (less than 2 at%). The main crystallographic phase formed is hexagonal AlN, with a small admixture of cubic AlN. The nitride layers are polycrystalline, with the average size of the crystallites weakly increasing from 4 nm to 10 nm with increasing the nitriding time. The atomic density of the nitride layers is determined to be $7.5 \cdot 10^{22}$ at/cm^3, which is about 20 % lower than the standard density of AlN bulk material.

T. Telbizova
E. Richter
W. Möller

Growth kinetics of nitride layer formed by ion nitriding of Al and $AlMg_{4.5}Mn$ alloy

The growth kinetics of nitride layer formed by ion nitriding of pure Al and $AlMg_{4.5}Mn$ alloy was investigated and compared. The ion nitriding was performed at an ion energy of 1.6 keV, a current density of 0.2 mA/cm^2, a substrate temperature of 400 °C and nitriding times from 5 min up to 4 h. NRA and AES were applied for determination of the layer thickness. SEM was used to study the surface morphology. For nitriding times shorter than 80 min both materials show similar nitriding kinetics where the nitride layer thickness grows linearly with time. For longer nitriding times a difference is observed. The nitride layers formed by ion nitriding of $AlMg_{4.5}Mn$ continue to grow linearly with time, so that a thickness of 4 µm is achieved after 4 h. In contrast, the layers produced by ion nitriding of Al have a limited layer thickness of about 1 µm obtained after nitriding during 80 min. These findings are correlated with different surface morphologies. Ion nitriding of Al results in formation of cracks and flaking, whereas the layers grown on$AlMg_{4.5}Mn$ are more continuous, consisting of macroscopic nitride particles, which are homogeneously distributed over the surface.

Biotechnological Materials

I. Zyganov
E. Wieser
A. Rogozin
M. Maitz
F. Prokert
E. Richter

Structure of TiO_{2-x} layers prepared by metal plasma immersion ion implantation and deposition (MPIIID)

Coating with TiO_{2-x} is a promising method to improve the blood compatibility of materials to be used for medical implants. TiO_{2-x} layers were deposited on oxidized Si using MPIIID from a plasma produced by cathodic arc evaporation (arc current 110 A) under addition of oxygen to the ambient near the substrate. The influence of the deposition parameters on the microstructure of these films was studied. Without negative bias amorphous and nanocrystalline structures are formed for high (180 sccm) and low (60 sccm) oxygen flow rate F, respectively. The crystalline phases formed with a negative bias of 2.5 kV are strongly dependent on F. High F results in dominating rutile contaminated by anatase. For low F a mixture of anatase and brookite is observed. Enhanced substrate temperature leads to better crystallization. Amorphous and nanocrystalline layers show higher blood clotting times than well-crystallized rutile films.

Supported by DAAD and INTAS

M.V. Vinnichenko[1]
M. Maitz
M.T. Pham
T. Chevolleau

Stainless steel corrosion behaviour in biological media probed by in-situ ellipsometry and AFM

The surface modification of austenitic stainless steel 304 and 316 L due to potentiodynamic corrosion tests has been studied. The current-voltage measurements were carried out in a specially designed cell that also permitted in-situ ellipsometric probing of the sample surface. Potentiodynamic tests were performed in phosphate buffered saline (PBS) and Dulbecco’s Modified Minimal Essential Medium (DMEM) at pH 7.4. After the corrosion tests the sample surfaces were studied by means of optical microscopy and AFM. The 316 L steel shows a higher corrosion potential and lower corrosion current in PBS than in DMEM. The 304 steel exhibits the opposite tendency. Ellipsometry is more sensitive than potentiodynamics to surface modification in the cathodic range. In the case of PBS and DMEM layers with different optical constants were formed. For potentiodynamics in DMEM removal of a surface layer in the first 2 min with further repassivation is characteristic while in PBS the surface layer starts to grow within first few seconds. This layer was observed for all samples after PBS by AFM. More abrupt changes of ellipsometric parameters with time were observed at lower corrosion current for each stainless steel grade.

Supported by DAAD

Collaboration: [1]Faculty of Physics, Kyiv Taras ShevchenkoUniversity, Ukraina

M.V. Vinnichenko[1]
M. Maitz
M.T. Pham
T. Chevolleau

Investigation of stainless steel surface modification in growing cell cultures

The surface alteration of materials in biological systems is an important problem in implantology. The modification of austenitic stainless steel 316L due to incubation in growing cell cultures (L929, polymorphonuclear neutrophils, SAOS-2) and cell culture media (DMEM and α-MEM) as control has been studied. The modified surfaces were probed in comparison with untreated ones by means of SE, XPS and AFM. Migration of Ni into the adsorbed layer was observed in all cases for samples after cell culture exposure. The protein layer thickness was ellipsometrically determined to be within 2.5 - 6.0 nm for all treated samples with parameterization of its optical constants in Cauchy approach. The study shows that for such biological treatments of stainless steel the protein adsorption is the dominating process in the first two weeks, which could play a role in the process of corrosion by the formation of complexes with metal ions.

Supported by DAAD

Collaboration: [1]Faculty of Physics, Kyiv Taras ShevchenkoUniversity, Ukraina

M. Maitz
S. Mukherjee
M.T. Pham

Reaction of bone forming cells to Ti based coatings deposited by plasma immersion ion implantation assisted deposition technique

Ti based coatings have been produced by plasma immersion ion implantation assisted deposition (PIIIAD) on stainless steel. The coatings deposited are Ti, TiAl, TiN and $Ti_{1-x}Al_xN$, where the value of x can be adjusted between 0 and 0.5 by adjusting the substrate bias. The coatings with nitrogen exhibit good mechanical properties. In order to investigate their suitability for medical implants the adherence of rat bone marrow cells as osteoblast progenitor cells to these was investigated in correlation with the deposition parameters and the surface morphology. The coatings were deposited at different bias voltages of 0 V, -1 kV and –2 kV. Apart from improving the adhesion between the coating and the stainless steel substrate, the bias can also be used to manipulate the surface roughness which is in the range of 10 – 80 nm. Rat bone marrow cells at the first passage were seeded out on the samples without serum, allowed to adhere for 5 hours, fixed with formaldehyde, fluorescent stained for the adhesion protein vinculin, and the cytoskeleton protein actin. The nuclei were couterstained with DAPI (4',6-Diamidino-2-phenylindole) There has been a good spreading of the cells and organisation of the cytoskeleton on Ti and coating; in general on the smoother samples produced with lower bias voltage the cell adhesion has been better than on the more rough samples. There have been no signs of necrotic cell death but a high rate (5 to 25 %) of pyknotic, fragmented nuclei has been found as hint for apoptotic cell death. This rate has been different for the different substrates, but there is no correlation to surface chemistry or surface structure. By the use of serum containing medium no more signs of apoptosis were found, also the cell adherence and spreading on the surface was nearly the same on all coatings. This indicates that apoptosis was mainly due to the lack of growth factors. Adsorbed plasma proteins mediate the first cell adherence and minimize the specific effect of the surface.

Supported by AvH

V. Romanova[1]
A. Kondyurin[2]
M. Maitz

FT-Raman and FTIR investigations of crosslinked polyurethaneurea films synthesised from solutions

Crosslinked polyurethaneurea films are intended to use as coatings of medical devices because of the good biocompatibility and mechanical properties. Polyurethaneureas based on polyoxitetramethylenglycol and polyoxipropyleneglycol with toluenediisocyanate and 3,3'-dichlor, 4,4'-diaminediphenylmethane have been synthesized in a solution with ethylacetate, acetone or methylethylketone as solvent. Intermolecular force constants of hydrogen bonds were calculated from FT-Raman and FTIR spectra. It is shown that these solvents modify the structure of the polymer during the polymerisation. Ethylacetate favors the formation of hydrogen bonds in the polyurethaneurea, whereas acetone and methylethylketone support the formation of the hard domains. By PIII using nitrogen ions further carbonisation is induced, and the polymer is made more resistant to biodegradation.

Supported by WTZ

Collaboration: [1]Natural Scientific Institute, Perm State University; [2]Institute of Technical Chemistry Perm, Russian Academy of Sciences, Russia

M.T. Pham
M. Maitz
H. Reuther
W. Matz
G. Steiner[1]

Biomolecules tethered to titanium surfaces

To promote interactions with bone-forming cells Ti surfaces were coated with extracellular matrix (ECM) proteins. The ECM proteins are known as ligands in reactions with cell surface receptors involved in bone physiology. The osteoblast-like cell line SAOS-2 was allowed to synthesize and assemble its own ECM on Ti substrates under standard cell culture conditions. Cells were then selectively removed resulting in Ti surfaces coated with a thin film of ECM (ECM-Ti). Studies by SEM, AFM, Imunofluorescence, XRD, and FTIR revealed surface features in sub-µm thickness containing ECM-characteristic components and structures. The responses of SAOS-2 cells to ECM-Ti were

examined and compared with those to the specific protein fibronectin FN and the adhesive peptide sequence RGDS covalently coupled to Ti. ECM-Ti was demonstrated to trigger native cell behavior by positively promoting cell attachment and spreading, while FN- and RGDS-Ti exhibited much lower bioactivity. A reason is seen in the complex structure of the ECM that cannot be simulated with single proteins and peptides.

Collaboration: [1]Institut für Analytische Chemie, Technische Universität Dresden

Ion Beam Analysis

C. Klein
R. Grötzschel
M. Mäder

Charge state distributions (CSD) of heavy ions after a close collision with Au atoms

Magnetic analyzers used in high-resolution RBS separate ions of equal energy but different charge. In the case of near surface scattering the charge state distribution of the emerging ions can deviate significantly from the equilibrium distribution. To convert the energy spectra into depth profiles the knowledge of the CSD of the emerging ions as a function of depth is necessary. For the analysis of very thin surface films CSD's resulting from a single collision of the primary ion with the target atom are very important. Therefore distributions for Li, C and F ions scattered under single collision conditions at Au atoms were measured at energies below 500 keV/amu. To this end sub-monolayers of Au were deposited onto a clean Si sample in a UHV scattering chamber. The measured distributions were compared with those resulting from scattering at thick targets, where the CSD is expected to be in equilibrium. It is found that the equilibrium mean charge state for Li ions is smaller than the mean charge state resulting from a single collision. For C and F ions the opposite behavior is observed. While the difference is very small for C ions it is pronounced for F ions where the corresponding distributions are shifted by about one charge unit. For Li and C ions the difference between mean equilibrium charge state and the mean charge state after a single collision is almost constant in the energy range considered. For F ions a slight decrease at higher energies is found. In conclusion the trend of an increasing difference between equilibrium and single collision charge state distributions with increasing nuclear charge presumed earlier could be corroborated.

C. Klein
R. Grötzschel
M. Mäder
A. Mücklich

Investigation of X-ray mirrors using high resolution RBS

The applicability of high resolution RBS (HRBS) with heavy ions for the investigation of thin films with thicknesses in the nanometer range was demonstrated at the Rossendorf Browne-Buechner-Spectrometer. To this end two different X-ray mirrors with nominal layer stack sequences of 50× (4.1 nm Si/2.74 nm Mo) and 30× (2.33 nm B_4C/1.9 nm Mo), respectively were analyzed with 2 MeV C-ions at a scattering angle of 35.5°. For both samples the first five Mo layers were analyzed and could be well resolved. In the case of the (B_4C/Mo) mirror a comparison of spectra taken at incident angles of 5° and 17.5° revealed a width of the first Mo-B_4C-interface of about 0.5 nm. The depth resolution obtained for deeper interfaces is limited by straggling and multiple scattering. In the case of the (Si/Mo) mirror the Si-Mo-interface (where Si is deposited on Mo) was found to be sharper than the Mo-Si-interface. These findings are in good agreement with TEM-measurements of the same samples which show a sharp interface for the (Mo/B_4C)-mirror and the formation of a intermixed layers for the (Mo/Si)-mirror. A calculation of the depth resolution reveals that heavy ions are especially useful for the investigation of very thin layers with a thickness of a few nanometers, whereas the resolution decreases faster with increasing depth than for lighter ions.

T. Wang[1]
U. Kreissig
D. Grambole
R. Grötzschel
F. Herrmann

Enhancement of the titanium surface oxidation resistance by hydrogen ion implantation

The influence of surface-near titanium hydride on the oxidation behavior of a special titanium alloy Ti225 was studied. The hydride-rich surface-near layers were formed by hydrogen ion implantation at room temperature using H_2^+ molecular ions at 25 keV/amu. The fluence was varied from $2{\cdot}10^{15}$ H/cm^2 to $6{\cdot}10^{17}$ H/cm^2. Prior to implantation the native oxide layer was chemically removed. After the implantation, the samples were stored in air at room tempe-

rature, and 60, 193 and 333 days after the implantation the area density of oxygen and the hydrogen depth profiles were measured by ERDA and NRA, respectively. The oxidation rate was found to be strongly dependent on the implanted hydrogen fluence. A significant decrease of the oxidation rate was observed at hydrogen fluences above $1{\cdot}10^{17}$ cm^{-2}. The amount of the surface oxygen in the sample implanted with a fluence of $6{\cdot}10^{17}$ H/cm^2 increased only by 23% during 273 days, whereas the amount in the untreated sample increased by more than a factor of 3. The hydrogen depth profiles reveal that the hydrogenation zone remains unchanged during the period of storage at room temperature.

Supported by MPG

Collaboration: [1]Institute of Modern Physics, Chinese Lanzhou, Chinese Academy of Sciences, P.R. China

T. Wang[1]
D. Grambole
F. Herrmann
F. Eichhorn
U. Kreissig
R. Grötzschel

Kinetics of titanium hydrogenation by hydrogen implantation

The hydrogenation in the titanium alloy Ti225 during hydrogen ion implantation has been studied with complementary use of NRA, ERDA, XRD and SEM. The samples were implanted at room temperature with 50 keV H_2^+ ions at fluences between $2{\cdot}10^{15}$ H/cm^2 and $6{\cdot}10^{17}$ H/cm^2. The measured hydrogen depth profiles deviate essentially from theoretical values predicted by SRIM, indicating a strong diffusion towards the surface and trapping at defects generated in course of implantation, whereas the retention increases with increasing fluence. Three hydrogen precipitation stages, which relate to different chemical states, were determined. The phase transformation from hexagonal close-packed (hcp) titanium to tetragonal TiH and then to TiH_2 was observed by XRD analysis when the fluence was increased from $2{\cdot}10^{16}$ and $6{\cdot}10^{17}$ H/cm^2. The formation of TiH_2 occurs at a fluence above $1{\cdot}10^{17}$ H/cm^2. Only TiH_2 was found after implantation with $6{\cdot}10^{17}$ H/cm^2, with the hydrogen concentration reaching a saturation level of about 23 at%, which is a factor of 3 higher than predicted by the phase diagram for the thermodynamic equilibrium. An inhomogeneous lateral distribution of the hydrogen was found by scanning microprobe ERDA. Blistering spots with a size of about 50 nm on the surface were observed by SEM which are believed to be induced by the TiH precipitates due to the lattice expansion by the higher lattice constant.

Supported by MPG

Collaboration: [1]Institute of Modern Physics, Chinese Lanzhou, Chinese Academy of Sciences, P.R. China

D.Jembrih-Simbürger[1,2]
C. Neelmeijer
O. Schalm[3]
P. Fredrickx[4]
M. Schreiner[1,2]
K. De Vis[5]
M. Mäder
D. Schryvers[4]
J. Caen[5]

The color of silver stained glass – Analytical investigations carried out with XRF, IBA, SEM/EDX and TEM

Glass treated at temperatures of 550 °C to 650 °C with both silver compounds and an inert alumino-silicate, such as ochre or clay, exhibits a wide variety of yellow color. It was the aim of this study to investigate the parameters of the manufacturing process of silver stained glass and to correlate them with the final color and color intensity. Therefore, defined mixtures of ochre and a silver compound (i.e. AgCl, $AgNO_3$, Ag_2SO_4, Ag_3PO_4 or Ag_2O) were prepared and applied on soda-lime glass. The firing process was varied within the temperature range of 563 °C to 630 °C. After the treatment the glass samples were analyzed with XRF, SEM/EDX and IBA (simultaneous PIXE, PIGE, RBS). The microstructure of individual silver particles was visualized by means of TEM after preparation of thin samples. The XRF results show that the highest amount of silver can be found on glass samples treated with silver stain mixtures containing Ag_2SO_4 while the lowest amounts were detected in the case of Ag_2O treatment. SEM/EDX shows that a low firing temperature (e.g. 563 °C) results in a higher silver concentration at the surface and a lower penetration depth. The 4 MeV external proton beam was used to measure the thickness and the Ag depth distribution of the Ag-rich surface layer. Cross-sectional SEM confirms the results from IBA. Thus, IBA proves suitable for studies of

intact originals.

Collaboration: [1]Institute of Humanities, Sciences and Technologies in Art, Academy of Fine Arts, Vienna, Austria; [2]Institute of Analytical Chemistry, Vienna University of Technology, Vienna, Austria; [3]University of Antwerp, Department of Chemistry, Antwerp-Wilrijk, Belgium; [4]University of Antwerp - RUCA, EMAT, Antwerp, Belgium; [5]Polytechnic University of Antwerp, Department Conservation/Restoration Glass, Antwerp, Belgium

Supported by EU , LSF-AIM

C. Neelmeijer
A. Siejek[1]
I. Sandner[1]
C. Hädrich[2]

Identification of tools used for creating historic hand drawings

For the study of drawing materials on paper the nearly background-free X-ray spectrum qualifies PIXE as a well-suited method. Proton beam intensities of only 200 pA and acquisition times of at most 30 seconds are sufficient to get significant signal from the applied substances, using the large area (80 mm^2) Si(Li) detector being available at the Rossendorf external beam set-up. Delicate hand drawings of the 15th – 17th century from the "Kupferstich-Kabinett Dresden" were under analysis. The interest of arts scientists relates to pigments of soft contours, light subfonts and gentle washouts. The challenge was to identify the types of these different painting materials on the very sensitive paper backing. Thus, lines from red chalk and silver pens were found. It was of special interest to reveal brownish and greyish tints which could be identified as ferro-gallic ink and lead from lead pens, respectively. In addition, PIXE enables to distinguish graphic tools made from carbon black (no characteristic X-ray line) and mineral black (Al and Si peaks). The simultaneous detection of RBS spectra allows to visualize individual techniques of paper grounding by chalk containing mash.

Collaboration: [1]Fachhochschule Köln, Fachbereich Restaurierung, Köln; [2]Staatliche Kunstsammlungen Dresden, Kupferstich-Kabinett, Dresden

Supported by BMBF

C. Neelmeijer[1]
A. Denker[2]

COST-G8: Participation at the EC action succeeding COST-G1

The main objective of the COST-G8 action is to achieve a better preservation and conservation of our cultural heritage by increasing the knowledge in museum objects through non-destructive analysis and testing and by improving the synergy between art historians, archeologists, conservators and natural scientists. The benefits are: (i) capability of answering questions related to museum objects including exchange of knowledge of the available non-destructive techniques and (ii) easy access of museums to experts and research facilities that provide such techniques. Within the international management committee of COST-G8 Germany is represented by both Forschungszentrum Rossendorf (Dresden) and Hahn-Meitner-Institut (Berlin). At the present status there are six approved project proposals for international museum/scientific collaboration of Germany with Norway, Austria, Greece and the UK. Among these, the Forschungszentrum Rossendorf joins projects (i) with the Academy of Fine Arts Vienna (Characterization of Iridescent Art Nouveau Glass) and (ii) with the ROTAX time of flight diffractometer at the ISIS spallation source at the Rutherford Appleton Laboratory, United Kingdom (Non-destructive Fingerprints for the Characterization of Böttger Stoneware).

Collaboration: [1]Hahn-Meitner-Institut, Ionenstrahllabor, Berlin

M. Mäder
C. Neelmeijer
A. Denker[1]
B. Schandert[2]
G. Kirchhoff[3]

Potential deterioration of art objects induced by ion beams

The problem of local modification of the physical and/or chemical properties of the object during analysis by the ion beam is a key factor in non-destructive characterization of art objects. Even a very gentle proton irradiation may cause visible darkening in insulators like colorless glasses or white porcelain. The formation of such color centers in samples of alkali silicate glasses and porcelain was studied by electron spin resonance (ESR) spectroscopy. Oxygen-associated trapped-hole centers in the silicate network were verified as origin

of these blackening. The generating mechanism of this point defect was found to be independent of the chemical composition. Optical absorption studies, however, indicate a dependence on both the composition of the material and the radiation fluence. A self-annealing process fades the visible deterioration during a few hours provided if the primary blackening did not exceed a critical limit. The annealing can be stimulated by energy supply, e.g. gentle heating or irradiation by light. In order to ensure non-destructivity during analysis a careful choice of the acceptable beam conditions and a special strategy of measurement (e.g. multiple data acquisition on several positions) is of importance when examining an art object made of glass or porcelain.

Collaboration: [1]Hahn-Meitner-Institut Berlin, [2]Institut für Festkörper- und Werkstoffforschung Dresden, [3]Institut für Werkstoff- und Strahltechnik Dresden

Semiconductor Materials

C. Zechner[1]
D. Matveev[1]
A. Erlebach[1]
S. Simeonov[2]
V. Menialenko[2]
R. Mickevicius[2]
M. Foad[3]
A. Al-Bayati[3]
A. Lebedev
M. Posselt

Technology computer aided design (TCAD) calibration of ultra-shallow junction profiles for advanced deep sub-µm CMOS processes

An accurate simulation of CMOS technologies down to channel lengths of 100 nm and below requires well-calibrated physical models obtained from comparison with experimental data. In order to calibrate the simulation of ion implantation and subsequent annealing, ultra-shallow profiles of As and B were considered. For this purpose, implantations were performed at following energies: (i) As: 0.2 – 10 keV, (ii) B: 0.2 – 10 keV, (iii) BF_2: 1 – 25 keV. The annealing was carried out at various time and temperature regimes, including typical spike anneals. Boron profiles were produced with and without pre-amorphization by Si or Ge implantation. The as-implanted and annealed profiles were analyzed by SIMS, spreading resistance profiling (SRP) and XTEM. The comparison of the as-implanted profiles with results of atomistic Crystal-TRIM simulations allowed the calibration of the few model parameters employed in the code. Annealing was successfully simulated within the framework of the models used in the process simulator DIOS, considering diffusion of pairs of silicon self-interstitials and dopants, interstitial traps, and interstitial and dopant clustering. A new model for dose loss was introduced which considers the dopant segregation in a thin surface layer on top of the silicon substrate.

Supported by ISE AG, Zürich, Switzerland

Collaboration: [1]ISE Integrated Systems Engineering AG, Zürich, Switzerland, [2]ISE Integrated Systems Engineering Inc., San Jose, CA, USA, [3]Applied Materials Inc., Santa Clara, CA, USA

A. Lebedev
M. Posselt
T. Feudel[1]
N. Variam[2]

Process and device simulation for tailoring of dopant profiles in advanced nMOS transistors

The properties of advanced CMOS transistors are strongly influenced by the dopant distribution in the transition region between the source (drain) and the channel. Tailoring of this distribution is achieved by appropriate halo and extension implants and subsequent annealing. Process and device simulations were performed to investigate the influence of the corresponding process parameters. The boundary condition used throughout the simulations was to keep the threshold voltage V_{Tsat} for the nominal nMOS transistor (sub-70 nm gate length) at 0.2 V. The following process conditions were studied: (i) B^+ halo implant: energy below 10 keV, tilt 45°, rotation 4x90°, dose varied to achieve V_{Tsat} = 0.2 V; (ii) As^+ extension implant: 0.5, 1.0, 2.0 keV, tilt 0°, 10^{15} cm^{-2}; (iii) RTA after both implants with special emphasis on soak and spike anneals (950...1100 °C). The model parameters employed in the simulation of the formation of the ultra-shallow extension profiles were calibrated using SIMS profiles of as-implanted and annealed samples, and sheet resistance data. The V_{Tsat} vs. L_{Gate} curve of the nMOS transistor was calculated. The dependence of the roll-off and roll-on behaviour on the process conditions considered is discussed. The influence of the gate-to-LDD-overlap on the device performance (drive current) was investigated.

Collaboration: [1]AMD Saxony Manufacturing GmbH, Dresden, Germany, [2]Varian Semiconductor Equipment Associates Inc., Gloucester, MA, USA

A. Lebedev
M. Posselt

Introduction of full-cascade simulation into the Crystal-TRIM-based implantation module of the commercial process simulator DIOS

In silicon technology the detailed knowledge of the defect structure formed by ion implantation is very important for the understanding and simulation of subsequent processes. In particular the effect of transient enhanced diffusion of dopants during annealing is caused by the presence of self-interstitials and/or

vacancies. In the previous Crystal-TRIM-based implantation module of the process simulator DIOS only the trajectories of the implanted ions were followed. The distribution of ballistically produced vacancies and displaced target atoms was determined approximately from the distribution of nuclear energy deposition using the Kinchin-Pease model. This procedure leads to identical profiles for both defect species. However, some effects appearing during annealing of implanted samples are assumed to be due to the mismatch between the spatial distributions of vacancies and self-interstitials. Furthermore, the previous procedure did not consider the motion of recoiled target atoms in collision cascades. This may lead to an incorrect spatial dependence of the defect concentration. In order to improve the estimation of self-interstitial and vacancy profiles, the implantation module of DIOS was modified. The simulation of collision cascades was introduced as an additional option and tested successfully. Splitting and duplication algorithms generally used in the implantation module of DIOS guarantee a high efficiency of the simulation without any loss of accuracy.

Supported by ISE AG, Zürich, Switzerland

A. Peeva
J. Kaschny
R. Kögler
W. Skorupa

Interaction between Si-interstitials and Helium-implantation-related defects for cavity stabilisation

The effect of interstitial-type defects on the evolution of He-implantation-induced cavities in Si was studied by TEM. Interstitial-type defects were formed by Si ion implantation into Si and subsequent annealing. The Si implantation energy and fluences were chosen in such a way to prevent the proximity of the surface and to create interstitial-type defects with different size, from small interstitial clusters to extended defects, in the projected ion range, R_P, region during annealing. The He ions were implanted (470 keV, $1\cdot10^{16}$ cm^{-2}) into the region of the Si interstitial-type defects. No visible cavities are formed in the as-implanted state after the He implantation. After an anneal at 700 °C for 30 min the TEM micrographs of both the reference sample only with He implant and the sample with He implant and the previously formed dislocations show existence of a cavity layer located in the R_P region. After longer annealing at 700 °C for 60 min, the reference sample shows no cavities while in the sample with the dislocations cavities are seen. The cavities are found to be located in the region where the pre-existing dislocations are observed. The cavities in silicon are known as a sink for interstitials. In the reference sample the flow of interstitials released by the interstitial type defects around the cavities can be captured by the cavity internal surface during annealing. If a great amount of interstitials is trapped at the cavity surface an epitaxial growth can occur, and the empty volume shrinks. The pre-existing dislocations are another sink and probably the preferred one for the interstitials. The pre-existing dislocations can getter the interstitials which in the reference sample are trapped at the internal surface of the cavities and, therefore, prevent the cavity disappearance.

R. Kögler
F. Eichhorn
J.R. Kaschny
A. Mücklich
H. Reuther
W. Skorupa
C. Serre[1]
A. Perez-Rodriguez[1]

Synthesis of nano-sized SiC precipitates in Si by simultaneous dual beam implantation of C^+ and Si^+ ions

Nanometer-sized SiC precipitates were in-situ synthesized in Si by simultaneous implantation with two ion beams of C^+ and Si^+ ions. The experiment was performed at the new Rossendorf *Double Implantation Chamber*. Results of simultaneous dual-beam implantation were compared with those of sequential dual-beam ion implantation and of single beam C^+ ion implantation. Remarkable differences were found in the content and the crystal perfection of SiC precipitates and also in the defect structure of the Si substrate. The SiC precipitates after dual beam synthesis were found to depend on the ion energy of the second beam and on the implantation mode, simultaneous or sequential. For suitable implantation conditions the simultaneous dual-beam synthesis can im-

prove the in-situ SiC formation compared to the single-beam synthesis. A higher density of SiC precipitates with better crystalline perfection was observed whereas their size was not changed. The second ion beam shifts the dynamic equilibrium of constructive and destructive processes for the SiC formation. A model is proposed assuming that SiC precipitation preferentially proceeds in regions with vacancy defects. The implantation process itself creates vacancy-dominated and also interstitial-dominated regions. The balance of the local point-defect composition is shifted by the second ion beam. In this way the conditions for SiC precipitation can be modified.

Collaboration: [1]Electronic Materials and Engineering, Dept. Electrònica, Universidad de Barcelona, Barcelona, Spain

G. Brauer
W. Anwand
W. Skorupa
A.G. Revesz[1]
J. Kuriplach[2]

Density gradient in the SiO_2/Si system demonstrated by PAS

Positron annihilation spectroscopy (PAS) of thermally grown and deposited SiO_2 films on silicon showed, for the first time in a non-destructive manner, that these films exhibit a gradient in their density. The gradient is most pronounced for oxide layers grown in dry oxygen. Oxidation in water-containing ambient results in an oxide with reduced gradient, similarly to the gradient in deposited oxides. These observations agree with earlier optical and other studies using stepwise etching or a set of samples of varying thickness. The investigations are accompanied by theoretical calculations of positron lifetimes, affinities and core electron contributions to Doppler broadening spectra for several phases (polymorphs) of SiO_2. An interesting feature is that not all polymorphs have the same coordination of Si and O atoms, which also affects the positron properties. The calculated quantities were compared to the experimental data of the SiO_2/Si interface. Moreover, this specific sensitivity of PAS for SiO_2/Si interfaces as well as the non-destructive manner of investigation are very promising for a deeper understanding of the nearest surrounding of semiconductor nanoclusters embedded in SiO_2 layers.

Collaboration: [1]Naval Research Laboratory, Washington/DC, USA, [2]Charles University, Prague, Czech Republic

J. Rinderknecht[1]
H. Prinz[1]
T. Kammler[1]
F. Berberich
E. Zschech[1]

***In situ* high-temperature diffraction studies of nanoscale Ni and Co-Ni layers**

Silicidation processes in nanoscale Ni and Co(Ni) layers, i.e. Co with several at% Ni, on silicon substrates were investigated. The phase formation sequences as well as the formation and transition temperatures between 160 °C and 750 °C were studied. An evacuated high-temperature diffraction chamber was used to perform *in-situ* grazing incidence diffraction studies. The impact of different silicon substrates, i.e. polycrystalline Si and (100) orientated Si single crystal substrates as well as the impact of different species (As, P) and different doses of dopants on the phase formation and transition processes were analyzed. In pure Ni samples on doped single crystalline silicon, the silicidation process starts at 160 °C with Ni_2Si. It is followed by NiSi at ~ 275-300 °C and ends with the formation of epitaxially grown $NiSi_2$ at 750 °C. On polycrystalline silicon Ni_2Si is stable up to 200-250 °C. At this temperature NiSi is formed and is stable up to 650 °C. The transition to polycrystalline $NiSi_2$ starts at 475 °C. In the case of the (Co,Ni) layers on silicon single crystal substrates, diffraction peaks of $(Co,Ni)_2Si$ for the doped substrates become visible at 275-300 °C. There are also diffraction peaks of (Co,Ni)Si visible at 275 °C. In each case (Co,Ni)Si is stable up to 475 °C, where it is transformed into $(Co,Ni)Si_2$. For non doped substrates $(Co,Ni)Si_2$ starts to form at 400 °C.

Collaboration: [1]AMD Saxony Manufacturing GmbH, Materials Analysis Department, Dresden

J. Gaca[*]
M. Wójcik[1]
J. Sass[1]
K. Mazur[1]
N. Schell
A. Bauer
F. Eichhorn

Structural studies of InGaAs/GaAs quantum well heterostructures

The real structure (lattice defects, disturbances in the chemical constitution and layer thickness) of strained InGaAs/GaAs quantum well layers influences their application for lasers and resonant-tunneling diodes. Various X-ray scattering techniques allow one to study this material non-destructively. However, the total thickness of the used heterostructures is very small (d < 50 nm) which results in a low scattering cross section. Therefore, the measurements were performed with X-ray synchrotron radiation with its high intensity and its very low divergence at ROBL. The determination of the chemical composition profile in the growth direction was carried out by computer simulation based on the Darwin dynamical diffraction theory. It was found that, (i) misfit dislocations are formed if the active layer thickness exceeds 30 nm, (ii) a lower growth rate results in greater discrepancy between obtained and expected results, and (iii) symmetric AlGaAs barriers below and above the active layer stabilize the profile of the InGaAs active layer.

Collaboration: [*]Institute of Electronic Materials Technology (ITME), Warsaw, Poland

Z. Zolnai[1]
N. Q. Khanh[1]
E. Szilagyi[2]
E. Kotai[2]
A. Ster[1]
M. Posselt
T. Lohner[1]
J. Gyulai[1]

Investigation of ion-implantation-induced damage in carbon and silicon sublattices of 6H-SiC

Single-crystal 6H-SiC samples were irradiated at room temperature with 200 keV Al^+ ions at fluences ranging from $3.5 \cdot 10^{13}$ to $2.8 \cdot 10^{14}$ cm^{-2}. Depth profiles of crystal defects both in the C and Si sublattices were measured by RBS/C using $^4He^+$ ions of 3.55 MeV. The direction of incidence was parallel to the <0001> axial channel direction. At this energy not only Si signals but also C signals can be detected, since the elastic cross-section of carbon is about six times higher than the Rutherford value. Damage in the C sublattice was found to be higher than in the Si one. Moreover, the C/Si damage ratio decreases with increasing fluence. The crystal defect profiles can be well simulated both by full-cascade SRIM and Crystal-TRIM programs. In the applied fluence range of Al implantation, effective displacement energies for C and Si sublattices were determined by comparing SRIM to RBS/C results.

Supported by SMWK

Collaboration: [1]Research Institute for Technical Physics and Materials Science, Budapest, Hungary, [2]Research Institute for Particle and Nuclear Physics, Budapest, Hungary

D. Panknin
C. Serre[1]
A. Pérez-Rodríguez[1]
A. Romano-Rodríguez[1]
R. Kögler
W. Skorupa

Ion beam synthesis of n-type doped buried SiC layers in Si

For the formation of n-doped 3C-SiC layers in (100)-Si by ion beam synthesis (IBS) two approaches were studied: i) doping by implantation of N^+ into the ion beam synthesized SiC layer, and ii) using a novel method based on pre-doping with N^+ and P^+ of the Si wafers before IBS of the buried SiC layer. In the first case the electrical data show a p-type overcompensation of the SiC layers doped with N^+. The structural (XRD) and in-depth (SIMS, spreading resistance) analysis of the samples suggests this overcompensation to be induced by p-type active defects related to the N^+ ion implantation damage. In the second case, the P^+-doped SiC layers always show n-type doping whereas the N^+ layers show n-type doping only for an implantation with low fluences. This is accompanied by a higher structural quality, similar to that of undoped material. Our electrical data, together with the absence of additional stress suggest that this technique could be suitable for avoiding effects related to the ion-implantation damage in the SiC lattice. In-depth analysis by SIMS reveals that the phosphorus distribution remains stable during the IBS process.

Collaboration: [1]Electronic Materials and Engineering (EME), Dept. Electrònica, Universidad de Barcelona, Barcelona, Spain

H. Weishart
V. Heera
W. Skorupa

Ion beam synthesis of doped diamond-SiC-heterostructures

Fabrication of diamond-SiC-heterostructures by synthesis of a thin SiC-layer within a diamond matrix has been successfully achieved by high-dose ion

B. Pécz[1]
A. Barna[1]

implantation of Si into diamond. Defects introduced into the diamond during Si-implantation facilitate a reaction of Si with C to form SiC. In order to retain the diamond structure, however, implantation was performed at 900 °C. A first characterization of the electrical properties of the implanted and annealed samples is done by four-point-probe measurements. The results indicate a highly conductive layer. Because Hall measurements shall be used to determine the carrier concentration, some samples are implanted through a specially designed mask to obtain a Hall bar structure. The existing Hall measurement apparatus has been extended with a new sample stage which can be used from LN-temperature up to 600 °C.

Supported by DFG

Collaboration: [1]Research Institute for Technical Physics and Materials Science, Budapest, Hungary

V. Heera
D. Panknin
W. Skorupa

p-type doping of SiC by high dose Al implantation - optimum processing conditions

The development of optimized processes for p-type doping of single crystalline SiC by ion implantation and subsequent annealing is a remaining challenge to SiC-device technology. Al is the most promising acceptor in SiC. However, also in the case of Al very high acceptor concentrations ($>10^{19}$ cm^{-3}) are necessary to obtain SiC layers with low resistivities (< 1 Ωcm). The physical consequences of such high impurity concentrations in SiC for the annealing of implantation damage and the electrical activation were investigated. A comparative study of several doping and annealing schemes used in our experiments and reported in the literature indicates the following optimum doping conditions: The optimum temperature range for implantation is between 400 °C and 600 °C. Higher implantation temperatures can deteriorate the electrical properties by the formation of secondary defects. Furnace annealing at temperatures between 1600 °C and 1700 °C yields the best activation results for Al doping with concentrations up to $5\cdot10^{20}$ cm^{-3}. At higher Al concentrations flash lamp annealing (20 ms, 2000 °C) is the superior process.

V. Heera
F. Eichhorn
A. Mücklich
W. Skorupa

The flux dependence of ion beam induced nanocrystallization of SiC

The ion beam induced crystallization (IBIC) of preamorphized SiC was studied as a function of the ion flux. 6H-SiC samples with an amorphous surface layer of 1.8 µm thickness were subjected to Si-irradiation (450 keV, $5\cdot10^{15}$ cm^{-2}) at a target temperature of 500 °C in order to stimulate the formation 3C-SiC nanocrystals up to a depth of 550 nm. The ion flux was varied from $3\cdot10^{11}$ $cm^{-2}s^{-1}$ to $3\cdot10^{13}$ $cm^{-2}s^{-1}$. The layers were analyzed by XRD under grazing incidence (0.35°) and XTEM. In contrast to previous assumptions, it was found that the nanocrystallite size depends only weakly on the ion flux. The correlation length which was determined from the XRD peak width increases slightly from 2.6 nm to 3.3 nm with increasing ion flux. Randomly oriented nanocrystalline 3C-SiC grains with a mean size of about 4 nm were detected by XTEM in all samples independent of the applied ion flux.

K.N.Madhusoodanan
V. Heera
W. Skorupa

Improved p-type doping of SiC by means of ion beam induced crystallization

The production of low-resistivity, p-type SiC is difficult due to deep acceptor levels in single crystalline SiC. Therefore, the electrical behavior of Al acceptors in nanocrystalline SiC was studied. Ion beam induced crystallization (IBIC) was used to induce crystal nucleation in pre-amorphized 6H- and 4H-SiC. An amorphous layer up to a depth of 500 nm was formed by high dose Al implantation at room temperature. Multiple-energy implantation was carried out to obtain a box-type Al acceptor profile. Crystallization in this amorphous layer is induced by further implantation of either Al or Si at an elevated temperature of 500 °C. Nanometer-size crystallites are formed under this IBIC

process. Electrical resistivity and Hall measurements were carried out on samples annealed at 1500 °C. The IBIC samples show low resistivity and high carrier concentration, indicating efficient p- type doping, in comparison with reference samples which do not contain nanocrystals. The results suggest that the technique can be considered as useful method for producing low resistivity p-type SiC layer.

Semiconductor Spectroscopy

T. Dekorsy
M. Helm
W. Seidel[1]
V.A. Yakovlev[2]

Second harmonic generation (SHG) below the Reststrahlen band of GaAs

The frequency doubling of laser light by crystals was first demonstrated by the generation of the second harmonic of a ruby laser in crystalline quartz in 1961 – representing the birth of nonlinear optics. The investigation of SHG in the far-infrared (FIR) remained largely unexplored due to the lack of high-power pulsed lasers which have become available as FELs. We investigated SHG in GaAs crystals for fundamental light frequencies below the fundamental optical phonon frequency at the FIR FEL facility FELIX, Netherlands. There exists the theoretical prediction that the nonlinear coefficient defining the intensity of the SHG light changes sign in this frequency range, since this coefficient has electronic and vibronic contributions of opposite sign. This sign reversal will lead to a zero crossing of the SHG intensity. Two clear minima in the SHG intensity were encountered at 58 µm and 66 µm, while a value of around 60 µm is predicted. The observation of two minima is puzzling since only a single sign reversal of the second order susceptibility is expected. Furthermore the spectral width of the minima was 1 µm FWHM only. These results do not fit into the existing quantum mechanical model. Regarding the importance of a complete description of the nonlinear susceptibility further experiments at FELIX are in progress.

Collaboration: [1]Institute for Nuclear and Hadron Physics, FZR; [2]Institute of Spectroscopy, Russian Academy of Sciences, Troitsk, Russia

K.J. Yee[1]
Y.S. Lim[1]
D.S. Kim[1]
T. Dekorsy

Generation mechanism of coherent LO phonons in GaAs multiple quantum wells

The excitation and detection of coherent phonons in bulk semiconductors and semiconductor heterostructures provides important information on nonlinear light-matter interaction on a femtosecond time scale. Although phonon spectroscopy performed by means of CW Raman spectroscopy is a well-established method, time-resolved coherent phonon spectroscopy is a relatively young field. Several different mechanisms have been proposed to be relevant for the impulsive excitation of coherent lattice vibrations by a femtosecond laser pulse. Some of them can be described on the base of impulsive Raman scattering, while some excitation mechanisms are distinctly different from known Raman interactions. One prominent example for a non-Raman type excitation is the ultrafast screening of electrical fields by a photo-generated electron-hole plasma in surface space charge fields of III-V semiconductors. We performed a systematic study of the excitation of coherent LO phonons in GaAs multiple quantum wells. Different excitation processes could be disentangled from the energy and polarization dependence of the exciting laser pulse. Under resonant excitation conditions at the first interband transitions the symmetry selection rules point towards a dominant impulsive Raman process, while under non-resonant conditions, i.e. into the continuum of the subbands, field screening dominates which does not depend on the exciting polarization.

Collaboration: * Department of Physics, Seoul National University, South Korea

O.V. Misochko[1]
N. Georgiev
T. Dekorsy
M. Helm

Observation of a hysteretic pseudogap behavior in high temperature superconductors via coherent phonons

One of the intriguing subjects in the physics of high temperature superconductors (HTSC) is their behavior above the superconducting transition temperature T_c, i.e. in the normal state. Above T_c anomalies are observed which are attributed to a pseudogap state in a temperature range above T_c, but below a crossover temperature T*. Although there exists no complete theory for the pseudogap regime, there is common agreement that the observed anomalies in

the pseudogap range are indications that some superconducting properties persist even above T_c. Time-resolved ultrafast spectroscopy of the carrier and lattice dynamics has been shown to provide insight into the dynamics of HTSC, such as the optical break-up of Cooper pairs and their subsequent relaxation as well as the excitation of coherent phonons. We performed a study of a close to optimally doped $YBa_2Cu_3O_{7-x}$ by optical pump-probe spectroscopy. Both the temperature dependence of the relaxation dynamics and the coherent excitation of the Ba A_g phonon mode exhibit an abrupt change at temperatures T_1* and T_2* *above* T_c. In addition T_1* and T_2* reveal a hysteresis depending on the direction of the temperature change. All these observation give evidence for the non-uniformity of the pseudogap

Supported by A. v. Humboldt Stiftung

Collaboration: * Institute of Solid State Physics, Russian Academy of Sciences, Chernogolovka, Moscow region, Russia

N. Georgiev
T. Dekorsy
M. Helm

Simulation of relaxation kinetics in quantum cascade lasers

Intersubband transitions in semiconductor quantum wells have been attracting increasing attention in various infrared optoelectronic device applications such as semiconductor lasers, detectors, and ultrafast all-optical switches or modulators. In recent years there was a drive towards systems realizing shorter-wavelength intersubband transitions extending into the NIR, which could be used for optical communication. We have proposed lattice-mismatched $In_xGa_{1-x}As/In_yAl_{1-y}As$ ($x>0.53$ and $y<0.52$) and lattice-matched InGaAs/AlAsSb quantum well structures on InP substrates for realizing quantum cascade lasers (QCL) operating at shorter wavelengths. The development of practical quantum cascade lasers from such a material requires the estimation of basic parameters like population inversion conditions and carrier relaxation rates within the structures. We have investigated numerically the dynamics of the coupled electron-phonon system of realistic $In_xGa_{1-x}As/In_yAl_{1-y}As$ and InGaAs/AlAsSb QCLs. We calculate carrier scattering rates and optical dipole matrix elements in order to obtain occupation probabilities, gain spectra, and threshold currents at different temperatures and injector conditions for optimized QCL performance.

N. Georgiev
M. Helm
T. Mozume[1]

Short wavelength intersubband transitions in InGaAs/AlAsSb quantum well structures

Intersubband transitions in the conduction band of quantum wells are gaining increasing interest for the development of mid-infrared cascade lasers, ultrafast modulators and switches. We have developed the MBE growth of a large-conduction-band-offset material system (~ 1.6 eV) with InGaAs/AlAsSb quantum wells on an InP substrate to achieve intersubband transitions < 2 µm (> 0.6 eV) using single and coupled double well structures. The near-infrared intersubband wavelength as well as the quality of the absorption and photoluminescence spectra (linewidth and peak intensity) in InGaAs/AlAsSb quantum wells are critically dependent on the interface quality owing to interdiffusion of the group III and V species between the well and the barrier material. We have observed improved optical response: the shift of the intersubband absorption peak to shorter wavelengths, narrower linewidth, and higher peak intensity in samples, where measures were taken to decrease the amount of the Sb atoms at the heterointerfaces.

Collaboration: [1]Femtosecond Technology Research Association, FESTA, Tsukuba, Japan

N. Georgiev,
A. Bauer,
F. Eichhorn,
M. Schell

Synchrotron characterization of ion beam induced quantum dots in III-V heterostructures

The synthesis of semiconductor quantum dots for applications in optoelectronics remains a challenging task. The self-organized growth in the Stranski-

T. Dekorsy, M. Helm, T. Bobek[1], S. Facsko[1], H. Kurz[1]

Krastanov growth mode during MBE is widely employed for the generation of quantum dots. Recently, the inverse mechanism has been shown to lead to the formation of regular nanoscale dot patterns on III-V surfaces. This mechanism relies on a surface instability during the ion-erosion of III-V surfaces under low energy Ar^+ sputtering. Depending on the ion energy nanoscale dots with diameters between 10 nm to 100 nm, an aspect ratio of 1, and a hexagonal ordering are obtained. We investigated ion sputtered $Ga_{0.8}In_{0.2}Sb/GaSb$ multiple quantum wells, where a single quantum well lies in the center of a 50 nm diameter dot, at the ROBL synchrotron beam line. An angular scan around the (004) Bragg peak of the GaSb substrate shows clear side maxima related to the lateral structure of the sample of 50 nm, in agreement with results obtained from SEM and AFM measurements. Furthermore the strain along the sputter direction was investigated at the top of the dots by radial scans of GaSb (400) in grazing-incidence/grazing-exit diffraction. These investigations will help in the understanding of the formation process of the quantum dots.

Supported by Bennigsen-Förder-preis of the MSWF, NRW

Collaboration: [1]Institute of Semiconductor Electronics, RWTH Aachen

Nanostructures

M. Strobel
K.-H. Heinig
W. Möller

Three-dimensional domain growth on the size scale of the capillary length: Effective growth exponent and comparative atomistic and mean-field simulations

The evolution of diffusively interacting nanoclusters is investigated by combined atomistic (kinetic lattice Monte Carlo method based on the nearest-neighbor Ising model) and mean-field (numerical integration of the governing reaction-diffusion equations) simulations. By expressing Monte Carlo parameters in terms of macroscopic thermodynamic quantities a well-defined interface between both methods is derived. Based on extensive Monte Carlo studies of the Gibbs-Thomson equation an explicit expression for the intrinsic capillary length is presented. Starting with high-temperature quenches, the evolution of nanoclusters is first studied by the atomistic model. The observed transient dynamics of coarsening is explained uniquely on the basis of the ratio of the capillary length to the mean cluster size. Using input data from the atomistic model, Ostwald ripening is also studied in parallel with the mean-field model. In a detailed study, the similarities and differences of both approaches are discussed and explained in terms of their statistical and deterministic natures. It is demonstrated that in contrast to the commonly applied linearized version of the Gibbs-Thomson relation in the mean-field approach only the use of the full exponential form provides a reasonable matching with the atomistic model.

T. Müller
K.-H. Heinig

Pearling instability of nanowires – predictions based on kinetic MC simulations

Kinetic 3D Lattice Monte Carlo (MC) simulations of the shape evolution of nanowires by thermally activated interface diffusion were performed. Interface minimization of wires leads to the Rayleigh (or pearling) instability. During heat treatment of a nanowire small random peristaltic thickness undulations amplify themselves, which finally results in the decay of the wire into a regular chain of nanoclusters (NCs). For temperatures above the roughening transition it could be shown that size and spacing of the NCs are in good agreement with predictions of the classical stability analysis of Rayleigh and Mullins. The competition between peristaltic undulations with different wavelengths (modes) results in the decay of the wire into equally-spaced NCs due to self-selection of the fastest growing mode. This mode selection was demonstrated by a Fourier analysis of the MC results. Other than in the analytical stability analysis it was found that short-wavelength modes develop first, whereas long-wavelength modes are missing initially.

Supported by EU

T. Müller
K.-H. Heinig
W. Möller
B. Schmidt

Nanocluster formation by phase separation in ultra-thin ion implanted gate oxides

Kinetic 3D lattice Monte-Carlo (MC) calculations of phase separation in very-low-energy ion implanted ultra-thin gate oxides were performed. Simulations show that for low ion fluences (low concentrations) the nanocluster (NC) formation proceeds via nucleation, growth and Ostwald ripening. However, for high fluences spinodal decomposition results in a laterally connected network of nanostructures resembling a conventional floating gate memory. In general, the Si/SiO_2 interface being in close neighborhood to the NCs has substantial influence on the NC evolution. During annealing a zone denuded by NCs forms above the interface, which serves as tunnel oxide for charging / decharging of NCs. Our predictions based on MC simulations are in qualitative agreement with TEM investigations of Si^+ implanted gate oxides. However, the experimental fluence necessary for Si NC formation exceeds the predicted one by up to an order of magnitude. Recently, the theoretical predictions initiated

experimental studies, which have shown that the discrepancy originates from oxidation of a large fraction of implanted Si. After ion implantation, a few tens of nm thick surface layer of the damaged SiO_2 soaks in atmospheric moisture. During subsequent annealing this moisture oxidizes the excess Si partly, especially for low-energy implantation.

Supported by EU

K.-H. Heinig
P. Novikov[1]
A.N. Larsen[2]
A. Dvurechenskii[1]

Simulation of ion-irradiation stimulated Ge nanocluster formation in gate oxides containing GeO_2

Process simulations were performed for a novel fabrication technique of Ge nanoclusters located in the thin gate oxide of a MOS field effect transistor which will be applied in non-volatile random access memories (nvRAMs). The simulations start from a thin GeO_2 layer buried in the gate oxide which might be produced by heteroepitaxy of a thin Ge layer in (001)Si followed by a special rapid thermal oxidation (RTO) avoiding Ge segregation. The process simulations predict that the recently reported transformation of such a GeO_2 layer into Ge nanoclusters by thermal annealing can be accelerated by ion irradiation. It is even more important that under ion irradiation the chemical reduction of GeO_2 should be achieved at lower process temperature. The limiting mechanism of the transformation of GeO_2 into Ge nanoclusters during thermal annealing is shown to be thermally activated detachment of Si monomers from the Si/SiO_2 interface into SiO_2. Thus, ion beam mixing of Si into SiO_2 stimulates the Ge nanocluster formation. The process simulations were performed by a specifically adapted and extended multicomponent kinetic Monte Carlo code.

Collaboration: [1]Institute of Semiconductor Physics, Novosibirsk, Russia, [2]Aarhus University, Aarhus, Denmark

Supported by EU

J. Schmidt
B. Schmidt

Optical characterization of Si nanoclusters embedded in SiO_2 obtained by alternate SiO_2 and Si sputtering and subsequent annealing

A novel technique to prepare planar arrangements of Si nanoclusters (NC) in a SiO_2 matrix was investigated, namely high temperature annealing of a sputter deposited SiO_2 / SiO_X ($x<2$) / SiO_2 film stack. Hereby the SiO_X film is prepared by alternate deposition of multiple sub-nanometer layers of Si and SiO_2 on a sample mounted to a rotating table. The effective O/Si ratio x can be tuned by varying the thickness of the Si sublayers. To investigate the annealing process of such SiO_X films, samples of ~70 nm SiO_X ($0.5 < x < 2$) on Si were exposed to a 30 s rapid thermal anneal at temperatures 800 °C < T < 1050 °C. The annealing does not change the content of excess Si determined by ellipsometry and RBS. The process of SiO_X phase separation in Si and SiO_2 was monitored by infrared (IR) transmission and photoluminescence (PL) measurements in the red spectral region, where emission is related to the presence of Si NCs. The frequency shift of the IR active Si-O-Si stretching vibration towards the value typical for SiO_2 reflects the progress in NC formation by phase separation. The frequency shift is larger for higher T and smaller x. For $x > 1$ the phase separation is still incomplete after annealing at 1050 °C. This is due to a high density of clusters with a smaller mean radius and therefore higher equilibrium concentration of Si monomers at the NC/SiO_2 interface. For all excess Si concentrations the maximum of the red PL emission shifts to lower energies with increasing T due to weaker confinement of electron-hole pairs in larger clusters. For higher T the maximum PL intensity is found at higher energy in samples with higher x.

Supported by DFG

J. Schmidt
B. Schmidt

MOS capacitors with Si nanoclusters embedded in the SiO_2 fabricated by alternate SiO_2 and Si sputtering and annealing

Si nanoclusters (NC) attract increasing interest due to their potential impact on optoelectronics, single electron devices and non-volatile memories. In a NC

memory cell, isolated Si NCs arranged in a plane within the gate oxide near the channel of a field effect transistor, act as electron traps. This application requires NCs having a narrow size distribution and a density of about 10^{12} cm^{-2}. MOS capacitors with a layer of isolated Si NCs embedded in the SiO_2 in direct tunneling distance to the Si substrate were prepared. For that SiO_2 (23nm) / SiO_X film stacks deposited by magnetron sputtering onto a ~ 2nm thermal SiO_2 film on Si were subjected to a 2 min rapid thermal annealing (RTA). The SiO_X composition x was varied between 1.3 and 1.9, the thickness d between 5 nm and 12 nm and the RTA temperature between 800 °C and 1050 °C. Charge trapping related to the NC layer after application of voltage pulses is evident from large shifts of the capacitance voltage curve which are not observed in the reference samples without NCs. Both positive and negative shifts are observed and attributed to addition and removal of electrons to respective from the clusters. Preliminary investigations of the charge retention behavior using the constant-capacity method indicate retention times >>10^5 s at room temperature.

Supported by DFG

B. Schmidt
K.-H. Heinig
M. Perego[1]
M. Fanciulli[1]

Atmospheric moisture penetration into ion-beam damaged SiO_2 surface layers studied by post-implantation exposure to N_2 with $H_2{}^{18}O$ humidity

Post-implantation water penetration from atmospheric humidity into the damaged SiO_2 surface layer has previously been studied by hydrogen depth profiling using nuclear reaction analysis (NRA). However, this experiment was not completely convincing, because hydrogen is always present in Si technology. Now, a more direct experiment was performed. A 100 nm thick thermal oxide layer on (001)Si was implanted with $5x10^{15}$ cm^{-2} Ge^+ ions of 20 keV. A second, identical sample was put in the implantation chamber, but protected from the ion beam. After implantation the chamber was filled with pure N_2 at 22 °C having 40% relative humidity of $H_2{}^{18}O$. The samples remained in the N_2 for 24 h. Then the depth profiles of the ^{18}O isotope, which occurs in nature only with 0.2 % abundance, in the SiO_2 surface layers were analyzed by ToF-SIMS. The measured ^{18}O depth profiles showed that near the SiO_2 surface the concentration of ^{18}O reaches up to 2 at% and the ^{18}O profile extends up to a depth of nearly 40 nm. This agrees with the hydrogen depth profiles measured previously by NRA. The identically treated but not implanted sample contained no ^{18}O exceeding the natural abundance.

Supported by EU

Collaboration: [1]Instituto Nationale per la Fisica della Materia, Laboratorio Materiali e Dispositivi per la Microelettronica, Agrate (MI), Italy

J. Zhao
L. Rebohle
T. Gebel
W. Skorupa

Modelling of the I-V characteristics of Ge implanted oxide layers using the SCL model

The electrical conduction mechanism of Ge-implanted SiO_2 films exhibiting room-temperature blue electroluminescence (EL) is of eminent interest for the understanding of the excitation mechanism of the EL. The current-voltage (I-V) characteristic of such Ge-implanted SiO_2 layers was investigated from room temperature up to 200 °C. For applied electric fields between 4.5 and 7 $MVcm^{-1}$ the I-V data can be modeled very well with the space charge limited (SCL) conduction mechanism in the trap-filled-limited (TFL) region. The current density J shows a power-law dependence $J \propto E^{\alpha}$ of the applied electric field E. The temperature dependence of α exhibits the typical behavior of TFL injection currents. For applied electric fields above 7 $MVcm^{-1}$ a weaker temperature dependence was observed. In this high-field region the charge transport mechanism can be explained by SCL currents which are superimposed by effects of Fowler-Nordheim tunneling, impact ionization and electron-hole recombination.

T. Gebel
L. Rebohle
A. Mücklich
H. Reuther
H. Fröb[1]
W. Skorupa

Microstructure and luminescence properties of Si /C co-implanted SiO_2 layers

Si^+ implanted SiO_2 films are known to exhibit strong blue light emission. In order to increase the electrical device stability, thin SiO_2 layers (350 nm) were co-implanted with Si^+ and C^+ ions and subsequently annealed at 1100 °C. The peak concentrations of excess Si and C amount to 5...10 at% in a depth ranging from 60 to 180 nm. The elemental depth distribution was investigated by AES and the microstructure by TEM. Small amorphous nanostructures consisting of $Si_yC_{1-y}O_x$ ($x < 2$) with sizes between 2 and 3.5 nm were observed in a depth region between 80 and 150 nm. Strong photoluminescence (PL) in the blue and yellow spectral region was achieved after excitation at 4.77 eV. In the electroluminescence (EL) spectra, for the lowest concentration (5%) a clear double-peak structure consisting of two maxima around 3.3 eV and 2.45 eV was observed whereas for 7.5 and 10 at% only one peak at 2.75 eV occurs. No remarkable changes in the EL spectra were observed with increasing electric fields. This means that the changes in the shape of the spectra for different Si/C concentrations are related to the different microstructure and not to the energy distribution of hot electrons. The Si/C rich oxide layers showed an improved electrical stability in comparison to the Ge/Sn implanted devices. This may be caused by the different types of defects capturing hot electrons during the high field operation.

Collaboration: [1]TU Dresden, Institut für Angewandte Photophysik

L. Rebohle
T. Gebel
H. Fröb[1]
W. Skorupa

Variations in the photoluminescence (PL) and electroluminescence (EL) spectra of Sn implanted thermally grown SiO_2 layers

The ion beam synthesis of group IV element rich SiO_2 layers is a promising approach for Si-based light emission. Thermally grown SiO_2 layers (200 nm) were implanted with 130 keV Sn^+ ions to fluences of 2.9 to $8.6 \cdot 10^{15}$ cm^{-2} and subsequently annealed. The PL and EL spectra show a main emission peak at around 3.2 eV implying that the emission is caused by the same luminescence center. However, for both, PL and EL, the luminescence is accompanied by a shoulder on the low energy side. For PL, this low energy shoulder increases for higher excitation energies. The PL excitation spectra of the two PL peaks reveal that the emission at 3.2 eV is related to the well-known excitation peak at 5.1 eV, whereas the emission at 2.6 eV shows a featureless PL excitation spectrum between 2.8 and 6.2 eV. Thus, the emission at 2.6 eV is obviously caused by a different luminescence center (LC). In EL the 2.6 eV peak is only present for low injection current densities. A first hypothesis assumes that the number of LC causing the 2.6 eV peak is reduced during operation at high electric fields due to impact ionization caused by hot electrons.

Collaboration: [1]TU Dresden, Institut für Angewandte Photophysik

T. Gebel
L. Rebohle
A. Nazarov[*]
I. Osiyuk[1]
W. Skorupa

Charge trapping effects in Ge implanted oxide layers

The electrical properties of Ge rich SiO_2 films exhibiting blue electroluminescence (EL) are of great interest for the understanding of the nature of the luminescence centers and the excitation mechanism of the EL. SiO_2 layers (80 nm) were implanted with 30 - 50 keV Ge^+ ions to fluences of $1.8 \cdot 10^{15}$ - $1.0 \cdot 10^{16}$ cm^{-2} and subsequently annealed. High-field electron injection was performed at a constant current density of $2 \cdot 10^{-5} Acm^{-2}$ corresponding to the typical EL operation regime. By applying a positive voltage to the gate contact electrons are injected from the Si substrate. The trapping behavior was investigated by two methods. First, using the HF-CV method the shift of the flat-band voltage was studied. Second, V(t), the change of the applied voltage during the time of constant current injection was detected which enables the calculation of the trapped charge. Since both methods are sensitive to different depth regions, the results imply the following scenario during the constant-

current stress: Electrons are trapped in the volume of the SiO_2 layer, but with increasing stress time also positive charges are trapped near the SiO_2/Si interface region. The trapping of positive charge may occur in oxygen deficiency centers, the same defects causing the EL. This would also explain the decrease of the luminescence efficiency after long-term operation at high electric fields.

Collaboration: [1]Institute of Semiconductor Physics, Kiev, National Academy of Sciences of the Ukraine

T. Gebel
J. von Borany
K.-H. Stegemann[1]
W. Skorupa

Investigation of the retention and endurance characteristics of Si^+ and Ge^+ implanted gate oxides

The long-term charge storage capability (data retention) and the endurance (number of write/erase cycles) of MOS capacitors with Si^+ or Ge^+ implanted SiO_2 layers (d = 20 nm) were investigated. The implanted impurity content within the SiO_2 was about 7 at%. For retention investigations programming with short-voltage pulses (± 12.5 V, 100 ms) was carried out. Afterwards the capacitors were stored at elevated temperature (100 °C…200 °C) up to two weeks without any bias applied to the gate, only occasionally interrupted by the measurement of the flatband voltage shift. For devices implanted with Si^+ the programming window remains stable even after a storage at 200 °C for 280 h, which confirms excellent retention behavior. Ge^+ implanted gate oxides show a sharp drop in the programming window already at room temperature (RT) and the retention is only of the order of 1000 s. One possible reason may be differences in the spatial trap distribution in Si^+ and Ge^+ implanted SiO_2 films which still has to be confirmed. For endurance investigations of the implanted MOS devices each write/erase-cycle consists of a ± 12.5 V pulse of 50 ms length. The obtained endurance for oxides implanted with $7\cdot10^{15}$ cm^{-2} is > 10^6 cycles. Referring to the possibility of using considerably lower programming times an endurance greater than 10^8 cycles can be envisioned.

Supported by SMWK

Collaboration: [1]Zentrum Mikroelektronik Dresden

Focused Ion Beams

G.L.R. Mair[1]
L. Bischoff
A.W.R. Mair[2]
Ch. Akmadaliev
C.J. Aidinis[1]
Th. Ganetsos[1]
C.A. Aleiev[1]

Investigation of the energy distribution of doubly-charged ions emitted from an alloy liquid metal ion source (LMIS)

Focused ion beams (FIB) employing LMISs can be used in a variety of applications including maskless ion implantation, integrated circuit inspection, repair and modification, lithography and SIMS. We investigate the energy spread, ΔE as a function of the emission current, *i*, for doubly-charged ions emitted by a $Au_{77}Ge_{14}Si_9$ alloy LMIS. For the ionic species of main interest, namely Ge^{++}, two modes were found with regard to the dependence of ΔE on *i*: in the first mode $\Delta E \propto i^{0.3}$, and in the second ?E ∝ i. The difference is attributed to changes in the composition of the alloy during field evaporation. The species Au^{++} and Si^{++} were also found to obey a $\Delta E \propto i^{0.3}$ law. In the case of Si^{++}, however, there is a deviation from this law at high currents.

Collaboration: [1]University of Athens, Department of Physics, Section of Solid State Physics, Greece; [2]University of Manchester, Faculty of Science and Engineering, UK

L. Bischoff
H. Tritschler[1]
J. Teichert

Microtools fabricated by focused ion beam processing

High speed steel (HSS) and especially tungsten carbide (WC) embedded in a Co matrix (7.5 %) are very promising materials for micro-tools like drills or milling cutters. Due to the small size of such devices (< 50 µm) and the extreme hardness of WC(Co) traditional mechanical techniques are not applicable. Focused ion beam milling is an alternative approach for processing this material. Three different prototypes of rotating milling cutters were fabricated on commercial HSS and WC blanks with a tip diameter of 50 µm by sputtering using a 35 keV Au^+ beam of 1.0 nA on the FIB system IMSA-100. In spite of the grain structure of WC(Co) smooth surfaces and sharp edges with radii in the nm-scale could be achieved. For accurate rotation of the tool during ion milling a special sample holder with an angle increment of 0.28° was employed. The prototypes were successfully tested under real-world conditions on a brass substrate at the University of Karlsruhe.

Collaboration: [1]Universität Karlsruhe (TH), Institut für Werkzeugmaschinen und Betriebstechnik

L. Bischoff
J. Teichert

Writing cobalt FIB implantation into 6H:SiC for $CoSi_2$ synthesis

Test microstructures were implanted with Co ions into 6H:SiC, n-type, doped with 10^{18} N/cm^3 using a 35 keV mass-selected focused ion beam working with a $Co_{36}Nd_{64}$ alloy liquid metal ion source. The fluence was varied in the range from $5x10^{16}$ cm^{-2} to $2.5x10^{17}$ cm^{-2} and the target temperature was RT and 400 °C, respectively. The resistivity was measured as a function of fluence, implantation and annealing temperature (t = 30 min, N_2 ambient). After annealing between 700 °C and 1000 °C the resistivity increased with temperature and dropped then down to a value below 1 mΩcm at 1250 °C. For higher annealing temperatures an Ar ambient was chosen but the resistivity increases which can be interpreted in terms of surface erosion. In the case of irradiation at RT and annealing at 1150 °C, 30 min in N_2 a diode like behavior between the Co implanted layer and the bulk SiC was found although the I-V characteristics showed the influence of parasitic resistors. SEM/EDX and µ-RBS measurements reveal that the Co is located in island like precipitates, which probably consist of silicides in the fully disrupted microstructure. From the experimentally determined sputtering yields the surface binding energies at the two temperatures were estimated.

L. Bischoff
J. Teichert

Optical pattern formation in a-SiC:H films by Ga^+ ion implantation

The optical modification effect of Ga^+ ion implantation in a-SiC:H films was

S. Kitova[1]
T. Tsvetkova[2]

investigated. As a result of the implantation a shift of the absorption edge to lower photon energies was observed. It is accompanied by a remarkable increase of the absorption coefficient up to two orders of magnitude in the measured photon energy range from 1.5 eV to 3.1 eV. The optical contrast thus obtained between implanted and unimplanted regions of the film material was applied for optical pattern formation using the computer controlled focused ion beam system IMSA-100 working with a Ga^+ liquid metal ion source. Possible applications for sub-micron lithography and high-density optical data storage have been suggested.

Collaboration: [1]Central Laboratory for Photoprocesses, Sofia, Bulgaria, [2]Institute of Solid State Physics, Sofia, Bulgaria

Ch. Akhmadaliev
L. Bischoff

Investigation of the ion acoustic effect at high energies - Experiments on the 3 MeV-Tandetron accelerator

Generation of elastic waves in different solid materials during irradiation with pulsed high-energy ion beams was investigated. Elastic waves occur mostly as a result of a momentum transfer from the beam particles and the thermal expansion of a small region of the sample under ion beam bombardment. For the detection of the acoustic waves two types of sensors were applied: a piezoelectric transducer (PZT) and a detector based on the tunneling effect. The signal from the sensor was amplified using an integrated broad-band-width preamplifier (amplification factor of about 80.000). The resulting signal was stored and analyzed on a PC. The PZT sensor showed a good sensitivity but its characteristic contains many resonances. For the tunneling based sensor no such disadvantage were found, but a further development to increase the sensitivity is necessary. All experiments were carried out using a Si ion beam with charge states from +2 up to +5 and energies from 4 to 15 MeV. The beam pulse duration was about 8 μs in the shortest case with a repetition time of about 1 ms. A linear dependence of the amplitude of the acoustic signal on the total power of the ion beam was measured. No significant dependence of the signal behavior on the different charge states of the ions was found.

Supported by DFG

Ch. Akhmadaliev
L. Bischoff

Development of a Scanning Ion Acoustic Microscope based on the IMSA-100 FIB system

The ion acoustic effect was applied for imaging of microstructures in order to investigate near subsurface features of a sample. In this system an intensity modulated focused ion beam was used at frequencies up to 4 MHz. For detecting the acoustic signal a PZT sensor with an integrated preamplifier was used. In order to obtain a maximum output signal, all measurements were made at the resonance frequency of the sensor. The signal from the preamplifier was filtered and amplified using a lock-in technique and displayed on a PC. The lateral resolution of this kind of microscope is a function of the modulation frequency and the target parameters. About 5 μm (FWHM) on a Si and 2 μm on a glass substrate were obtained. A further increase of the frequency was not possible on the IMSA-100 FIB system due to restrictions caused by the blanking system. Also the dependence of the signal amplitude on the FIB current density investigated, showing only a weak increase upon focusing.

Supported by DFG

Equipment

M. Friedrich
W. Bürger
S. Turuc

Operation and development of the electrostatic accelerators

The ***2 MV VdG accelerator*** has been used mainly for RBS analysis. The charging system of the belt has been changed from the multi-needle charge spray to an arrangement with tungsten foil pieces (thickness 50 µm) touching the belt. In this way the degradation of the insulating gas by the intensive glow discharge at the needles is avoided (with respect to the future use of SF_6). Furthermore, the foil charging operates at a considerably lower voltage resulting in a lower electric stress of the belt.

The ***5 MV Tandem*** has been applied mainly for ion beam analysis and high-energy implantation. In January the basic maintenance of the accelerator – starting in September 2000 - was completed. Especially, the acceleration tube set was exchanged and the overvoltage protection spark gap assembly was reconstructed. The new HVEE tubes show a very low radiation level due to an excellent secondary electron suppression which results in an improved beam stability. The voltage conditioning turned out to be slower and less stable than expected. The accelerator can again be operated up to the original nominal voltage of 5 MV. A higher voltage appears to be possible but was not applied so far. The beam line from the tandem to the high-resolution ERDA magnetic spectrometer has been set up mechanically with most of the control equipment.

The ***3 MV Tandetron*** has been applied mainly for high-energy implantation and ion beam analysis. In December, after 8 years of stable operation, a partial breakdown of the 30 kHz high voltage power transformer made a shutdown necessary. In 2001 the total operating hours of the high-energy accelerators were 1480 h (VdG), 1920 h (Tandetron) and 2190 h (Tandem, starting in February 2001).

R. Grötzschel
U. Kreissig
C. Klein
M. Mäder
T. Wang[1]

The QQDS magnetic spectrometer "Little John" at the 5 MV tandem accelerator

The magnetic spectrometer "Little John", developed by Gils et al. for nuclear reaction studies at the Karlsruhe cyclotron, was reconstructed and installed at the 5 MV tandem accelerator. This instrument can be used both for materials analysis (RBS, ERDA, NRA) with high depth resolution and for ion- solid interaction studies in transmission geometry. The spectrometer consists of two quadrupoles, one 60° dipole with a mean orbit radius of 1.5 m and one sextupole, providing a particle rigidity of 2.5 Tm. This QQDS configuration allows a variable dispersion by placing the focal plane detector at different positions behind the magnets. The maximum focal plane length of 0.5 m corresponds to relative energy ranges E_{min}/E_{max} of 0.65 near the magnets and 0.81 at the most distant position. The calculated values of the energy resolution dE/E at these positions amount to $7 \cdot 10^{-4}$ and $3.8 \cdot 10^{-4}$. The spectrometer can be rotated around the vertical axis of the UHV scattering chamber and connected to ports at fixed angles of 0°, 15°, 30°, 45°, and 60°, respectively. Channeling measurements can be accomplished in a wide temperature range from 25 K to about 2000 K using different goniometers. A silicon multistrip PSD and a one-dimensional position sensitive ionization chamber telescope can be used as focal plane detectors.

Collaboration: [1]Institute of Modern Physics Lanzhou, Chinese Academy of Sciences, P. R. China

M. Friedrich
W. Pilz
N. Bekris[1]
M. Glugla

A compact AMS facility for tritium depth profiling

Depth profiling measurements of tritium in carbon samples have been performed at a dedicated AMS facility equipped in a first step with an air-insulated 100 kV tandem accelerator. The samples were cut from the inner wall of the

M. Kiisk[2]
V. Liechtenstein[3]

fusion experiment JET Culham/UK and prepared in the Forschungszentrum Karlsruhe. At the air-insulated 100 kV tandem accelerator both a gas stripper and diamond-like carbon (DLC) stripper foils have been tested. After successful tests of the long-lived DLC stripper foils a compact SF_6-insulated 100 kV tandem accelerator was constructed and installed in the AMS facility. The 15° analysing magnet was replaced by a 90° magnet to reduce some disturbing background signals. Test measurements at this compact AMS facility have been performed with standard samples from the LLNL Livermore/USA (TiH_2) and from the Tritium Laboratory of the IFIN-Horia Hulubei Bucharest/Romania (tritium in carbon). Depth profiles of other light elements (D, Li, Be, C, etc.) can be measured simultaneously in a SIMS mode without acceleration of the considered ions using the 100 kV tandem.

Collaboration: [1]Forschungszentrum Karlsruhe, [2]University of Lund, Sweden, [3]RRC Kurchatov Institute, Moscow, Russia

Others

J. Cizek[1]
I. Prochazka[1]
O. Melikhova[1]
G. Brauer
W. Anwand
R. Kuzel[1]
M. Cieslar[1]
R.K. Islamgaliev[2]

Defect distributions in ultra-fine grained copper from combining PAS, TEM and XRD

Ultra-fine grained (UFG) materials exhibit a number of unusual properties which are known to be connected with a significant volume fraction of grain boundaries. UFG copper, produced by high-pressure torsion, was studied by means of PAS (slow positron implantation spectroscopy, lifetime and Doppler broadening spectroscopy), TEM and XRD in order to identify defects and their spatial distribution and depth profile. Two types of defects could be identified, i.e. dislocations in the distorted regions along grain boundaries and vacancy clusters consisting of 3-4 vacancies. There is no change in grain size as a function of the distance of the center of the sample discs. The mean coherent domain size close to the surface was found to be 80 $\pm$ 20 nm and slightly increases with depth. The concentration of microvoids is found to decrease with depth and depends on the distance from the center of the sample disc, being lowest in the center. No position dependence of the concentration of dislocations is found.

Supported by BMBF

Collaboration: [1]Charles University, Prague, Czech Republic; [2]Ufa State Aviation Technical University, Ufa, Russia

Glossary

AES	Auger electron spectroscopy
AFM	Atomic force microscopy
AMS	Atomic mass spectrometry
CEMS	Conversion electron Mössbauer spectroscopy
CMOS	Complementary metal-oxide-semiconductor
CV	Capacitance-voltage-characteristics
CVD	Chemical vapor deposition
DLC	Diamond-like carbon
ECR	Electron-cyclotron-resonance
EL	Electroluminescence
ERDA	Elastic recoil detection analysis
ESRF	European Synchrotron Radiation Facility, Grenoble
FEG	Field emission gun (at the TEM)
FIB	Focused ion beam
FIR	Far infrared
FTIR	Fourier transform infrared spectroscopy
FWHM	Full width at half maximum
GDOS	Glow discharge optical spectroscopy
GIXRD	Gracing incidence X-ray diffraction
GMR	Giant magnetoresistance
GRID	Gammy-ray induced Doppler-broadening
IBA	Ion beam analysis
IBIC	Ion beam induced crystallization
IBAD	Ion beam assisted deposition
HSS	High speed steel
IBS	Ion beam synthesis
IV	Current-voltage-characteristics
MBE	Molecular beam epitaxy
MOS	Metal-oxide-semiconductor
NIR	Near infrared
NRA	Nuclear reaction analysis
PAS	Positron annihilation spectroscopy
PECVD	Plasma enhanced chemical vapor deposition
PIGE	Proton-induced Gamma-ray emission
PIII	Plasma immersion ion implantation
PIIIAD	Plasma immersion ion implantation assisted deposition
PIXE	Proton-induces X-ray emission

PL	Photoluminescence
PSD	Position sensitive detector
PVD	Physical vapor deposition
ROBL	**RO**ssendorf Synchrotron **B**eam**L**ine (at the ESRF)
RBS	Rutherford backscattering spectroscopy
RBS/C	Rutherford backscattering spectroscopy under channelling conditions
RF	Radio frequency
RTA	Rapid thermal annealing
SE	Spectroscopic ellipsometry
SEM	Scanning electron microscopy
SIMS	Secondary ion mass spectrometry
SPIS	Slow positron implantation spectroscopy
SQUID	Superconducting quantum interferometer device
SRIM (TRIM)	Computer program “Stopping and Ranges of Ions in Matter”
STM	Scanning tunnel microscope
TEM	Transmission electron microscopy
XANES	X-ray absorption near-edge spectroscopy
XPS	X-ray photoelectron spectroscopy
XRD	X-ray diffraction
XRF	X-ray fluorescence analysis
XTEM	Cross-section transmission electron microscopy

Supporting Institutions

AIF	Arbeitsgemeinschaft Industrieller Forschungsvereinigungen e.V.
AvH	Alexander-von-Humboldt Stiftung
BMBF	Bundesministerium für Bildung und Forschung
BMWI	Bundesministerium für Wirtschaft
DAAD	Deutscher Akademischer Austauschdienst
DFG	Deutsche Forschungsgemeinschaft
EU	European Union
MPG	Max-Planck-Gesellschaft
SMWK	Sächsisches Staatsministerium für Wissenschaft und Kunst
SMWA	Sächsisches Staatsministerium für Wirtschaft und Arbeit
WTZ	Programs of „Scientific-Technical-Cooperation”

Statistics

Publications

Abramof, E., Beloto, A. F., Ueda, M., Günzel, R., Reuther, H.,
Reciprocal space mapping of silicon implanted with nitrogen by plasma immersion ion implantation,
Nucl. Instr. Meth. B **175-177** (2001) 229

Aidinis, C., Mair, G.L.R., Bischoff, L., Papadopoulos, I.,
A study of the temperature dependence of the energy spread and energy deficit of a Ge^{++} ion beam produced by a liquid metal alloy ion source,
J. Phys. D: Appl. Phys. **34** (2001) L 14

Akhmadaliev, Ch., Bischoff, L., Teichert, J., Kazbekov, K.,
Ion acoustic microscopy for imaging of buried structures based on a focused ion beam,
Microel. Eng. **57 – 58** (2001) 659

Anwand, W., Brauer, G., Hasegawa, M., Dersch, O., Rauch, F.,
A study of positron properties in quartz crystals and synthetic silica glass,
Acta Phys. Polonica A **99** (2001) 321

Anwand, W., Brauer, G., Panknin, D., Skorupa, W.,
Ion implantation induced defects in 6H-SiC and their annealing behaviour,
Mat. Sci. Forum **363-365** (2001) 442

Anwand, W., Brauer, G., Skorupa, W.,
Evolution of ion implantation-caused vacancy-type defects in 6H-SiC probed by slow positron implantation spectroscopy,
Appl. Surf. Sci. **184** (2001) 247

Barbiellini, B., Kuriplach, J., Anwand, W., Brauer, G.,
Calculation of positron characteristics in silicon carbide,
in: Silicon carbide – materials, processing and devices, Mat. Res. Soc. Symp. Proc. Vol. **640**, Eds. A.K. Agarwal, J.A. Cooper, Jr., E. Janzen, M. Skowronski (Materials Research Society, Warrendale/PA, 2001) p. H.5.25.1

Barradas, N.P., da Silva, M.F., Soares, J.C., Kreissig, U., Arnoldbik, W., Cardoso, S., Freitas, P.P.,
High resolution IBA analysis of spin dependent tunnel junctions,
Modern Phys. Lett. B **15** (2001) 1288

Bauer, A., Reischauer, Ph., Kräusslich, J., Schell, N., Matz, W., Goetz, K.,
Structure refinement of the silicon carbide polytypes 4H and 6H: unambiguous determination of the refinement parameters,
Acta Cryst. A **57** (2001) 60

Beloto, A. F., Ueda, M., Abramof, E., Senna, J. R., Leite, N. F., da Silva, M. D., Reuther, H.,
Porous silicon implanted with nitrogen by plasma immersion ion implantation,
Nucl. Instr. Meth. B **175-177** (2001) 224

Belov, A.Yu., Jäger, H.U.,
Elastic properties of diamond-like amorphous carbon films grown by computer simulation of ion-beam deposition process,
Mat. Res. Soc. Symp. Proc. **648** (2001) P6.53.

Berberich, F., Matz, W., Kreissig, U., Richter, E., Schell, N., Möller, W.,
Structural characterisation of hardening of Ti-Al-V alloys after nitridation by plasma immersion ion implantation,

Appl. Surf. Sci. **179** (2001) 13

Berg, S., Möller, W., Rie, K.T., (Eds.)
Plasma Surface Engineering. Proceedings of the 7th Int. Conf. on Plasma Surface Engineering
Surf. Coat. Technol. **142-144** (2001)

Bischoff, L., Teichert, J., Ganetsos, T., Mair, GLR.,
Effect of temperature on the electric emission characteristics of liquid metal alloy ion sources,
J. Vac. Sci. Technol. B **19** (2001) 76

Bischoff, L., Teichert, J., Hausmann, S.,
Dose rate dependence of irradiation damage in silicon,
Nucl Instr. Meth. B **178** (2001) 165

Bischoff, L., Teichert, J.,
Writing cobalt FIB implantation into 6H:SiC,
Appl. Surf. Sci. **184** (2001) 336

Bischoff, L., Teichert, J., Heera, V.,
Focused ion beam sputtering investigations on SiC,
Appl. Surf. Sci. **184** (2001) 372

Bobek, T., Facsko, S., Dekorsy, T., Kurz, H.,
Ordered quantum dot formation on GaSb surfaces during ion sputtering,
Nucl. Instr. Meth. B **178** (2001) 101

Borodin, V.A., Heinig, K.-H., Schmidt, B., Oswald, S.,
Oxidation of Ge implanted into SiO_2 layers: Modeling and XPS,
Nucl. Instr. Meth. B **178** (2001) 115

Calcagno, L., Hallen, A., Martins, R., Skorupa, W.,
Amorphous and crystalline silicon carbide: Material and applications,
Appl. Surf. Sci. **184** (2001) complete volume

Cumblidge, S.E., Catchen, G.L., Motta, A.T., Brauer, G., Böhmert, J.,
Effects of neutron irradiation and thermal annealing on model alloys using positron annihilation techniques,
in: Effects of radiation on materials. 20th Int. Symp., Williamsburg/VA 2000,
Eds. S.T. Rosinski, M.L. Grossbeck, T.R. Allen, A.S. Kumar, ASTM STP 1405 (American Society for Testing and Materials, West Conshohocken/PA, 2001) p. 247

Danesh, P, Pantchev, B., Grambole, D., Schmidt, B.,
Depth distributions of hydrogen and intrinsic stress in a-Si:H films prepared from hydrogen-diluted silane,
J. Appl. Phys. **90** (2001) 3065

Dekorsy, T.,
Bloch Oszillationen und ihre Kopplung an optische Phononen,
Physikalische Blätter **57** (2001) 67

Dubiel, S. M., Cieslak, J., Zukrowski, J., Reuther, H.,
Spin-density enhancement in a ^{119}Sn implanted (110)Cr single crystal as evidenced by Mössbauer spectroscopy,
Phys. Rev. B **63** (2001) 060406

Ecker, K.H., Berger, A., Grötzschel, R, Persson, L., Wätjen, U.,

Antimony implanted in silicon - A thin layer reference material for surface analysis,
Nucl. Instr. Meth. B **175** (2001) 797

Facsko, S., Bobek, T., Dekorsy, T., Kurz, H.,
Ordered quantum dot formation by ion sputtering,
Phys. Stat. Sol. B **224** (2001) 537

Facsko, S., Kurz, H., Dekorsy, T.,
Energy dependence of quantum dot formation by ion sputtering,
Phys. Rev. B **63** (2001) 165329

Fitting, H.-J., Barfels, T., Schmidt, B., von Czarnowski, A.,
Cathodoluminescence depth profiling of Ge-implanted SiO_2 layers,
Solid State Phenom. **78-79** (2001) 119

Fitting, H.-J., Barfels, T., Trukhin, A.N., Schmidt, B.,
Cathodoluminescence of crystalline and amorphous SiO_2 and GeO_2,
J. Non-Cryst. Solids **279** (2001) 51

Fitz, C., Kolitsch, A., Fukarek, W.,
Stress relaxation during annealing of boron nitride films,
Thin Solid Films **389** (2001) 173

Fradin, J., Thome, T., Grynszpan, R.I., Thome, L., Anwand, W., Brauer, G.,
Damage induced by argon ion implantation in cubic zirconia,
Mat. Sci. Forum **363-365** (2001) 514

Fradin, J., Thome, T., Grynszpan, R.I., Thome, L., Anwand, W., Brauer, G.,
Precursory stage of damage production in argon irradiated cubic zirconia,
Nucl. Instr. Meth. B **175** (2001) 516

Friedrich, M., Pilz, W., Sun, G., Penzhorn, R.-D., Bekris, N., Behrisch, R., García-Rosales, C.,
Tritium depth profiling by AMS in carbon samples from fusion experiments,
Physica Scripta T **94** (2001) 98

Funke, H., Bernhard, G., Claußner, J., Jansen, K.-H., Matz, W., Nitsche, H., Oehme, W., Reich, T., Röllig, D.,
Technical description of the radiological safety system for X-ray absorption spectroscopy experiments on radioactive samples at the Rossendorf Beamline,
Kerntechnik **66** (2001) 195

Ganetsos, Th., Mair, G. L. R., Bischoff, L., Teichert, J., Kioussis, D.,
A study of liquid metal alloy ion sources for the production of ions of interest in the microelectronics industry,
Solid State Electronics **45** (2001) 1049

Ganetsos, T., Aidinis, C., Bischoff, L., Mair, GLR, Teichert, J., Panknin, D., Papadopoulos, I.,
Liquid metal ion source-produced germanium ions for maskless ion implantation,
J. Phys. D: Appl. Phys. **34** (2001) L 11

Gebel, T., Rebohle, L., Zhao, J., Borchert, D., Fröb, H., Borany, J. von, Skorupa, W.,
Ion beam synthesized based formation of Ge - rich thermally grown silicon dioxide layers: a promising approach for a silicon based light emitter,
Mat. Res. Soc. Symp. Proc. **638** (2001) F18.1

Gebel, T., Borany, J. von, Thees, H.-J., Wittmaack, M., Stegemann, K.-H., Skorupa, W.,

Non-volatile memories based on Si^+ – implanted Gate oxides,
Microel. Eng. **59** (2001) 247

Grötzschel, R., Klein, C., Kruse, O.,
The Rossendorf broad-range magnetic spectrometer for high resolution RBS and NRA,
Nucl. Instr. Meth. B **183** (2001) 3

Gueorguiev, Y., Kögler, R., Peeva, A., Panknin, D., Mücklich, A., Yankov, R.A., Skorupa, W.,
Trans-projected-range effect in proximity gettering of impurities in silicon,
Vacuum **62** (2001) 309

Günzel, R., Hornauer, U., Rogozin, A.I., Astrelin, V.T.,
Basic investigation of an integrated modulator for plasma immersion ion implantation,
Surf. Coat. Technol. **136** (2001) 47

Günzel, R., Shevchenko, N., Matz, W., Mücklich, A., Celis, J. P.,
Structural investigation and wear resitance of submicron TiN coatings obtained ba a hybride plasma immersion ion implantation process,
Surf. Coat. Technol. **142-144** (2001) 978

Heinig, K.-H., Schmidt, B., Strobel. M., Bernas, H.,
Inverse Ostwald Ripening and self-organization of nanoclusters due to ion irradiation,
Mat. Res. Soc. Proc. **650** (2001) R9.6.1

Heinig, K.-H., Schmidt, B., Strobel, M., Bernas, H.,
Inverse Ostwald ripening and self-organization of nanoclusters due to ion irradiation,
Mat. Res. Soc. Proc. **647** (2001) O14.6

Heera, V.,
Ion beam synthesis of SiC-diamond-heterostructures,
Comp. Semicond. **7** (2001) 43

Heera, V., Skorupa, W., Stoemenos, J., Pécz, B.,
High dose implantation in 6H-SiC,
Mat. Sci. Forum **353-356** (2001) 579

Heera, V., Panknin, D., Skorupa, W.,
P-type doping of SiC by high dose Al implantation – problems and progress,
Appl. Surf. Sci. **184** (2001) 307

Helm, M., Strasser, G.,
Correlation of vertical transport and infrared absorption in GaAs/AlGaAs superlattices,
Proc. 25th Conf. Phys. Semicond., Eds. N. Miura and T. Ando (Springer, Berlin 2001) p.715

Hennig, C., Panak, P., Reich, T., Roßberg, A., Raff, J., Selenska-Pobell, S., Matz, W., Bucher, J. J., Bernhard, G., Nitsche, H.,
EXAFS investigation of uranium(VI) complexes formed at Bacillus cereus and Bacillus sphaericus surfaces,
Radiochim. Acta **89** (2001) 625

Hu, Y.F., Shan, Y.Y., Beling, C.D., Fung, S., Xie, M.H., Cheung, S.H., Tu, J., Brauer, G., Anwand, W., Tong, D.S.Y.,
GaN thin films on SiC substrates studied using variable energy positron annihilation spectroscopy,
Mat. Sci. Forum **363-365** (2001) 478

Jagielski, J., Kopcewicz, M., Matz, W., Grötzschel, R., Thomé, L.,

Phase transformations in nitrogen-implanted iron layers,
Nucl. Instr. Meth. B **175-177** (2001) 448

Jagielski, J., Piatkowska, A., Matz, W., Richter, E., Gawlik, G., Turos, A.,
Structural and micromechanical properties of ion-beam mixed tungsten-on-steel system,
Vacuum **63** (2001) 671

Jembrih, D., Neelmeijer, C., Schreiner, M., Mäder, M., Ebel, M., Svagera, R., Peev, M.,
Iridescent Art Nouveau glass – IBA and XPS for the characterisation of thin iridescent layers,
Nucl. Instr. Meth. B **181** (2001) 698

Kentsch, U., Tyrroff, H., Zschornack, G., Möller, W.,
Retention of the potential energy of multiply charged argon ions incident on copper,
Phys. Rev. Lett. **87** (2001) 105504

Kleinsorge, B., Rodil, S.E., Adamopoulos, G., Robertson, J., Grambole, D., Fukarek, W.,
Hydrogen and disorder in diamond-like carbon,
Diam. Rel. Mat. **10** (2001) 965

Klimenkov, M., Matz, W., Nepijko, S., Lehmann, M.,
Crystallisation of Ge nanoclusters in SiO_2 caused by electron irradiation in TEM,
Nucl. Instr. Meth. B **179** (2001) 209

Klimenkov, M., Nepijko, S.A., Matz, W., Bao, X.,
The study of Ti doped ZSM-5 zeolite particles and acvities inside them,
J. Cryst. Growth **231** (2001) 577

Klimenkov, M., Borany, J.von., Matz, W., Eckert, J., Wolf, M., Müller, K.-H.,
Structure and magnetic properties of Co nanoclusters fabricated by ion beam synthesis in SiO_2 films,
Appl. Phys. A **73** (2001) DOI 10.1007/s003330100915

Kögler, R., Peeva, A., Eichhorn, F., Kaschny, J.R., Voelskow, M., Skorupa, W., Hutter, H.,
Implantation induced defects in silicon detected by Cu decoration technique,
Electrochem. Soc. Proc. **29** (2001) 133

Kögler, R., Peeva, A., Kaschny, J.R., Skorupa, W., Hutter, H.,
Defect engineering and prevention of impurity gettering at Rp/2 in ion-implanted silicon,
Solid. State Phenom. **82-84** (2001) 399

Kögler, R., Peeva, A., Werner, P., Skorupa, W., Gösele, U.,
Gettering centres in high-energy ion-implanted silicon investigated by point defect recombination,
Nucl. Instr. Meth. B **175** (2001) 340

Kokkoris, M., Kossionides, S., Vlastou, R., Aslanoglou, X.A., Grötzschel, R., Nsouli, B., Kuznetsov, A., Petrovic, S., Paradellis, T.,
Determination of parameters for channeling of protons in SiC polytype crystals in the backscattering geometry,
Nucl. Instr. Meth. B **184** (2001) 319

Kokkoris, M., Kossionides, E., Vlastou, R., Aslanoglou, X.A., Grötzschel, R., Paradellis, T.,
Determination of stopping power of channeled " –particles in SiO_2 in the backscattering geometry,
AIP Conf. Proceedings **576**, Melville, New York (2001) 7

Kokkoris, M., Vlastou, R., Aslanoglou, X.A., Kossionides, E., Grötzschel, R., Paradellis, T.,
Determination of the stopping power of channeled protons in SiO_2 in the backscattering geometry,
Nucl. Instr. Meth. B **173** (2001) 411

Lazar, M., Ottaviani, L., Locatelli, M.L., Raynaud, D., Planson, D., Morvan, E., Godignon, P., Skorupa, W., Chante, J.P.,
High electrical activation of aluminium and nitrogen implanted in 6H-SiC at room temperature by RF annealing,
Mat. Sci. Forum **353-356** (2001) 571

Madhusoodanan, K. N., Heera, V., Panknin, D., Skorupa, W.,
Spreading resistance measurements at nano-crystalline SiC induced by ion beam induced crystallization,
Appl. Surf. Sci. **184** (2001) 209

Malkow, T., Arce-Garca, L., Kolitsch, A., Schneider, D., Bull, S.J., Page, T.F.,
Mechanical properties and characterisation of very thin CN"x films synthesised by IBAD,
Diam. Rel. Mat. **10** (2001) 2199

Mändl, S., Günzel, R., Hammerl, C., Richter, E., Rauschenbach, Möller, W.,
PIII-nitriding of boron implanted stainless steel,
Surf. Coat. Technol. **136** (2001) 176

Martin, J., Bischoff, L., Wannemacher, R.,
Microscopy of ion-beam generated fluorescent color center patterns in LiF,
Opt. Commun. **188** (2001) 119

Masri, P., Rouhani Laridjani, M., Pezoldt, J., Yankov, R.A., Skorupa, W.,
$(AlN)_X(SiC)_{1-X}$ buried layers implanted in 6H-SiC: A theoretical study of their optimised composition,
Appl. Surf. Sci. **184** (2001) 383

Matz, W., Schell, N., Neumann, W., Bøttiger, J., Chevallier, J.,
A two-magnetron sputter deposition chamber for in situ observation of thin film growth by synchrotron radiation scattering,
Rev. Sci. Instr. **72** (2001) 3344

Michely, T., Kalff, M., Comsa, G., Strobel, M., Heinig, K.-H.,
Step edge diffusion and step atom detachment in surface evolution: ion erosion of Pt(111),
Phys. Rev. Lett. **86** (2001) 2589

Mohsen, M., Ismail, H., Ashry, A., Brauer, G., Mohamed, S.,
Lattice defects in industrial Al probed by positrons,
Mat. Sci. Forum **363-365** (2001) 216

Müller, T., Heinig, K.-H., Schmidt, B.,
Formation of Ge nanowires in oxidized silicon V-grooves by ion beam synthesis,
Nucl. Instr. Meth. B **175-177** (2001) 468

Müller, T., Heinig, K.-H., Schmidt, B.,
Shape evolution of oxidized silicon V-grooves during high dose ion implantation,
Nucl. Instr. Meth. B **178** (2001) 109

Müller, T., Schmidt, B., Heinig, K.-H., Mücklich, A., Möller, W.,
Synthesis of spatially controlled nanostructures by ion implantation in V-grooves on (001)Si surfaces,
Mat. Res. Soc. Proc. **647** (2001) O10.2

Nagel, M., Dekorsy, T., Brucherseifer, M., Haring-Bolivar, P., Kurz, H.,
Characterization of polypropylene thin-film microstrip lines at millimeter and submillimeter wavelengths,
Microw. Opt. Techn. Lett. **29** (2001) 97

Nancheva, N., Docheva, P., Anwand, W., Brauer, G.,
Characterization of Sn films on silicon by slow positron implantation spectroscopy,
Acta Phys. Polonica A **99** (2001) 435

Nicht, E.-M., Brauer, G., Tempus, G.,
Longtime aging behaviour of the alloy Al-2024 characterized by positron annihilation spectroscopy,
Acta Phys. Polonica A **99** (2001) 441

Ottaviani, L., Lazar, M., Locatelli, M.L., Heera, V., Voelskow, M., Skorupa, W.,
Investigation of Al-implanted 6H- and 4H-SiC layers after fast heating rate annealings,
Appl. Surf. Sci. **184** (2001) 330

Österman, J., Hallen, A., Anand, S., Linnarson, M. K., Andersson, H., Aberg, D., Panknin, D., Skorupa, W.,
Techniques for depth profiling of dopants in 4H-SiC,
Mat. Sci. Forum **353-356** (2001) 559

Panknin, D., Gebel, T., Skorupa, W.,
Flash lamp annealing of implantation doped p- and n-type 6H-SiC,
Mat. Sci. Forum **353-356** (2001) 587

Panknin, D., Stoemenos, J., Eickhoff, M., Heera, V., Skorupa, W.,
The beneficial role of flash lamp annealing on the epitaxial growth of 3C-SiC on Si,
Appl. Surf. Sci. **184** (2001) 377

Panknin, D., Stoemenos, J., Eickhoff, M., Heera, V., Vouroutzis, N., Krötz, G., Skorupa, W.,
Improvement of the 3C-SiC/Si interface by flash lamp annealing,
Mat. Sci. Forum **353-356** (2001) 151

Panknin, D., Wirth, H., Mücklich, A., Skorupa, W.,
Electrical and microstructural properties of higly boron-implantation doped 6H-SiC,
J. Appl. Phys. **89** (2001) 3162

Pantchev, B., Danesh, P., Kreissig, U., Schmidt, B.,
Dependence of electrical conductance of a-Si:H films on Na concentration in glass substrate,
Opto-Electronics Rev. **9** (2001) 431

Pantchev, B., Danesh, P., Savatinova, I., Liarokapis, E., Schmidt, B., Grambole, D.,
The effect of structural disorder on mechanical stress in a-Si : H films,
J. Phys. D - Appl. Phys. **34** (2001) 2589

Pecz, B., Barna, A., Heera, V., Fontaine, F., Skorupa, W.,
TEM investigations of Si implanted natural diamond,
Mat.Sci. Forum **353-356** (2001) 199

Peeva, A., Fichtner, P.F.P., Behar, M., Koegler, R., Skorupa, W.,
Helium implantation induced metal gettering in silicon at half of the projected ion range,
Nucl. Instr. Meth. B **175** (2001) 176

Persson, P. O. A., Skorupa, W., Panknin, D., Kuznetsov, A., Hallen, A., Hultman, L.,
Structural defects in ion implanted 4H-SiC epilayers
Mat.Res.Soc.Symp.Proc. **640** (2001) H6.2.1

Pham, M.T., Maitz, M.F., Grambole, D., Herrmann, F., Reuther, H., Richter, E.,
Surface stimuli to precipitating hydroxyapatite on titanium,
J. Mat. Sci. Lett. **20** (2001) 295

Piazza, F., Arnal, Y., Grambole, D., Herrmann, F., Kildemo, M., Lacoste, A., Relihan, G., Golanski, A.,
Influence of the process parameters on the properties of hydrogenated amorphous carbon thin films deposited using ECR plasma,
Thin Solid Films **383** (2001) 196

Piazza, F., Grambole, D., Herrmann, F., Relihan, G., Barthe, M. F., Desgardine, P., Golanski, A.,
Incorporation of hydrogen and oxygen into (t)a-C:H thin films deposited using DECR plasma,
Mat. Res. Soc. Proc. **675** (2001) W10.3.1

Piekoszewski, J., Chmielewski, A.G., Licki, J., Sartowska, B., Werner, Z., Barson, S.D., Skeldon, P., Thompson, G.E., Richter, E., Wieser, E., Cerny, I., Hnilica, F., Fürbacher, I.,
Laboratory-unit investigations of palladium-treated titanium foil for dry scrubber application,
Rad. Phys. Chem. **62** (2001) 253

Posselt, M.,
Improving the understanding of ion-beam-induced defect formation and evolution by atomistic computer simulations,
Mat. Res. Soc. Proc. **647** (2001) O2.1.1

Posselt, M., Belko, V., Chagarov, E.,
Influence of polytypism on elementary processes of ion-beam-induced defect production in SiC,
Nucl. Instr. Meth. B **180** (2001) 17

Posselt, M., Bischoff, L., Teichert, J.,
Influence of dose rate and temperature on ion-beam-induced defect evolution in Si investigated by channeling implantation at different doses,
Appl. Phys. Lett. **79** (2001) 1444

Posselt, M., Teichert, J., Bischoff, L., Hausmann, S.,
Dose rate and temperature dependence of Ge range profiles in Si obtained by channeling implantation,
Nucl. Instr. Meth. B **178** (2001) 170

Pritzkow, W., Vogl, J., Berger, A., Ecker, K., Grötzschel, R., Klingbeil, P., Persson, L., Riebe, G., Wätjen, U.,
Contribution of ICP-IDMS to the certification of antimony implanted in a silicon wafer - comparison with RBS and INAA results,
Fresenius J. of Analytical **371** (2001) 867

Prokert, F., Noetzel, J., Schell, N., Wieser, E., Matz, W., Gorbunov, A.,
Reflectivity and diffraction study of cross-beam pulsed laser deposited Co/Cu multilayers,
Thin Solid Films **394** (2001) 164

Rebin, M., Henrion, W., Stauss, P., Diesner, K., Panknin, D.,
Optical investigations of ß-$FeSi_2$ with and without Cr addition,
J. Appl. Phys. **90** (2001) 5018

Rebohle, L., Borany, J. von, Borchert, D., Fröb, H., Gebel, T., Helm, M., Möller, W., Skorupa, W.,
Efficient blue light emission from silicon: The first integrated Si-based optocoupler,
Electrochem. Solid State Lett. **7** (2001) G57

Rebohle, L., Gebel, T., Fröb, H., Reuther, H., Skorupa, W.,
Ion beam processing for Si/C-rich thermally grown SiO_2 layers: photoluminescence and microstructure,
Appl. Surf. Sci. **184** (2001) 156

Rebohle, L., Gebel, T., Borany, J. von, Fröb, H., Borchert, D., Skorupa, W.,
Strong visible electroluminescence from Ge- and Sn-implanted silicon dioxide layers,
Mat. Sci. Eng. C **19** (2001) 373

Rebohle, L., Gebel, T., Borany, J. von, Skorupa, W., Helm, M., Pacifici, D., Franzò, G., Priolo, F.
Transient behavior of the strong violet electroluminescence of Ge-implanted SiO_2 layers,
Appl. Phys. B **74** (2001) 53

Reuther, H., Behr, G., Teresiak, A.,
Determination of the hyperfine parameter of α-$FeSi_2$ by angle dependent Mössbauer spectroscopy on single crystals,
J. Phys.: Condens. Matter **13** (2001) L225

Richter, E., Piekoszewski, J., Prokert, F., Stanislawski, J., Walis, L., Wieser, E.,
Alloying of silicon on Ti6Al4V using high – intensity pulsed plasma beams,
Vacuum **63** (2001) 523

Rizza, G.C., Strobel, M., Heinig, K.-H., Bernas, H.,
Ion irradiation of gold inclusions in SiO_2: Experimental evidence for inverse Ostwald ripening,
Nucl. Instr. Meth. B **178** (2001) 78

Schell, N., Matz, W., Eichhorn, F., Prokert, F., Berberich, F.,
Synchrotron radiation studies of thin films and implanted layers with the materials research endstation of ROBL,
J. Alloys Comp. **328** (2001) 105

Schmidt, B., Heinig, K.-H., Mücklich, A.,
Evolution of ion beam synthesized Au nanoclusters in SiO_2 under ion irradiation,
Mat. Res. Soc. Proc. **647** (2001) O11.20.1

Schweitz, K. O., Chevallier, J., Bøttiger, J., Matz, W., Schell, N.,
Hardness in Ag/Ni, Au/Ni and Cu/Ni multilayers,
Phil. Mag. A **81** (2001) 2021

Sendezera, E.J., Davidson, A.T., Anwand, W., Brauer, G., Nicht, E.-M.,
Positron annihilation lifetime study of pure and doped LiF,
Mat. Sci. Forum **363-365** (2001) 386

Seppälä, A., Rauhala, E., Grötzschel, R.,
Lattice location of implanted tellurium in GaN heteroepitaxial films,
J. of Phys. D: Appl. Phys. **34** (2001) 269

Serre, C., Panknin, D., Perez-Rodriguez, A., Romano-Rodriguez, A., Morante, J. R., Kögler, R., Skorupa, W., Esteve, J., Acero, M. C.,
Structural and electrical characterization of ion beam synthesized and n-doped SiC layers,
Mat. Sci. Forum **353-356** (2001) 591

Serre, C., Perez-Rodriguez, A., Romano-Rodriguez, A., Morante, J.R., Esteve, J., Acero, M.C., Koegler, R., Skorupa, W.,
SICOI (silicon carbide-on-insulator) structures. Technology and characterisation,
In "Progress in Semiconductor-On-Insulator Structures and Devices Operating at Extreme Conditions",
Eds. F. Balestra and A. Nazarov, NATO ASI Series, Kluwer Academic Publishers B.V. (Dordrecht, The Netherlands), 2001

Serre, C., Panknin, D., Perez-Rodriguez, A., Romano-Rodriguez, A., Morante, J. R., Kögler, R., Skorupa, W., Esteve, J., Acero, M. C.,
Ion beam synthesis of n-type doped SiC layers,
Appl. Surf. Sci. **184** (2001) 367

Silva, D.L. da, Fichtner, P.F.P., Peeva, A., Behar, M., Koegler, R., Skorupa, W.,
The effects of implantation temperature on He bubble formation in silicon,
Nucl. Instr. Meth. B **175** (2001) 335

Spiga, S., Ferrari, S., Fanciulli, M., Schmidt, B., Heinig, K.-H., Grötzschel, R., Mücklich, A., Pavia, G.,
Kinetics of ion beam synthesis of Sn and Sb in SiO_2 layers,
Mat. Res. Soc. Proc. **647** (2001) 011.23.1

Stan-Sion, C., Behrisch, R., Coad, J.P., Kreissig, U., Kubo, F., Lazarev, V., Lindig, S., Mayer, M., Nolte, E., Peacock, A., Rohrer, L., Roth, J.,
Hydrogen isotope depth profiling in carbon samples from the erosion dominated inner vessel walls of JET,
J. Nucl. Mat. **290** (2001) 491

Strasser, G., Gianordoli, S., Schrenk, W., Gornik, E., Mücklich, A., Helm, M.,
MBE-grown GaAs/AlGaAs and strained InGaAs/AlGaAs/GaAs quantum cascade lasers,
J. Crystal Growth **227-228** (2001) 197

Strobel, M., Heinig, K.-H., Michely, T.,
Mechanisms of pit coarsening in ion erosion of fcc(111) surfaces: a kinetic 3D lattice Monte-Carlo study,
Surf. Sci. **486** (2001) 136

Strobel, M., Heinig, K.-H., Michely, T.,
Three-dimensional kinetic lattice Monte-Carlo simulation of ion erosion of fcc(111) surfaces,
Nucl. Instr. Meth. B **178** (2001) 105

Strobel, M., Heinig, K.-H., Möller, W.,
Three-dimensional domain growth on the size scale of the capillary length: Effective growth exponent and comparative atomistic and mean field simulations,
Phys. Rev. B **64** (2001) 245422

Strobel, M., Heinig, K.-H., Möller, W.,
Understanding ion beam synthesis of nanostructures: Modeling and atomistic simulations,
Mat. Res. Soc. Proc. **647** (2001) O2.3

Telbizova, T., Chevolleau, T., Möller, W.,
Nitrogen incorporation and loss during ion nitriding of Al,
Nucl. Instr. Meth. B **184** (2001) 347

Telbizova, T., Parascandola, S., Prokert, F., Barradas, N.P., Richter, E., Möller, W.,
Ion nitriding of Al: growth kinetics and characterisation of the nitride layer,
Surf. Coat. Technol. **142-144** (2001) 1028

Thome, T., Fradin, J., Grynszpan, R.I., Anwand, W., Brauer, G.,
Positron implantation depth profiles in alpha-irradiated 18 carats gold,
Nucl. Instr. Meth. B **178** (2001) 342

Thome, T., Fradin, J., Grynszpan, R.I., Anwand, W., Brauer, G.,
Depth-dependence recovery of helium-implanted 18 carats gold-silver alloy,

Mat. Sci. Forum **363-365** (2001) 484

Tyschenko, I.E., Zhuravlev, K.S., Vandyshev, E.N., Misiuk, A., Yankov, R.A., Rebohle, L., Skorupa, W.,
Study of photoluminescence in SiOxNy films implanted with Ge ions and annealed under the conditions of hydrostatic pressure,
Semiconductors **35** (2001) 129

Tyschenko, I.E., Rebohle, L., Talochkin, A.B., Kolesov, B.A., Voelskow, M., Misiuk, A., Skorupa, W.,
Blue-green photoluminescence from silicon dioxide films containing Ge^+ nanocrystals formed under conditions of high hydrostatic pressure annealing,
Solid. State Phenomena **82-84** (2001) 607

Tyschenko, I.E., Zhuravlev, K.S., Vandyshev, E.N., Misiuk, A., Rebohle, L., Skorupa, W., Yankov, R.A., Popov, V.P.,
Enhancement of the intensity of violet and green photoluminescence from Ge^+ ion-implanted SiO_xN_y films caused by hydrostatic pressure during annealing,
Optical Materials **17** (2001) 99

Ueda, M., Reuther, H., Günzel, R., Beloto, A. F., Abramof, E., Berni, L. A.,
High dose nitrogen and carbon shallow implantation in Si by plasma immersion ion implantation,
Nucl. Instr. Meth. B **175-177** (2001) 715

Vlastou, R., Fokitis, E., Kokkoris, M., Kossionides, S., Koubouras, G., Grötzschel, R.,
Characterization of multilayer thin film optical filters using RBS,
AIP Conf. Proceedings **576**, Melville, New York (2001) 436

Weima, J.A., von Borany, J., Kreissig, U., Fahrner, W.R.,
Quantitative analysis of carbon distribution in steel used for thermochemical polishing of diamond films,
J. Electrochem. Soc. **148** (2001) G607

Werner, Z., Piekoszewski, J., Barcz, A., Grötzschel, R., Prokert, F., Stanislawski, J., Szymczyk, W.,
Alloying of Pd into Ti by pulsed plasma beams
Nucl. Instr. Meth. B **175-177** (2001) 767

Wieteska, K., Wierzchowski, W., Graeff, W., Turos, A., Grötzschel, R.,
Synchrotron studies of implanted $In_xGa_{1-x}As$,
J. of Alloys and Compounds **328** (2001) 193

Yee, K. J., Lim, Y. S., Dekorsy, T., Kim, D. S.,
Mechanism for the generation of coherent longitudinal-optical phonons in GaAs/AlGaAs multiple quantum wells,
Phys. Rev. Lett. **86** (2001) 1630

Invited Talks

Bischoff, L., Teichert, J.,
Application of focused ion beams in materials research,
12th Int. School VEIT`01, Varna, Bulgaria, Sept. 17-21, 2001

Borany, J. von, Heinig, K.-H., Klimenkov, M., Rebohle, L., Schmidt, B., Skorupa, W., Stegemann, K.-H.,
Ion beam synthesis of semiconductor nanoclusters in SiO_2 films for opto- and microelectronic applications,
12th Int. School VEIT´01, Varna, Bulgaria, Sept.17-21, 2001

Dekorsy, T.,
Bloch Oszillationen und ihre Kopplung an optische Phononen,
DPG Frühjahrstagung, Hamburg, March 26-30, 2001

Heera, V., Panknin, D., Skorupa, W.,
The p-type doping of SiC by high dose Al-implantation - Problems and progress,
E-MRS Spring Meeting, Strasbourg, France, June 5-8, 2001

Heinig, K.-H., Schmidt, B., Strobel, M., Bernas, H.,
Inverse Ostwald ripening and self-organization of nanoclusters due to ion irradiation,E-MRS 2001 Spring Meeting, Strasbourg, France, June 5-8, 2001

Heinig, K.-H., Schmidt, B., Müller, T., Bernas, H.,
Inverse Ostwald ripening,
Gordon Research Conference, Kimball Union Academy, Meriden, NH, USA, July 1 – 6, 2001

Heinig, K.-H., Schmidt, B., Müller, T., Bernas, H.,
Effects of ion irradiation on metal and semiconductor nanostructures in SiO_2,
11th Conference on Radiation Effects in Insulators REI11, Lisbon, Portugal, Sept 3 – 7, 2001

Heinig, K.-H.,
Microstructural processes in ion irradiated materials,
CECAM Workshop on Modelling Materials: From Atoms to Microstructures, Lyon, France, Sept. 18-21, 2001

Helm, M.,
Subband physics in semiconductor quantum structures and the Rossendorf FEL programme,
Rank Prize Funds Symposium on Applications of Free Electron Lasers, Grasmere, U.K., Sept. 17-20, 2001

Hornauer, U., Günzel, R., Richter, E., Wieser, E., Möller, W., Dettenwanger, F., Schütze, M.,
Protection of TiAl allyos against high temperature oxidation by chlorine plasma immersion ion implantation,
SMMIB 2001, Marburg, Sept. 9-14, 2001

Kolitsch, A., Fitz, C., Fukarek, W., Möller, W.,
Real time in situ stress measurements of ion beam assisted deposition of BN thin films,
E-MRS Strasbourg, France, June 5-8, 2001

Kurz, H., Facsko, S., Bobek, T., Dekorsy, T.,
Ion-induced formation of quantum dots,
APS March Meeting 2001, Seattle, USA, March 12-16, 2001

Möller, W.,
Fundamentals of ion-surface interaction,
12th Int. School VEIT-2001, Varna, Bulgaria, Sept. 17-21, 2001

Möller, W.,
Grundlagen der Ionen-Festkörper-Wechselwirkung,
Sommerschule "Nukleare Sonden und Ionenstrahlen", Bad Blankenburg, Sept. 24-28, 2001

Möller, W.,
Cubic boron nitride thin films: Recent developments,
Int.Conf. Frontiers of Surface Engineering 2001, Nagoya, Japan, Oct. 29 – Nov 2, 2001

Neelmeijer, C., Mäder, M.,
The merits of PIXE in revealing painting techniques,
9th Int. Conf. on Particle-Induced X-ray Emission and its Analytical Applications, Guelph, Canada, June 8-12, 2001

Rebohle, L., Borany, J. von, Fröb, H., Gebel, T., Helm, M., Skorupa, W.,
Ion beam synthesized nanoclusters for silicon-based light emission,
7th Europ. Conf. on Accelerators in Appl. Res. and Techn., University of Surrey, Guildford, UK, Aug. 21-24, 2001

Skorupa, W., Rebohle, L., Gebel, T.,
Group-IV nanocluster formation by ion beam synthesis,
31th Europ. Solid State Device Research Conf. (ESSDERC), Nürnberg, Sept.10-14, 2001

Skorupa, W., Rebohle, L., Gebel, T.,
Ion beam synthesis of nanocluster-rich SiO_2-layers: Electrical and optical properties,
IV Int. School on Physics in Materials Science: Nanomaterials and nanostructures - Fabrication, properties, physical models, Jaszowiec, Poland, Sept. 23-29, 2001

Conference Contributions

Akhmadaliev, Ch., Bischoff, L., Teichert, J., Kazbekov, K., Köhler, B.,
Ion acoustic microskopy for imaging of buried structures based on a focused ion beam system,
DPG Tagung 2001, Hamburg, March 26-30, 2001

Akhmadaliev, Ch., Bischoff, L., Teichert, J., Kazbekov, K.,
Ion acoustic imaging of microstructures using a focused ion beam system,
3rd Int. Conf. on Nuclear and Radiation Physics, Almaty, Republic of Kazakstan, June 4-7, 2001

Akhmadaliev, Ch., Bischoff, L., Teichert, J., Kazbekov, K.,
Ion acoustic microscopy based on IMSA-100 focused ion beam system,
12th Int. School VEIT`01, Varna, Bulgaria, Sept. 17-21, 2001

Anwand, W., Brauer, G., Skorupa, W.,
Evolution of ion implantation-caused vacancy-type defects in 6H-SiC probed by slow positron implantation spectroscopy.
E-MRS Spring Meeting, Strasbourg, France, June 5-8, 2001

Anwand, W., Brauer, G., Skorupa, W.,
Vacancy-type defects in 6H-SiC caused by N^+ and Al^+ high fluence co-implantation,
9th Int. Workshop on Slow Positron Beam Techniques for Solids and Surfaces (SLOPOS-9), Dresden, Germany, Sept. 16-22, 2001

Anwand, W., Brauer, G., Wirth, H., Skorupa, W., Coleman, P.G.,
The influence of substrate temperature on the evolution of ion implantation induced defects in epitaxial 6H-SiC,
9th Int. Workshop on Slow Positron Beam Techniques for Solids and Surfaces (SLOPOS-9), Dresden, Germany, Sept. 16-22, 2001

Arazi, A., Bürger, W., Foestermann, T., Niello, J.F., Knie, K., Korschinek, G., Richter, E., Rugel, G., Wallner, A., Wallner, C.,
AMS measurents of the $^{25}Mg(p,\gamma)^{26}Al$ reaction at stellar energies,
DPG-Tagung, Erlangen, March 20, 2001

Arazi, A., Faestermann, T., Niello, J.F., Knie, K., Korschinek, G., Richter, E., Rugel, G., Wallner, A., Wallner, C.,
AMS measurents of the $^{25}Mg(p,\gamma)^{26}Al$ reaction at stellar energies,
Astronomy with radioaktivities III, Ringberg, May 23-26, 2001

Barfels, T., Schmidt, B., Czarnowski, A. von, Fitting, H.-J.,
Cathodoluminescence depth profiling by electron beam energy variation,
European Microbeam Analysis Society Meeting, Tampere, Finland, May 6-10, 2001

Bartels, A., Dekorsy, T., Kurz, H.,
Wavelength tunable femtosecond Ti:sapphire ring laser with up to 1.5 GHz repetition rate,
Conf. on Lasers and Electro Optics 2001, Baltimore/MD, USA, May 6-11, 2001

Belov, A., Jäger, H.U.,
Calculation of intrinsic stresses in amorphous carbon films grown by molecular dynamics simulation: from atomic to macroscopic scale,
E-MRS 2001 Spring Meeting, Strasbourg, France, June 5-8, 2001

Belov, A., Jäger, H.U.,
Elastic constants of diamond - like amorphous carbon films: the effect of internal stresses,

E-MRS 2001 Spring Meeting, Strasbourg, France, June 5-8, 2001

Berberich, F., Matz, W., Kreißig, U., Schell, N., Richter, E., Möller, W.,
Strukturelle Charakterisierung der Härtung von Ti-Al-V Legierungen nach Plasma-Immersions-Ionen-Implantation mit Stickstoff,
65. Physikertagung, Hamburg, März 26-30, 2001

Bischoff, L., Teichert, J.,
Writing cobalt FIB implantation into 6H:SiC,
E-MRS Spring Meeting, Strasbourg, France, June 5-8, 2001

Bischoff, L., Teichert, J. Heera, V.,
Focused ion beam sputtering investigations on SiC,
E-MRS Spring Meeting, Strasbourg, France, June 5-8, 2001

Bischoff, L., Teichert, J., Kitova, S., Tsvetkova, T.,
Optical pattern formation in a-SiC:H films by Ga^+ ion implantation,
12th Int. School VEIT`01, Varna, Bulgaria, Sept. 17-21, 2001

Borany, J. von, Gebel, T., Skorupa, W., Stegemann, K.-H., Thees, H.-J., Wittmaack, M.,
Non-volatile memories based on Si^+-implanted gate oxides,
12th Conf. on Insulating Films on Semiconductors (INFOS'2001), Udine, Italy, June 20-23, 2001

Boudreault, G., Elliman, R.G., Grötzschel, R., Gujrathi, S.C., Jeynes, C., Lennard, W.N., Rauhala, E., Sajavaara, T., Timmers, H., Weijers, T.D.M.,Round Robin: Measurement of H implants in Silicon by ERD,
15th Int. Conf. on Ion Beam Analysis, Cairns, Australia, July 15-20, 2001

Cizek, J., Prochazka, I., Melikhova, O., Brauer, G., Anwand, W., Kuzel, R., Cieslar, M., Islamgaliev, R.K.,
Investigation of spatial distribution of defects in ultra-fine grained copper,
9th Int. Workshop on Slow Positron Beam Techniques for Solids and Surfaces (SLOPOS-9), Dresden, Germany, Sept. 16-22, 2001

Danesh, P., Pantchev, B., Savatinova, I., Liarokapis, E., Schmidt, B.,
Effect of ion implantation on the structural properties of a-Si:H films,
12th Int. Summer School VEIT 2001, Varna, Bulgaria, Sept.17-21, 2001

Donchev, T., Tsaneva, V., Nurgaliev, T., Spasov, A., Gravier, L., Ansermet, J. Ph., Petrov, I., Petrova, V., Matz, W., Groetzschel, R., Pignard, S., Vincent, H.,
YBCO/LSMO and LSMO/YBCO double layer deposition by off-axis magnetron sputtering and strain effects,
12th Int. School VEIT 2001, Varna, Bulgaria, Sept.17-21, 2001

Donchev, T., Tsaneva, V., Spasov, A., Vlakhov, E.S. Vlakhov, Groetzschel, R., Matz, W., Wieser, E.,
Deposition of $La_{0.7}Sr_{0.3}MnO_3$ base layer for LSMO/YBCO heterostrukture by off-axis R.F. magnetron sputtering
12th Int. School VEIT 2001, Varna, Bulgaria, Sept.17-21, 2001

Dubiel, S. M., Cieslak, J., Zukrowski, J., Reuther, H.,
Spin-density enhancement in the presurface zone of chromium,
Int. Conf. on the Applications of the Mössbauer Effect, Oxford, England, Sept. 2-7, 2001

Eichhorn, F., Kögler, R., Mücklich, A., Schell, N., Matz, W.,
Structural relation between Si and SiC formed by carbon ion implantation,
E-MRS 2001 Spring Meeting, Strasbourg, France, June 5 - 8, 2001

Facsko S., Bobek T., Kurz H., Dekorsy T.,
Ordered quantum dot arrays via sputtering,
Gordon Conference "Material Processes Far from Equilibrium", Meriden/NH, USA, July 1-6, 2001

Fradin, J., Grynszpan, R.I., Thome, L., Anwand, W., Brauer, G.,
Fluence dependence of damage production in Y-stabilized cubic zirconia by rare-gas ion irradiation,
9th Int. Workshop on Slow Positron Beam Techniques for Solids and Surfaces (SLOPOS-9), Dresden, Germany, Sept. 16-22, 2001

Friedrich, M., Bürger, W., Turuc, S., Tyrroff, H.,
New developments at the Rossendorf electrostatic accelerators,
35th Symp. for Northeastern Accelerator Personnel (SNEAP), Lund, Sweden, Oct. 22-25, 2001

Fritsche, B., Chevolleau, T., Kourtev, J., Kolitsch, A., Möller, W.,
Plasma diagnostic of an RF magnetron Ar/N_2 discharge,
12th Int. School VEIT, Varna, Bulgaria, Sept.17-21, 2001

Funke, H., Reich, T., Bernhard, G., Matz, W.,
The radiochemistry station for x-ray absorption spectroscopy experiments at ROBL,
2nd Int. Workshop JINR Synchrotron Radiation Source: DELSY-2001, Dubna, Russia, April 2-6, 2001

Ganetsos, Th., Mair, G.L.R., Bischoff, L.,
Temperature dependence of the electronics characterization and mass spectra of liquid metal alloy ion sources,
IFES 2001, 47th InternationalField Emission Symposium, Berlin, Germany, July 29 - Aug. 3, 2001

Gebel, T., Rebohle, L., Howitz, S., Borany, J. von, Skorupa, W.,
Silizium basierte Lichtemitter: Neue Möglichkeiten für Lab-on-Chip Systeme?
2. Biosensor Symposium, Tübingen, Germany, April 01-03, 2001

Gebel, T., Rebohle, L., Zhao, J., Borany, J. von, Stegemann, K.H., Mrstik, B., Skorupa, W.,
Ion beam synthesized group IV nanoclusters in SiO_2 layers: a promising approach for non-volatile memories and silicon based light emitters,
MRS Spring Meeting, San Francisco, USA, April 16-20, 2001

Gebel, T., Voelskow, M., Skorupa, W., Mannino, G., Privitera, V., Priolo, F., Napolitani, E., Carnera, A.,
Flash lamp annealing with millisecond pulses for ultra shallow boron profiles in silicon
E-MRS 2001 Spring Meeting, Strasbourg, France, June 4-8, 2001

Gebel, T., Borany, J. von, Thees, H.-J., Wittmaack, M., Stegemann, K.-H., Skorupa, W.,
Non-volatile memories based on Si^+ – implanted Gate oxides,
Int. Conf. on Insulating Films On Semiconductors (INFOS 2001), Udine, Italy, June 20-23, 2001

Ghosh, A.W., Jönsson, L., Wilkins, J.W., Dekorsy, T., Bartels, A., Kurz, H.,
Coupled Bloch-phonon modes in superlattices,
Quantum Electronics and Laser Science Conference 2001, Baltimore/MD, USA, May 6-11, 2001

Golanski, A., Grambole, D., Hommet, J., Herrmann, F., Kern, P., Mc Donnel, L., Piazza, F., Stoquert, J.-P.,
Nano-structured amorphous carbon films synthesized using DECR plasma,
MRS Spring Meeting, San Francisco, USA, April 16-20, 2001

Grigorov, K., Beshkov, G., Maciel, H. S., Djouadi, A., Matz, W., Anguelov, Ch., Velchev, N.,
AlN films obtained by broad energy nitrogen ion implantation and Rapid Thermal Annealing Process,
Int. Conf. Diamond 2001, Budapest, Hungary, Sept. 1-4, 2001

Grigorov, K., Donchev, T., Tsaneva, V., Spasov, A., Matz, W., Groetzschel, R.,
RBS and ion channelling study of YBCO/STO and YBCO/LSMO/STO structures oxygen content estimated by X-ray diffraction,
12th Int. School VEIT 2001, Varna, Bulgaria, Sept.17-21, 2001

Günzel, R., Matz, W., Ivanov, Yu.F., Shevchenko, N., Rotshtein, V.P.,
Pulsed electron-beam treatment of high-speed steel: structure-phase transformations and wear resistance,
Int. Conf. on Pulsed Power Applications, Gelsenkirchen, March 27 - 29, 2001

Günzel, R., Rogozin, A., Brutscher, J., Demski, M., Filaiov, A.,
Generation of high voltage pulses for plasma–based ion implantation devices,
6th Int. Workshop on Plasma-based Ion Implantation, Grenoble, France, June 25-28, 2001

Heinig, K.-H., Schmidt, B., Müller, T.,
Nanocluster formation: Atomistic simulations and impact of atmospheric moisture.
Projekttreffen NEON, CEMES/CNRS, Toulouse, France, Jan 31 – Feb 4, 2001

Heinig, K.-H., Schmidt, B., Müller, T.,
Tailoring the size and size distribution of nanoclusters through ion irradiation,
Annual Meeting of the German Physical Society, Hamburg, March 26-30, 2001

Heinig, K.-H., Schmidt, B., Borany, J. von, Müller, T., Bernas, H.,
Self-organization of nanostructures with ion beams,
E-MRS Spring Meeting, Strasbourg, France, June 5-8, 2001

Heinig, K.-H., Novikov, P.,
Ion-irradiation stimulated Ge nanocluster formation in gate oxides containing GeO_2,
Projekttreffen NEON, Uni Århus, Denmark, August 19-21, 2001

Heinig, K.-H., Novikov, P., Larsen, A.N., Dvurechenskii, A.,
Simulation of ion-irradiation stimulated Ge nanocluster formation in gate oxides containing GeO_2,
11th Conference on Radiation Effects in Insulators REI11, Lisbon, Portugal, Sept 3 – 7, 2001

Hornauer, U.,
Cl Plasma-Immersions-Ionenimplantation zur Verbesserung des Hochtemperaturoxidationsverhaltens von TiAl,
VIII. Erfahrungsaustausch "Oberflächentechnologie mit Plasmaprozessen", Mühlleithen, March 13-15, 2001

Jäger, H.U.,
Understanding of ta-C film deposition by means of atomistic simulations,
International Conference on Materials for Advanced Technologies (ICMAT 2001), Singapore, July 1-6, 2001

Jiraskova, Y., Brauer, G., Schneeweiss, O., Blawert, C., Anwand, W., Coleman, P.G.,
The migration of defects and nitrogen atoms in nitrided surface layers of austenitic stainless steel followed by microscopic methods,
9th Int. Workshop on Slow Positron Beam Techniques for Solids and Surfaces (SLOPOS-9), Dresden, Germany, Sept.16-22, 2001

Klein, C., Grötzschel, R., Mäder, M.,
Charge state distributions of heavy ions after scattering at surface atoms,
15th Int. Conf. on Ion Beam Analysis, Cairns, Australia, July 15-20, 2001

Knapp, W., Bischoff, L., Teichert, J.,

Solidified liquid metal ion source – formation of a nanoemitter,
12th Int. School VEIT`01, Varna, Bulgaria, Sept. 17-21, 2001

Kögler, R.,
Evidence of vacancy-defects in ion-implanted silicon,
Treffen des 39. Arbeitskreises Punktdefekte, Dresden, Feb.12-13, 2001

Kögler, R., Peeva, A., Kaschny, J.R., Skorupa, W., Hutter, H.,
Prevention of impurity gettering in the Rp/2 region of ion-implanted silicon by defect engineering,
E-MRS Spring Meeting, Strasbourg, France, June 5-8, 2001

Kögler, R., Peeva, A., Eichhorn, F., Kaschny, J.R., Voelskow, M., Skorupa, W., Hutter, H.,
Implantation induced defects in silicon detected by Cu decoration technique,
Symp. on Crystalline Defects and Contamination: their Impact and Control in Device Manufacturing, DECON 2001, Nürnberg, Germany, Sept.13-14, 2001

Kögler, R., Peeva, A., Kaschny, J.R., Skorupa, W., Hutter, H.,
Defect engineering and prevention of impurity gettering at Rp/2 in ion-implanted silicon,
9th Int. Autum Meeting Gettering and Defect Engineering in Semiconductor Technology, GADEST 2001, St. Tecla, Italy, Sept.30-Oct.3, 2001

Komori, K, Yasuhira, T., Wang, X.L., Ogura, M., Först, M., Dekorsy, T., Kurz, H.,
Ultrafast Dynamics of excitons in crescent-shaped GaAs quantum wires,
Quantum Electronics and Laser Science Conference 2001, Baltimore/MD, USA, May 6-11, 2001

Krause-Rehberg, R., Börner, F., Redman, F., Kögler R., Panknin, D., Skorupa, W., Egger, W., Kögel, G., Triftshäuser, W.,
Slow positron defect profiling with enhanced depth resolution
9th Int.Workshop on Slow Positron Beam Techniques for Solids and Surfaces, (SLOPOS-9), Dresden, Germany, Sept. 16-22, 2001

Krause-Rehberg, R., Börner, F., Redman, F., Kögler, R., Kliemann, R., Skorupa, W., Egger, W., Kögel, G., Triftshäuser, W.,
Identification of getter defects in high-energy self-implanted silicon at Rp/2,
ICDS-21, Giessen, Germany, July 2001

Krause-Rehberg, R., Börner, F., Redman, F., Gebauer, J., Kögler, R., Skorupa, W., Kögel, G., Egger, W., Sperr, P., Triftshäuser, W.,
The microscopic nature of gettering defects at Rp/2 in high-energy self-implanted silicon,
9th Int. Conf. on Defects - Recognition, Imaging and Physics in Semiconductors (DRIP IX), Rimini, Italy, Sept. 24-28, 2001

Kreissig, U., Liechtenstein, V.K., Grötzschel, R.,
A combination of ΔE-E gas ionisation chamber and time-of-flight technique for heavy ion ERDA,
15th Int. Conf. on Ion Beam Analysis, Cairns, Australia, July 15-20, 2001

Kuriplach, J., Anwand, W., Brauer, G., Skorupa, W.,
Positron characteristics of various SiO_2 polymorphs,
9th Int. Workshop on Slow Positron Beam Techniques for Solids and Surfaces (SLOPOS-9), Dresden, Germany, Sept. 16-22, 2001

Lebedev, A., Posselt, M., Feudel, T., Variam, N.,
Tailoring of dopant profiles in advanced nMOS transistors,
E-MRS 2001 Spring Meeting, Strasbourg, France, June 5-8, 2001

Linss, V., Pfeifer, T., Halm, T., Hoyer, W., Richter, F., Schell, N.,
Calculation of the unstressed lattice spacing of Al-doped c-Bn thin films using data from synchrotron radiation diffraction experiments,
12th Int. School VEIT 2001, Varna, Bulgaria, Sept.17-21, 2001

Mäder, M., Neelmeijer, C., Schreiner, M.,
Non-destructive composition analysis of glass artefacts for precaution,
1st Int. Conf. „Hyalos Vitrum Glass – History, Technology and Conservation of Glass and Vitreous Materials in the Hellenic World“, Rhodes, Greece, April 1-4, 2001

Madhusoodanan, K.N., Heera, V., Panknin, D., Skorupa, W.,
Spreading resistance measurements at nano-crystalline SiC produced by ion beam induced crystallization,
E-MRS Spring Meeting, Strasbourg, France, June 5-8, 2001

Maitz, M.F.,
The Mat*Med* Database,
MatMed EU Project meeting, Rhodos, Greece, May 9-11, 2001

Maitz, M.F., Pham, M.T., Matz, W., Reuther, H., Richter, E.,
Ion beam treatment of titanium surfaces for enhancing deposition of hydroxyapatite from solution,
E-MRS Spring Meeting, Strasbourg, France, June 5-8, 2001

Maitz, M.F., Pham, M.T.,
Promoted calcium-phosphate precipitation from solution for improved biocompatibility by ion implantation,
SMMIB 2001, Marburg, Sept. 9-14, 2001

Maitz, M.F., Günzel, R., Pham, M.T., Langping, W., Chu, P., Richter, E.,
Ta implantation and deposition for increased X-Ray visibility and hemocompatibility of vascular stents,
5th Asian Symp. on Biomedical Materials, Hongkong, Dec. 9-12, 2001

Maitz, M.F., Pham, M.T., Matz, W., Reuther, H., Steiner, G., Richter, E.,
Hydroxyapatite precipitation on Na implanted titanium,
5th Asian Symp.on Biomedical Materials, Hongkong, Dec. 9-12, 2001

Masri, P., Rouhani Laridjani, M., Pezoldt, J., Yankov, R.A., Skorupa, W.,
$(AlN)_X(SiC)_{1-X}$ buried layers implanted in 6H-SiC: A theoretical study of their optimised composition,
E-MRS Spring Meeting, Strasbourg, France, June 5-8, 2001

Matz, W., Schell, N., Eichhorn, F., Prokert, F., Reich, T., Funke, H., Berberich, F.,
ROBL - A synchrotron radiation beamline for radiochemistry and materials research,
2nd Int. Workshop JINR Synchrotron Radiation Source: DELSY-2001, Dubna, Russia, April 2-6, 2001

Müller, T., Heinig, K.-H., Schmidt, B.,
Template-directed ion beam synthesis of Ge nanowires using V-grooves,
Annual Meeting of the German Physical Society, Hamburg, March 26-30, 2001

Müller, T., Heinig, K.-H., Schmidt, B.,
Self-assembly of nanowires and pearling instability at ion beam synthesis,
E-MRS 2001 Spring Meeting, Strasbourg, France, June 5-8, 2001

Müller, T.,
Nanocluster formation by low energy ion implantation – basic mechanisms,
Projekttreffen NEON, Uni Århus, Denmark, Aug. 19-21, 2001

Oswald, S., Schmidt, B., Heinig, K.-H.,
Einfluss von Ionenstrahlparametern auf die Phasenidentifizierung an Ge Nanopartikeln mittels XPS Tiefenprofilen,
Tagung Festkörperanalytik, Chemnitz, June 25-28, 2001

Ottaviani, L., Lazar, M., Locatelli, M.L., Heera, V., Voelskow, M., Skorupa, W.,
Investigation of Al-implanted 6H- and 4H-SiC layers after fast heating rate annealings,
E-MRS Spring Meeting, Strasbourg, France, June 5-8, 2001

Ottaviani, L., Lazar, M., Locatelli, M.L., Chante, J.P. Heera, V., Skorupa, W., Voelskow, M.., Torchio, P.,
Annealing studies of Al-implanted 6H-SiC in an induction furnace,
9th Int. Conf. on Defects - Recognition, Imaging and Physics in Semiconductors (DRIP IX), Rimini, Italy, Sept. 24-28, 2001

Panknin, D., Skorupa, W.,
P-doping of epitaxial 6H-SiC by boron implantation: Electrical and structural properties,
E-MRS Spring Meeting, Strasbourg, France, June 5-8, 2001

Panknin, D., Stoemenos, J., Eickhoff, M., Heera, V., Skorupa, W.,
The beneficial role of flash lamp annealing on the epitaxial growth of 3C-SiC on Si,
E-MRS Spring Meeting, Strasbourg, France, June 5-8, 2001

Pantchev, B., Danesh, P., Grambole, D., Schmidt, B.,
Development of a-Si:H films during plasma-enhanced CVD from hydrogen-diluted silane,
5th Europ. Res. Conf. Photovoltaic Devices - High Efficiency Solar Cells, Tomar, Portugal, Sept. 8-13, 2001

Pantchev, B., Danesh, P., Kreissig, U., Schmidt, B.,
Elastic recoil detection analysis of ion-exchanged soda-lime glass substrates for a-Si:H devices,
12th Int. Summer School VEIT 2001, Varna, Bulgaria, Sept.17-21, 2001

Pécz, B., Tóth, L., Heera, V., Skorupa, W.,
Synthesis of epitaxial diamond grains in cubic SiC by high temperature carbon implantation,
12th Int. Conf. on Microscopy of Semiconducting Materials (MSM XII), Oxford, March 25-29, 2001

Peeva, A., Fichtner, P.F.P., Kögler, R., Behar, M., Skorupa, W.,
Helium implantation induced metal gettering in silicon at Rp/2,
39. Arbeitskreis Punktdefekte, Dresden, Feb. 12-13, 2001

Peeva, A., Kaschny, J., Kögler, R., Skorupa, W.,
Stabilisation of He cavities in silicon by interstitial type defects,
9th Int. Autumn Meeting on Gettering and Defect Engineering in Semiconductor Technology (GADEST 2001), Catania, Italy, Sep. 30-Oct. 3, 2001

Peikert, M., Wieser, E., Möller, W., Reuther, H., Wenzel, C.,
Enhanced thermal stability of Ta-based thin diffusion barrier by ion implantation,
12th Int. School VEIT 2001, Varna, Bulgaria, Sept.17-21, 2001

Piazza, F., Grambole, D., Herrmann, F., Relihan, G., Barthe, M.F., Desgardine, P., Golanski, A.,
Incorporation of hydrogen and oxygen into (t)a-C:H thin films deposited using DECR plasma,
MRS Spring Meeting, San Francisco, USA, April 16-20, 2001

Posselt, M.,
Atomistische Computersimulation der Defektbildung und –evolution in Si bei Ionenimplantation,
39. Arbeitskreis Punktdefekte, Dresden, Germany, Feb. 12-13, 2001

Prokert, F., Gorbunov, A., Schell, N.,
Ausnutzung der anomalen Streuung bei Reflektivitätsuntersuchungen an Fe-Cr-Doppelschichten mittels Synchrotronstrahlung,
9. DGK-Tagung, Bayreuth, March 12 - 15, 2001

Rebohle, L., Borany, J. von, Fröb, H., Gebel, T., Skorupa, W.,
Luminescence properties of ion-beam synthesized „point defects“ in silicon dioxide,
39. Arbeitskreis Punktdefekte, Dresden, Feb.12-13, 2001

Rebohle, L., Gebel, T., Borany, J. von, Fröb, H., Klimenkov, M., Skorupa, W.,
Strong blue photo- and electroluminescence from tin implanted silicon dioxide,
MRS Spring Meeting, San Francisco, USA, April 16-20, 2001

Rebohle, L., Gebel, T., Fröb, H., Reuther, H., Skorupa, W.,
Luminescence investigations at thin SiO_2 layers after Si- and C-Coimplantation,
E-MRS Spring Meeting, Strasbourg, France, June 5-8, 2001

Rebohle, L., Gebel, T., Borany, J. von, Fröb, H., Borchert, D., Skorupa, W.,
Strong visible electroluminescence from Ge- and Sn-nanocluster rich silicon dioxide layers,
E-MRS Spring Meeting, Strasbourg, France, June 5-8, 2001

Rebohle, L., Gebel, T., Borany, J. von, Skorupa, W., Helm, M.,
Si-based light emission from Ge- implanted SiO_2 layers: Electric and optoelectronic properties,
10th Int. Conf. on Modulated Semiconductor Structures, Linz, July 23-27, 2001

Reuther, H., Behr, G.,
Determination of the hyperfine parameters of iron silicides by angle dependent conversion electron Mössbauer spectroscopy on single crystals,
Int. Conf. on the Applications of the Mössbauer Effect, Oxford, England, Sept. 2-7, 2001

Revesz, A.G., Anwand, W., Brauer, G., Hughes, H.L., Skorupa, W.,
Density gradient in SiO_2 films on silicon as revealed by positron annihilation spectroscopy,
9th International Workshop on Slow Positron Beam Techniques for Solids and Surfaces (SLOPOS-9), Dresden, Germany, September 16-22, 2001

Revesz, A.G., Anwand, W., Brauer, G., Hughes, H.L., Skorupa, W.,
Density gradient in SiO_2 films on silicon as revealed by positron annihilation spectroscopy,
32nd Semiconductor Interface Specialists Conference, Washington/DC, USA, Nov. 29 –Dec. 01, 2001

Richter, E., Piekoszewski, J., Wieser, E., Prokert, F., Stanislawski, J., Walis, L., Reuther, H.,
Modification of titanium surface by its alloying with silicon using intensive pulsed plasma beams,
SMMIB 2001, Marburg, Sept. 9-14, 2001

Richter, E., Prokert, F., Reuther, H., Helm, M.,
Ion beam synthesis of magnesium diboride,
SMMIB 2001, Marburg, Sept. 9-14, 2001

Richter, E., Telbizova, T., Möller, W.,
Growth kinetic and properties of nitride layers produced by low energy ion nitriding and plasma immersion ion implantation of Al and Al alloys,
SMMIB 2001, Marburg, Sept. 9-14, 2001

Rogozin, A., Günzel, R.,
Integrated high voltage modulator for plasma immersion ion implantation,
6th Int. Workshop on Plasma-based Ion Implantation, Grenoble, France, June 25-28, 2001

Romanus, H., Spieß, L., Knedlik, Ch., Cimalla, V., Panknin, D., Skorupa, W., Ecke, G., Gottfried, K.,
High temperature stable contacts to SiC based on tungsten compounds,
E-MRS Spring Meeting, Strasbourg, France, June 5-8, 2001

Sánchez-García, M.A., Ristic, J., Calleja, E., Pérez-Rodríguez, A., Serre, C., Romano-Rodríguez, A., Morante, J.R., Koegler, R., SkorupaW.,
Growth and characterisation of III-Nitrides on SiC/Si(111) susbtrates by Molecular Beam Epitaxy,
North American MBE Conference, Providence, USA, Oct. 2001

Schmidt, B. Heinig, K.-H., Müller, T., Stegemann, K.-H,
Self-organized NC-layers by conventional ion implantation,
Status report WP2: Fundamental related experiments,
NEON-Project Meeting, Aarhus, Denmark, Aug. 20-21, 2001

Schmidt, B., Grambole, D., Herrmann, F.,
Impact of ambient atmosphere on as-implanted amorphous insulating layers,
11th Int. Conf. on Radiation Effects in Insulators (REI-11), Lisbon, Portugal, Sept. 3-7, 2001

Schmidt, J., Schmidt, B.,
Investigation of MOS structures with embedded Si-nanocrystals obtained by r.f. sputtering,
12th Int. School VEIT 2001, Varna, Bulgaria, Sept 17-21., 2001

Schmidt, J., Schmidt, B., Beyer, V.H.,
MOS-structures with embedded nanocrystalline silicon prepared by rf-sputtering,
65. Physikertagung und Frühjahrstagung des Arbeitskreises Festkörperphysik (AKF) der DPG, Hamburg, March 26-30, 2001

Serre, C., Pérez-Rodríguez, A., Romano-Rodríguez, A., Morante, J.R., Esteve, J., Acero, M.C., Panknin, D., Koegler, R., Skorupa, W.,
Ion beam synthesis of SiC on insulator structures,
199th Meeting of the Electrochemical Society, 10th Int. Symp.on Silicon-On-Insulator Technology and Devices, Washington, USA, March 2001

Serre, C., Pankin, D., Pérez-Rodríguez, A., Romano-Rodríguez, A., Morante, J.R., Kögler, R., Skorupa, W., Esteve, J., Acero, M.C.,
Ion beam synthesis of n-type doped SiC layers,
E-MRS Spring Meeting, Strasbourg, France, June 5-8, 2001

Skorupa, W., Pecs, B., Dobos, L., Heera, V.,
Ion beam synthesis of carbon-related phases in silicon carbide and diamond: A new approach to N-doped diamond layers?
MRS Spring Meeting, San Francisco, USA, April 16-20, 2001

Skorupa, W., Peeva, A., Gueorguiev, Y., Kögler, R.,
Metal gettering in the Rp/2 region and beyond Rp of buried implants in silicon: The two sides of the same medal?
MRS Spring Meeting, San Francisco, USA, April 16-20, 2001

Telbizova, T., Chevolleau, T., Möller, W.,
Dependence of nitrogen incorporation on beam energy during ion nitriding of Al,
Int. Conf. on Plasma Based Ion Implantation, Grenoble, France, Jun. 25-28, 2001

Turos, A., Gaca, J., Wojcik, M., Grötzschel, R., Nageswara Rao, S.V.S., Siddiqui, A.M., Pathak, A.P.,
Strain and compositional profile determination ion ion bombarded heterostructures by the complementary use of RBS/channeling and high resolution X-ray diffraction,
15th Int. Conf. on Ion Beam Analysis, Cairns, Australia, July 15-20, 2001

Ueda, M., Silva, M., Otani, C., Reuther, H., Yatsuzuka, M., Lepienski, C., Berni, L.A.,
Improvement of tribological properties of Ti6Al4V by nitrogen plasma immersion ion implantation,
Int. Conf. on Frontiers of Surface Engineering 2001, Nagoya, Japan, Oct. 28 – Nov. 1, 2001

Ueda, M., Reuther, H., Dias, F. G., Rangel, E., Cruz, N.,
Nitrogen plasma ion implantation of Al5052 alloy,
Int. Conf. on Frontiers of Surface Engineering 2001, Nagoya, Japan, Oct. 28 – Nov. 1, 2001

Ujvari, T., Kolitsch, A., Toth, A., Mohai, M., Bertoti, I.,
XPS characterization of the composition and bonding states of elements in CN layers prepared by ion beam assisted deposition,
12th Europ. Conf. on Diamond, Diamond-like Materials, Carbon Nanotubes, Nitrides and Silicon Carbides, Budapest, Hungary, Sept. 2001

Walterfang, M., Keune, R., Reiche, R., Oswald, S., Dobler, M., Reuther, H.,
Tiefenselektive Phasenanalyse der α-$FeSi_2$-Bildung nach Beschuß von β-$FeSi_2$ mittels DCEMS, XPS und AES,
65. Physikertagung, Hamburg, March 26-30, 2001

Walterfang, M., Kruijer, S., Keune, W., Dobler, M., Reuther, H.,
Depth analysis of buried iron disilicide formation by Fe ion implantation into Si,
Int. Conf. on the Applications of the Mössbauer Effect, Oxford, England, Sept. 2-7, 2001

Werner, Z., Piekoszewski, J., Staniliawski, J., Barcz, A., Grötzschel, R., Szymczyk, W., Chmielewski, A.G., Skeldon, P., Bonilla, F.A., Thompson, G.E.,
Palladium profiles in titanium surface-treated by high-intensive plasma pulses,
SMMIB 2001, Marburg, Sept. 9-14, 2001

Wielunski, L.S., Grambole, D., Kreissig, U., Grötzschel, R., Harding, G., Szilágyi, E.,
Hydrogen depth resolution in multilayer metal structures, comparison of elastic recoil detection and resonant nuclear reaction method,
15th Int. Conf. on Ion Beam Analysis, Cairns, Australia, July 15-20, 2001

Wieser, E., Noetzel, J., Peikert, M., Reuther, H.,Wenzel, C., Tselev, A.,
Formation of metastable structures in metalls and alloys,
4th Int. Ural Seminar, Snezhinsk, Russia, Feb. 25–March 3, 2001

Zechner, C., Matveev, D., Erlebach, A., Simeonov, S. Menialenko, V., Mickevicius, R., Foad, M., Al-Bayati, A., Lebedev, A., Posselt, M.,
TCAD calibration of USJ profiles for advanced deep sub-µm CMOS processes,
E-MRS 2001 Spring Meeting, Strasbourg, France, June 5-8, 2001

Zolnai, Z., Khanh, N.Q., Szilagyi, E., Kotai, E. Ster, A., Posselt, M., Lohner, T., Guylai, J.,
Investigation of ion implantation induced damage in the carbon and silicon sublattices of 6H-SiC,
12th European Conf. on Diamond, Diamond-Like Materials, Carbon Nanotubes, Nitrides and Silicon Carbide, Budapest, Hungary, Sept. 2-7, 2001

Zyganov, I., Wieser, E., Matz, W., Reuther, H., Oswald, S., Pham, M.T., Richter, E.,
Modification of titanium by ion irradiation of calcium and/or phosphorus,
4th Int. Ural Seminar, Russia, Snezhinsk, Feb.25–March 3, 2001

Zyganov, I., Wieser, E., Matz, W., Reuther, H., Richter, E.,
Modification of the alloy Ti-6Al-4V by ion implantation of calcium and/or phosphorus,
SMMIB 2001, Marburg, Sept. 9-14, 2001

Zyganov, I., Wieser, E., Matz, W., Reuther, H., Richter, E.,
Modification of the Ti-6Al-4V alloy by ion implantation of Ca and/or P,
12th Int. School VEIT´01, Varna, Bulgaria, Sept.17-21, 2001

Lectures

Belov, A.Y.,
Atomic-level and average stresses in diamond-like amorphous carbon films grown by computer simulation,
MPI für Metallforschung, Stuttgart, Aug. 15, 2001

Berberich, F.,
In situ Untersuchungen der Phasentransformation und der mechanischen Eigenschaften stickstoffimplantierter Ti-6Al-4V Legierungen,
TU Chemnitz, May 18, 2001

Berberich, F.,
In situ study of the phase transformation and the correlated mechanical degradation of nitrogen implanted Ti-6Al-4V alloys,
ESRF PhD Seminar, Grenoble, Feb. 22, 2001

Berberich, F.,
In situ study of the phase transformation and the correlated mechanical properties of nitrogen implanted Ti-6Al-4V alloys,
ESRF Seminar, Grenoble, Oct. 23, 2001

Berberich, F.,
In situ Untersuchungen der Phasentransformation und der mechanischen Eigenschaften stickstoffimplantierter Ti-6Al-4V Legierungen
HMI Berlin, Oct. 31, 2001

Bischoff, L.,
Der Fokussierte Ionenstrahl in der Nanotechnologie,
TU Dresden, Dec. 5, 2001

Borany, J. von,
Emitter doping of Si solar cells by phosphorous plasma-immersion ion implantation,
Universität Konstanz, Jan. 11, 2001

Borany, J. von,
Ionenstrahlmodifizierung und Synthese von Halbleiter-Nanoclustern in dünnen Gatedielektrika für Flash- und EEPROM-Anwendungen,
Kickoff-Meeting zum Projekt „Konsul“, Infineon Dresden, Aug. 23, 2001

Dekorsy T.,
Coherent phonons and phonon co-variances,
FOM Institute AMOLF, Amsterdam, Netherlands, Jan. 29, 2001

Dekorsy T.,
Coherent phonons,
TU Wien, Austria, May 28, 2001

Dekorsy T.,
Von der Femtosekunden Spektroskopie zur –Technologie,
FZR Kolloquium, May 31, 2001

Dekorsy T.,
Zeitaufgelöste Spektroskopie an Halbleiterheterostrukturen mit dem Freie-Elektronen Laser,
ELBE Palaver, Nov. 1, 2001

Eichhorn, F.,
Ionenstrahlsynthese von SiC in Si: Strukturelle Untersuchungen,
FSU Jena, April 6, 2001

Eichhorn, F.,
Ion beam synthesis of SiC in Si: Real structure analysis at ROBL,
ESRF Monday Seminar, April 23, 2001

Gebel, T.,
Neue Möglichkeiten für integrierte optische Systeme in Siliziumtechnologie durch Lichtemission aus Nanostrukturen
TU Chemnitz, March 19, 2001

Gebel, T.,
Lichtemission aus Nanostrukturen: Neue Ansätze für integrierte optische Systeme in Siliziumtechnologie,
VDI – Forum Nanoworld, Hannover Messe 2001, Hannover, April 24, 2001

Gebel, T.,
Blaue Lumineszenz aus Nanostrukturen,
2. Fachforum "Nanotechnologie", OTTI-Technik Kolleg, Würzburg, Oct. 24, 2001

Gebel, T.,
Emitterarray (violet/UV) für die Biotechnologie,
Kompetenzzentrum Nanotechnologie "Ultradünne funktionale Schichten", Dresden, Nov. 29, 2001

Gebel, T.,
Si-and Ge-nanoclusters in ion implanted SiO_2: Electrical properties and memory applications,
Inst. of Semicond. Phys., Ukraine, Acad. of Sciences, Nov.16, 2001

Grötzschel. R.,
Elementanalytik dünner Schichten mit MeV-Ionenstrahlen,
IFW Dresden, April 2001

Heinig, K.-H.,
Züchtung und Zähmung von Nanostrukturen mit Ionenstrahlen,
Forschungszentrum Jülich, Institut für Schichten und Grenzflächen, August 29, 2001

Helm, M.,
Elektronen in künstlichen Halbleiterstrukturen: vom Modellsystem für Quantenmechanik und Festkörperphysik zum Quantenbauelement,
Physikkolloquium TU Dresden, Jan. 23, 2001

Helm, M.,
Der Freie-Elektronen-Laser in Dresden/Rossendorf und seine Anwendungen in der Infrarot-Spektroskopie von Halbleitern und anderen Systemen,
Universität Giessen, Jan. 25, 2001

Helm, M.,
Infrarotspektroskopie von Halbleiterquantenstrukturen: vom Modellsystem zum Infrarot- und THz Bauelement,
Max-Born-Institut für Nichtlineare Optik und Kurzzeitspektroskopie, Berlin, April 9, 2001

Helm, M.,
Infrared spectroscopy of semiconductor quantum structures and the ion-beam and free-electron-laser facilities at Rossendorf,

Lawrence Berkeley National Laboratory, Berkeley, CA, USA, Sept. 6, 2001

Jäger, H.U.,
MD-Simulation der Bildung von ta-C-Schichten bei C^+ Ionendeposition,
MPI für Plasmaphysik, Garching, May 17, 2001

Klein, C.,
Hochauflösende Rutherford-Ionenstreuung mit schweren Ionen,
MPI für Plasmaphysik, Garching, July 5, 2001

Klein, C.,
Hochauflösende RBS mit schweren Ionen,
Arbeitstreffen FSI 2001, Freiberg, Oct. 3-5, 2001

Kolitsch, A.,
In situ diagnostics of stress evolution and relaxation at BN deposition by IBAD,
KFKI Budapest, Hungary, Sept. 2001

Maitz, M.F.,
Principles of biological testing of implant materials,
Kyiv Taras Shevchenko University, Faculty of Physics, May 3, 2001

Maitz, M.F.,
Grundlagen der Gerinnungsaktivierung an Fremdmaterialien,
3. Thüringer Biomaterial-Kolloquium, Jena, Nov. 9, 2001

Maitz, M.F.
Principles of biomaterials testing,
Southwest Jiaotong University, Chengdu, China, Dec.14, 2001

Möller, W.,
Ionenstrahlen in der Materialforschung,
FhI für Keramische Technologien und Sinterwerkstoffe, Dresden, June 18, 2001

Möller, W.,
Grundlagen der Ionen-Festkörper-Wechselwirkung,
Sommerschule "Nukleare Sonden und Ionenstrahlen", Bad Blankenburg, Sept. 24, 2001

Möller, W.,
Ions for materials research: surface modification and analysis at Rossendorf,
Institute of Applied Physics, University of West Bohemia, Pilsen, Tschechien, Dec. 20, 2001

Müller, T.,
Synthesis and decay of nanowires,
Ionenstrahltreffen, Uni Augsburg, Oct. 1-2, 2001

Neelmeijer, C.,
Zerstörungsfreie substantielle Analyse von (Böttger-)Steinzeug am externen Protonenstrahl,
Ehrenfried Walther von Tschirnhaus – Kolloquium zu seinem 350. Geburtstag,
Blockhaus Dresden, Germany, April 10, 2001

Rebohle, L.,
Ion beam synthesized nanoclusters for silicon-based light emission,
Inst. für Festkörperelektronik, TU Wien, Nov. 6, 2001

Rebohle, L.,

Ion beam synthesis of nanoclusters for silicon-based light emission,
Inst. of Semicond. Phys., Ukraine, Acad. of Sciences, Nov.16, 2001

Richter, E.,
Industrielles Anwendungspotenizial der Plasma-Immersions-Ionenimplantation,
Innovationsforum „Neuartige Applikationsfelder für die plasmagestützte Oberflächentechnik", Zittau, April 5-6, 2001

Richter, E.,
Die unsichtbare Kraft – Ionen veredeln Materialoberflächen,
Werkstoff-Forum Hannover Messe 2001, April 23–27, 2001

Schmidt, B.,
Umgebungseinflüsse auf ionenimplantiertes SiO_2,
Ionentreffen, University Augsburg, Oct. 1-2, 2001

Skorupa, W.,
Ion beam-related defect studies of the Semiconductor Materials Department at the FZ Rossendorf,
Kungl Tekniska Högskolan (Royal Institute of Technology), Stockholm, Sweden, May 4, 2001

Skorupa, W.,
Nanocluster in SiO_2-Schichten durch Ionenstrahlsynthese,
II. Phys. Inst., Univ. Göttingen, June 18, 2001

Skorupa, W.,
Ladungshafteigenschaften ionenimplantierter Ge-reicher SiO_2-Schichten,
TU München, Oct. 20, 2001

Skorupa, W.,
Activities of the Semiconductor Materials Department at the FZ Rossendorf,
Inst. of Semicond. Phys., Ukraine, Acad. of Sciences, Nov.16, 2001

Wieser, E.,
Studies of ion beam modification of metalls and alloys,
Lipetsk State Technical University, Lipetsk, Russia, March 7, 2001

Reports

Beyer, E., Jäger, H.U., Lichte, H., Möller, W., Schultrich, B., Schultrich, H.,
Modellierung und experimentelle Untersuchung der Bildung superharter, amorpher Kohlenstoffschichten durch energiereiche Teilchen,
Schlussbericht für die FuE-Vorhaben Be 1875/2, Li 346/13, Mo 297/9 der DFG, Oct.10. 2001

Borany, J. von, Fontaine, F., Heera, V.,
Implantationsdotierung von Diamantschichten für Mikrosystemanwendungen,
Abschlussbericht zum BMBF-Projekt 16SV 548/2, June 2001

Borany, J. von, Gebel, T., Grötzschel, R., Heinig, K.-H., Klimenkov, M., Schmidt, B.,
Physikalische und technologische Grundlagen zum Engineering von Nanoclustern für nichtflüchtige Speicherzellen,
Abschlussbericht zum SMWK/SMWA-Verbundprojekt 4-7531.50-03-844-98/4, June 2001

Borany, J. von, Beyer, V.,
Entwicklung eines Justierdetektors für Elektronenstrahlanlagen,
Zwischen- und Abschlussbericht zum BMBF/Leica Projekt „JD-50“, April/Oct. 2001

Brauer, G.,
PAS an nanoclusterreichen SiO_2 – Schichten
SMWK: 7531.50-02-844-01/0, Zwischenbericht 02.07.2001, Abschlußbericht 09.01.2002

Brauer, G.,
Positron annihilation spectroscopy of metals with complex structure
BMBF/IB: Projekt CZE 00/035, Jahresbericht 2001, 12.12.2001

Köhler, B., Bischoff, L.,
Entwicklung einer neuen Technologie zur Probenpräparation für die Transmissions-Elektronenmikroskopie (TEM) auf der Basis der Ionenfeinstrahlbearbeitung
Abschlußbericht SMWK Projekt 7/2001 und FZR-329, August 2001

Möller, W., Posselt, M.,
TRIDYN_FZR User manual,
FZR-317, April 2001

Müller, T.,
Ion beam synthesis of Ge nanowires,
FZR-309, Januar 2001

Stephan, I., Böhmert, B., Prokert, F., Scholz, A.,
Bestrahlungsexperimente an Reaktordruckbehälterstählen am Rossendorfer Forschungsreaktor RFR,
FZR/FWSM – 02/2001, March 2001

Teichert, J., Borany, J. von,
Entwicklung einer Niederenergie-Implantationskammer mit einem neuartigen Bremslinsensystem,
FZR-323, May 2001

Tyrroff, H., Richter, B., Neumann, W.,
Strahlkopplung von Tandetron-Beschleuniger und Ionenimplanter zur Durchführung von Mehrstrahl-experimenten im Forschungszentrum Rossendorf,
FZR-308, Januar 2001

Patents

Gebel, T., Skorupa, W., Borany, J. von, Rebohle, L., Borchert, D., Fahrner, W. R.,
Integrierter Optokoppler und Verfahren zu seiner Herstellung,
Offenlegungsschrift DE 100 11 258 A1, Sept. 20, 2001

Gebel, T., Voelskow, M., Heera, V., Panknin, D., Eickhoff, M., Skorupa, W.,
Verfahren zur Behandlung heteroepitaktischer Halbleiterschichten auf Silizium-Substraten,
Erfindungsanmeldung beim Deutschen Patentamt, DE 101 27 073.9 (01.06.2001)

Gebel, T., Voelskow, M., Heera, V., Panknin, D., Eickhoff, M., Skorupa, W.,
Verfahren zur Behandlung heteroepitaktischer Halbleiterschichten auf Silicon-on-insulator(SOI)-Substraten,
Erfindungsanmeldung beim Deutschen Patentamt, DE 101 27 074.7 (01.06.2001)

Schmidt, B., Bischoff, L., Eng, L.,
Verfahren zur Herstellung von integrierten Abtastnadeln,
DE 10057656

Tsvetkova, T., Teichert, J., Bischoff, L.,
Schichtmaterial für optisch informationsträger und Lichtmasken sowie Verfahren zur Herstellung des Schichtmaterials,
Erfindungsanmeldung beim Deutschen Patentamt, AZ 101 43 616.5, 06.09.2001

PhD Theses

Fitz, C.,
Entwicklung und Relaxation mechanischer Spannungen in Bornitridschichten,
TU Dresden, Nov. 13, 2001

Hauschild, T.,
Investigating interatomic solid-state potentials using Crystal-GRID: a study of applicability,
TU Dresden, April 19, 2001

Parascandola, S.,
Nitrogen transport during ion nitriding of austenitic stainless steel,
TU Dresden, April 23, 2001

Awards

Dekorsy T.,
Gustav-Hertz Award of the German Physical Society 2001
DPG Frühjahrstagung, Hamburg, March 28, 2001

Laboratory Visits

Berberich, F.,
ESRF, Grenoble, France, June 6 – 17; Nov. 20 – 25, 2001

Borany, J. von,
ESRF, Grenoble, France, Nov. 17 – 22, 2001

Dekorsy, T.,
RWTH Aachen, June 27-29, 2001

Dekorsy, T.,
Free-Electron Laser Facility FELIX, Rhijnhuizen, Netherlands, Aug. 6-17, 2001

Eichhorn, F.,
ESRF, Grenoble, France, Apr. 20 - 24; Sept. 18 – 24, 2001

Fritsche, B.,
Institute of Technology, Linköping University, Linköping, Sweden, Oct.15-29, 2001

Gago, R.,
Institute of Technology, Linköping University, Linköping, Sweden, Oct.15-29, 2001

Gebel, T.,
Fa. JIPELEC, Meylan, France, April 4-5, 2001

Gebel, T.,
Institute of Semiconductor Physics, Ukrainian Academy of Science, Kyiv, Nov.15-18, 2001

Heinig, K.-H.,
CEMES/CNRS, Toulouse, France, Jan 31 – Feb 4, 2001

Heinig, K.-H.,
Uni Aarhus, Denmark, July 20-21, 2001; Aug. 19-21, 2001

Heinig, K.-H.,
Forschungszentrum Jülich, Aug. 28-29, 2001

Kreher, J.,
ESRF, Grenoble, France, Sept. 26 – Oct. 2, 2001

Matz, W.,
ESRF, Grenoble, France, March 21 - 27; June 5 - 7; Aug. 15 - 24, 2001

Müller, T.,
CEMES/CNRS, Toulouse, France, Jan. 31 – Feb. 4, 2001

Müller, T.,
Uni Aarhus, Denmark, July 20-21, 2001; Aug. 19-21, 2001

Müller, T.,
Forschungszentrum Jülich, Aug. 28-29, 2001

Müller, T.,
Uni Augsburg, October 1-2, 2001

Panknin, D.,
Aristotle University Thessaloniki, Greece, June 23-26, 2001

Panknin, D.,
Fa. EADS, München, May 7-8, 2001

Prokert, F.,

ESRF, Grenoble, France, Feb. 2-6; March 2-7; June 15-22; Nov. 24 – 28, 2001
Rebohle, L.,
Inst. für Festkörperelektronik, TU Wien, November 5-7, 2001

Rebohle, L.,
Institute of Semiconductor Physics, Ukrainian Academy of Science, Kyiv, Nov.15-18, 2001

Reuther, H.,
DESY Hamburg, April 3-4, 2001

Scholz, A.,
ESRF, Grenoble, France, Jan. 24–31, 2001

Skorupa, W.,
J.I.P.ELEC, Meylan, France, April 4-5, 2001

Skorupa, W.,
Kungl Tekniska Högskolan, Royal Institute of Technology, Stockholm, Sweden, May 3-5, 2001

Skorupa, W.,
Fa. EADS, München, May 7-8, 2001

Skorupa, W.,
II. Phys. Institut, Univ. Göttingen, June 18-19, 2001

Skorupa, W.,
Aristotle University Thessaloniki, Greece, June 23-26, 2001

Skorupa, W.,
Institute of Semiconductor Physics, Ukrainian Academy of Science, Kyiv, Nov.15-18, 2001

Guests

V.V. Afanas'ev,
Katholieke Univ. Leuven, Belgium, Nov.8-10, 2001

E. Alonso,
Institut für Integrierte Systeme der ETH Zürich, Zürich, Switzerland, Oct. 20-Nov. 2, 2001

V. Astrelin,
Institute of Nuclaer Physics Novosibirsk, Russia, Sept. 1–Oct. 19, 2001

A.H.A. Azzam,
Nuclear Research Center, Cairo, Egypt, Dec. 2001

F. Becvar,
Charles University, Prague, Czech Republic, Dec 10-15, 2001

V.I. Belko,
Belorussian State University, Minsk, Belarus, Nov. 1-30, 2001

H. Bernas,
CSNSM Orsay/Paris, France, Oct. 10–Nov. 4, 2001

D. Bhattacharya,
Nuclear Science Centre, New Delhi, India, Sept.16.-Sept. 20, 2001

J.P. Biersack,
Hahn-Meitner-Institut Berlin, Germany, Dec. 6-7, 2001

V. Borodin,
Russian Research Centre "Kurchatov Institute", Moscow, Russia, April 22–June 23; Oct. 20–Nov. 30, 2001

J. Camassel,
University Montpellier, France, March 8-11, 2001

J. Cizek,
Charles University, Prague, Czech Republic, April 9–16; Nov 12-25, 2001

A.V. Dvurechenskii,
Institute of Semiconductor Physics, Novosibirsk, Russia, Sept. 24– Oct.13, 2001

G.A. Elawadi,
Nuclear Research Center, Cairo, Egypt, Dec. 2001

P.F.P. Fichtner,
Fed. Univ. of Rio Grande dol Sul, Porto Alegre, Brasilien, Feb.8-17, 2001

J. Fradin,
ENSAM, Paris, France, Feb 8-28, 2001

R. Gago Fernández,
Feb. 5-April 25, 2001

Fei Gao,

Pacific Northwest National Laboratory, Richland, WA, USA, Nov. 4-18, 2001

K.Grigorov,
Institute of Electronics, Bulgarian Acad. of Sciences, Sofia, Apr. 23 – 27, 2001

V. Hnatowicz,
Nuclear Physics Institute of Academy of Sciences of Czech Republic, June 18-19, 2001

J. Jagielski,
Institute of Electronic Materials Technologie, Warsaw, March 5–10, 2001

M. Kalitzova,
Bulgarian Acad. of Sciences, Sofia, Bulgaria, March 5-16, 2001

J. Kalkman,
FOM Institut Amsterdam, Netherlands, Sept.10–14, 2001

S. Kaschieva,
Bulgarian Acad. of Sciences, Sofia, Bulgaria, March 16-April 20, 2001

J. R. A. Kaschny,
Fed. Univ. of Rio Grande dol Sul, Porto Alegre, Brasilien, Jan.1- April 26, 2001

A. Kondyurin,
Russian Academy of Sciences Perm, Russia, April 1– May 31; Sept. 1-Dec. 31, 2001

I. Kondyurina,
University of Perm, Russia, Dec. 7-31, 2001

J. Kourtev,
Bulgarian Academy of Sciences, Sofia, Bulgaria, Feb. 1-28, 2001

G. Kuri,
HASYLAB at DESY, Hamburg, Sept. 24-29, 2001

J. Kuriplach,
Charles University, Prague, Czech Republic, Apr 2-12; 19-30; Oct 3–18; Oct 24-Nov 7, 2001

M. Lebedev,
Institute for Solid State Physics, Chernogolovka, Russia, Nov. 14 –Dec. 12, 2001

M. Linnarsson,
Kungl Tekniska Högskolan, Royal Institute of Technology, Stockholm, Sweden, Oct.14-15, 2001

A. Mackova,
Nuclear Physics Institute of Academy of Sciences of Czech Republic, June 18-19, 2001

R. McMahon,
University of Cambridge, UK, June 28-29, 2001

O.V. Misochko,
Institute for Solid State Physics, Chernogolovka, Russia, July-Dec., 2001

N. Morrison,
University of Cambridge, UK, June 28-29, 2001

S. Mukherjee,
Institute for Plasma Research, FCIPT, Gandhinagar, India, June 1 - Dec. 31, 2001

J. Narojdczyk,
Radom, Poland, March 19-24; April 2-6, 2001

A. Nazarov,
Ukrain. Academy of Sciences, Kiyv, Ukraine, Aug. 1-31, 2001

G. Nechitailo,
Institute of Biochemical Physics, Moskau, Nov. 25-Dec 31, 2001

P. Novikov,
Institute of Semiconductor Physics, Novosibirsk, Russia, March 26–June 23; Sept. 17–Dec. 8, 2001

I. Osiyuk,
Ukrain. Academy of Sciences, Kiyv, Ukraine, Aug. 1-31, 2001

J. Österman,
Royal Institute of Technology, Kista Sweden, Jan. 22-28, 2001

V. Ovchinnikov,
Institute of Electrophysics, Jekaterinenburg, Russia, May 28– June 25, 2001

B. Pakrash,
Katholische Universität Leuven, Belgien, Feb. 2-16, 2001

A. Pathak,
University of Hyderabad, India, May 19–June 16, 2001

V. Perina,
Nuclear Physics Institute of Academy of Sciences of Czech Republic, June 18-19, 2001

P.O.A. Persson,
Linköping University, Sweden, Aug. 19–25, 2001

J. Piekoszewski,
Soltan Institute of Nuclear Studies, Otwock/Poland, Jan. 23. – Febr. 02; March 14-24; Aug. 27– Sept. 5; Nov. 26 – Dec. 06, 2001

I. Prochazka,
Charles University, Prague, Czech Republic, May 2-9; Nov 26-Dec 10, 2001

A.G. Revesz,
Revesz Associates, Bethesda/MD, USA, March 14 - April 1; Sept.15-22, 2001

A.W. Robertson-Mair,
University of Manchester, June 18- Aug. 17, 2001

V. Romanova,
Russian Academy of Sciences Perm, Russia, April 1– May 31, 2001

N. Shevchenko,
University of Tomsk/Russia, Jan.1–April 30, 2001

A.H.M. Soliman,

Nuclear Research Center, Cairo, Egypt, Dec. 2001

A. Ster,
Research Institute for Technical and Materials Science, Budapest, Hungary, March 25–April 7, 2001

J. Stoemenos,
University Thessaloniki, Greece, March 8-11, 2001

B.G. Svensson,
Kungl Tekniska Högskolan, Royal Institute of Technology, Stockholm, Sweden, Oct.14-15, 2001

A. Turos,
Institute of Electronic Materials Technologie, Warsaw, March 4–10, 2001

V. Valtsifer,
Russian Academy of Sciences Perm, Russia, Sept. 1–15, 2001

M. Vinnichenko,
Kyiv Taras Shevchenko University Kiev/Ukraina, Dec. 1, 2000–Feb 27, 2001; June 1-Aug. 28, 2001

J. Wang,
July 17- Oct. 13, 2001

C. Zechner,
ISE Integrated System Engineering AG, Zürich, Switzerland, Nov. 1-2, 2001

W.J. Zhao,
Peking University, China, Sept. 22-26, 2001

I. Zyganov,
University of Lipetsk/Russia, Jan. 26–Feb.19; Sept. 1-Dec. 17, 2001

V.A.Yakovlev,
Institute for Spectroscopy, Troitsk, Russia, Aug.1-30, 2001

European Large Scale Facility Visitors

G. Abrasonis,
University of Poitiers, France, Nov. 18-Dec.1, 2001

C. Angelov,
Institute for Nuclear Research and Nuclear Energy, Sofia, Bulgaria, Aug. 16-31, 2001

N.P. Barradas
Nuclear and Technological Institute, Sacavem, Lisboa, Portugal, Feb.24-26; April 29-May5; Dec. 16-21, 2001

A. Bartkowiak-Kurska,
Institute of Electronic Materials Technology Warsaw, Poland, March 12-23, 2001

J. Brttiger,
University of Aarhus, Denmark, Feb. 24-26, 2001

B. Brijs,

IMEC Leuven, Belgium, Oct. 22-26, 2001

R.N. Bugoi,
Institute of Atomic Physics, Bucharest, Romania, April 17-29, 2001

B. Constantinescu,
Institute of Atomic Physics, Bucharest, Romania, April 17-29, 2001

T. van Dillen,
FOM Amsterdam, Netherlands, Feb. 24-26, 2001

R. Hellborg,
University of Lund, Sweden, Feb. 24-26, 2001

A. Hörling,
Linköping University, Sweden, Sept. 9-16, 2001

M. Kalitzova,
Institute of Solid State Physics, Sofia, Bulgaria, March 5-19, 2001

A. Karydas,
Institute of Nuclear Physics, Athens, Greece, Nov. 11-16, 2001

M. Kokkoris,
Institute of Nuclear Physics, Athens, Greece, June 23-July 1, 2001

S. Kossionides,
Institute of Nuclear Physics, Athens, Greece, Sept. 17-22, 2001

C.A. Londos,
University of Athens, July 1 – 15, 2001

D. Music,
Linköping University, Sweden, March 12-16, 2001

J. Narojczyk,
Technical University Radom, Poland, March 19-24; April 2-7, 2001

J. Neidhardt
Linköping University, Sweden, May 27- June 9, 2001

B. Pakrash,
Katholieke Universiteit Leuven, Belgium, Feb. 2-16, 2001

A. Ratajczak,
Institute for Nuclear Studies, Swierk, Poland, March 5-23, 2001

S. Spiga,
Laboratorio MDM-INFM Agrate, Italy, April 22-May 11, 2001

A.M. Szekeres,
Institute of Solid State Physics, Sofia, Bulgaria, April 4 - May 5, 2001

S. Tinchev,
Bulgarian Academy of Sciences, Sofia, Bulgaria, Feb. 24-26, 2001

T. Tsvetkova,
Institute of Solid State Physics, Sofia, Bulgaria, Jan. 20 – Feb. 23; Oct. 10-24, 2001

I. Vickridge,
Universite de Paris, France, Feb. 24-26, 2001

E. Vlakhov,
Institute of Solid State Physics, Sofia, Bulgaria, April 23-May 7; Nov. 5-18, 2001

R. Vlastou-Zannis,
National Technical University of Athens, Greece, June 23-July 1, 2001

R.G. van Welzenis,
Eindhoven University, Netherlands, Feb. 24-26, 2001

Z. Werner,
Soltan Institute of Nuclear Studies, Otwock/Poland, March 19-24; June 6-9; Nov. 26–30, 2001

C. Zarkadas,
Institute of Nuclear Physics, Athens, Greece, Nov. 11-16, 2001

Marie Curie Training Site

M. Kiisk,
Lund University, Sweden, June 9-Dec. 12, 2001

S. Nauwelaerts,
Katholieke Universiteit Leuven, Belgium, Sept. 9-Dec. 22, 2001

E. Pecheva,
University Sofia, Bulgaria, April 1-Oct. 31, 2001

A. Razpet,
University of Ljubljana, Slowenia, Sept. 7- Dec. 31, 2001

Seminar of the Institute

J. Christen - Universität Magdeburg
Optische Mikrocharakterisierung komplexer Galliumnitrid-Heterostrukturen
April 12, 2001

T. Drüsedau - Universität Magdeburg
Reichweiten und Gasdichtereduzierung bei der Sputter-Deposition
Oct. 18, 2001

R. Fischer - MPI für Plasmaphysik, Garching
Datenanalyse mit der Bayesschen Wahrscheinlichkeitstheorie - Beispiele aus der Oberflächenphysik und Ionenstrahldiagnostik
Jan. 25, 2001

H. Hahn - TU Darmstadt
Synthese und Eigenschaften von nanostrukturierten Materialien
Feb. 8, 2001

G. Marletta - University of Catania
Enhanced adhesion of biological systems to irradiated polymer surfaces
Italy, July 12, 2001

P. Reinke - Universität Göttingen
Interfaces with carbon thin films: reactivity and electronic properties
Nov. 8, 2001

C. M. Schneider - IFW Dresden
Magnetismus ultradünner Schichtsysteme: Grundlagen und Anwendungsaspekte
April 19, 2001

L. Thomé - CSNSM Orsay
Application of ion beams to nuclear waste issues
France, June 14, 2001

J. Weber - TU Dresden
Wasserstoff in Halbleitern - Grundlagen und Anwendungen
Feb. 1, 2001

H. P. Winter - TU Wien
Wege zum detaillierten Verständnis der inelastischen Wechselwirkung langsamer Ionen mit atomar reinen Festkörperoberflächen
Nov. 15, 2001

W. D. Zeitz - HMI Berlin
Untersuchungen des Verhaltens von Bor in Si-Ge-Mischkristallen mit Hilfe der ß-NMR
May 17, 2001

Other Seminars

V.V.Afanas'ev - Katholieke Univ. Leuven, Belgium
Electron trapping in SiO_2: Intrinsic defects and the role of hydrogen
Nov.9, 2001

E. Alonso - Institut für Integrierte Systeme der ETH Zürich, Switzerland
Concentration dependent dopant diffusivity for high dose implants
Oct. 29, 2001

A. Anders - Lawrence Berkeley Laboratory, USA
Fortschritte in Richtung präzis kontrollierter, vollständig ionisierter Bogenplasmen
April 4, 2001

D. Bhattacharya - NSC New Delhi, India
Ion beam mixing and ion beam synthesis
Sept. 18, 2001

R. Beyer – TU Chemnitz
Möglichkeiten und Grenzen der Charakterisierung nanoclusterhaltiger SiO_2-Schichten mittels Kapazitätsspektroskopie von MOS-Strukturen
Jan. 11, 2001

J.P. Biersack - Hahn-Meitner-Institut Berlin
TRIM-Rechnungen zu Damage-Verteilungen (Korrekturen und Verbesserungen),
Neue Rechnungen zur elektronischen Stopping Power von Protonen in Si
Dec. 7, 2001

T. Chudoba - TU Chemnitz
Nano indentation - state of the art and new developments
Nov. 26, 2001

M. Dhayal - UMIST Manchester, UK
Time resolved measurements of ion energy distribution function in a pulsed RF gas discharge
Oct. 4, 2001

F. El-Hossary - University Sohag, Egypt
Plasma nitriding and carbonitriding of stainless steel and aluminium using Rf ICP
Sept. 12, 2001

S. Estreicher - Physics Department, Texas Tech. University, Lubbock, USA
The H_2 molecule in semiconductors: an angel in GaAs, a devil in Si
Nov. 26, 2001

P.F.P. Fichtner - Fed. Univ. of Rio Grande dol Sul, Porto Alegre, Brasil
Nucleation and growth behaviour of Cu/Al-precipitates in He-implanted and annealed aluminium
Feb.15, 2001

R. Frank - Universität Tübingen
Optische Methoden in der Bioanalytik
Dec.10, 2001

Fei Gao - Pacific Northwest National Laboratory, Richland, USA
Multi-scale computer simulation of silicon carbide
Nov. 9, 2001

G. K. Hubler - Naval Research Laboratory, Washington, USA
Ion-beam based materials studies
Sept. 17, 2001

M. Huisman - University of Amsterdam, The Netherlands
Ion beam analysis of O and H in switchable mirrors and magnetic tunnel junctions
April 4, 2001

M. Kalitzova - Bulgarian Acad. of Sciences, Sofia, Bulgaria
Present status of Ta_2O_5 as an active dielectric
March 5-16, 2001

H.M. Katsch - Universität Essen
Charakterisierung von Radiofrequenzentladungen in Sauerstoff und Chlor mit kapazitiver und induktiver Anregung
Oct. 22, 2001

G. Kuri - DESY Hamburg
MeV ion implantation and ion scattering studies in semiconductors,
Sept. 28, 2001

M. Linnarsson - Kungl Tekniska Högskolan (Royal Institute of Technology), Stockholm, Sweden
Solubility limit and precipitate formation in Al-doped 4H-SiC
Oct.15, 2001

R. Mc Mahon, N. Morrison - Dept. of Engineering, Univ. of Cambridge, UK
Modelling of energy transient beam processing for semiconductor materials: The FLASiC approach,
June 29, 2001

A. Nazarov - Institute of Semiconductor Physics, Ukrain. Academy of Sciences, Kiyv, Ukraine
High-temperature processes of charge instability in the buried oxide ofSOI-materials and MOSFETs
Aug. 10, 2001
Fowler-Nordheim electron injection and charge trapping in the buried oxide of SOI structures
Aug. 17, 2001

K. Nordlund - Helsinki University, Finland
Computer simulation of ion and plasma modification of fusion reactor materials
April 20, 2001

V. Ovchinnikov
Deep ranging structural transformations in $FePd_2Au$ and Fe-Cr by ion irradiation,
June 22, 2001

A.G. Revesz - Revesz Associates, Bethesda, USA
The evolution of the Si - SiO_2 interface structure:
I. The Si - SiO_2 interface / II. The structure and properties of SiO_2 films on silicon
March 28, 2001

E. Schomburg - Universität Regensburg
Ultrafast domain formation in semiconductor superlattices
Oct. 4, 2001

G. Schütz - Universität Würzburg
Magnetismus im zirkular polarisierten Röntgenlicht
June 8, 2001

C. Stan-Sion - IFIN-HH Bukarest, Romania
Tritium-AMS an Fusionsproben
Sept. 6, 2001

M. Strobel - Catania University, Italy
Ion erosion of fcc(111) surfaces: a kinetic lattice Monte Carlo study
March 1, 2001

J. Sun - Changchun Inst. of Physics, Chin. Acad. of Sciences, Changchun, P.R. of China
Blue electroluminescence from reactive sputtering Si-rich SiO_2, Si_3N_4 thin films and Si/SiO_2 superlatices
Nov.14, 2001

H. Whitlow - Lund Institute of Technology, Sweden
Swift heavy ion beams - an universal tool for frontier materials research
Jan 29, 2001

M. Zacharias - MPI für Mikrostrukturphysik Halle
Size controlled Si nanocrystals and Er doping for photonic applications
Nov. 7, 2001

V. Zorin - Institute of Applied Physics, Nishni Novgorod, Russia
High current multi-charged ion source based on an ECR discharge sustained by millimeter wave radiation
Jan 9, 2001

Meetings organized by the institute

Infrared and THz Radiation: Generation and Applications,
Forschungszentrum Rossendorf, Dresden, Germany, Jan. 18-20, 2001
Organizers: M. Helm, E. Grosse, W. Seidel, T. Dekorsy

9th Int. Workshop on Slow Positron Beam Techniques for Solids and Surfaces (SLOPOS-9),
Dresden, Germany, Sept. 16-22, 2001
Organizers: W. Anwand, G. Brauer

12th International Summer School "Vacuum, Electron, and Ion Technologies“,
Varna, Bulgaria, Sept. 17-21, 2001
Organizers: Bulgarian Academy of Sciences, Institute of Electronics / FZ Rossendorf

3rd Summer School "Nuclear Probes and Ion Beams“,
Bad Blankenburg, Thuringia, Sept. 24-28, 2001
Organizers: FZ Rossendorf / HMI Berlin

Projects based on external funds

05/1997 - 04/2001 European Union, within the BRITE-EURAM-Project EU
Plasma immersion ion implantation for enhancing high precision machining with tools of complexy geometry
Dr. R. Günzel, Tel.: 0351 260 2462 r.guenzel@fz-rossendorf.de

11/1997 - 10/2002 European Union, within TMR Network EU
Synthesis, structure and properties of new carbon based hard materials
Dr. A. Kolitsch, Tel. 0351 260 3348 a.kolitsch@fz-rossendorf.de

03/1998 - 02/2002 European Union, within TMR Network EU
European Network on defect engineering of advanced semiconductor devices
Dr. K.-H. Heinig, Tel.: 0351 260 3288 k.h.heinig@fz-rossendorf.de

07/1998 - 12/2001 Sächsisches Staatsministerium für Wissenschaft und Kunst SMWK
Blue electroluminescence from nanoscaled semiconductor structures
Dr. W. Skorupa, Tel.: 0351 260 3612 w.skorupa@fz-rossendorf.de

10/1998 - 11/2001 Deutsche Forschungsgemeinschaft DFG
Ion-acoustic microscopy using focused ion beams
Dr. L. Bischoff; Tel.: 0351 260 2963 l.bischoff@fz-rossendorf.de

11/1998 -10/2001 Deutsche Forschungsgemeinschaft DFG
Modeling and experimental investigation of the formation of superhard amorphous carbon layers by energetic particles
Dr. H.-U. Jäger, Tel.: 0351 260 3373 h.u.jaeger@fz-rossendorf.de

01/1999-12/2001 WTZ with Russia BMBF
Nanocluster formation by means of ion implantation
Dr. K.-H. Heinig, Tel.: 0351 260 3288 k.h.heinig@fz-rossendorf.de

07/1999 - 06/2002 WTZ with Bulgaria BMBF
Investigation of the cluster emission characteristics of liquid metal ion source with the aim to produce focused cluster beams
Dr. L. Bischoff, Tel.: 0351 260 2963 l.bischoff@fz-rossendorf.de

01/2000 - 12/2001 DAAD (VIGONI-Program with Italy) DAAD
ROS-CAT: Luminescence and point defect studies
Dr. W. Skorupa, Tel.: 0351 260 3612 w.skorupa@fz-rossendorf.de

02/2000 - 01/2003 European Union within "Transnational Access to Major Research Infrastructures" as a Large-Scale Facility EU
Center for Application of Ion Beams in Materials Research
Dr. A. Kolitsch, Tel. 0351 260 3348 a.kolitsch@fz-rossendorf.de

03/2000 - 03/2003 Bilaterales Abkommen BAS – FZR JRP
Applications of Focused Ion Beam Systems for Optical Data Storage and other Uses in Optoelectronics and Photonics
Dr. L. Bischoff, Tel.: 0351 260 2963 l.bischoff@fz-rossendorf.de

04/2000 - 03/2002 Deutsche Forschungsgemeinschaft DFG
Investigation of vacancy-type defects in ion beam treated silicon carbide by means of positron annihilation spectroscopy

Dr. G. Brauer, Tel.: 0351 260 2117 g.brauer@fz-rossendorf.de

06/2000 - 03/2002 Deutsche Forschungsgemeinschaft DFG
Modification of SiC-layers by ion beam stimulated recrystallization and phase formation
Dr. Viton Heera, Tel.: 0351 260 3343 v.heera@fz-rossendorf.de

06/2000 - 05/2002 WTZ with Czech Republic WTZ
Positron annihilation spectroscopy of metals with a complex structure
Dr. G. Brauer, Tel.: 0351 260 2117 g.brauer@fz-rossendorf.de

07/2000 – 10/2001 Bundesministerium für Bildung und Forschung BMBF
Entwicklung eines Si-Justierdetektors für Elektronenstrahlanlagen mit einem Linearitätsbereich bis 8 A $cm^2 \cdot \mu m^2$ bei einer Elektronenenergie von 50 keV
Dr. J. von Borany, Tel.: 0351 260 3378 j.v.borany@fz-rossendorf.de

08/2000 - 08/2003 Deutsche Forschungsgemeinschaft DFG
Ion beam synthesis of doped diamond-SiC-heterostructures
Dr. V. Heera; Tel.: 0351 260 3343 v.heera@fz-rossendorf.de

09/2000 - 08/2002 Deutsche Forschungsgemeinschaft DFG
Dynamische in situ Untersuchung der Entstehung von kompressiven Spannungen in Bornitrid-Schichten und des Einflusses von Verunreinigungen und Wachstumsparametern
Prof. W. Möller, Tel.: 0351 260 2245 w.moeller@fz-rossendorf.de

10/2000 - 09/2002 Bundesministerium für Wirtschaft BMWi
Enhanced oxidation resistance of new light construction materials for high temperature application by ion implantation
Prof. E. Wieser, Tel.: 0351 260 3096 e.wieser@fz-rossendorf.de

10/2000 - 03/2003 Sächsisches Staatsministerium für Wirtschaft und Arbeit SMWA
Aufsticken von Edelstahl, Teilthema „Plasma-Immmersions-Implantation“
Dr. E. Richter, Tel.: 0351 260 3326 e.richter@fz-rossendorf.de

01/2001 - 12/2003 WTZ with Ukraine WTZ
Luminescence and memory effects in SiO_2 layers containing Si/Ge nanoclusters
Dr. W. Skorupa, Tel.: 0351 260 3612 w.skorupa@fz-rossendorf.de

01/2001- 01/2004 European Union, Growth Project EU
Nanoclusters for Electronics (NEON)
Dr. K.-H. Heinig, Tel.: 0351 260 3288 k.h.heinig@fz-rossendorf.de

02/2001 - 11/2001 Sächsisches Staatsministerium für Wissenschaft und Kunst SMWK
Flash lamp supported deposition of 3C-SiC films
Dr. D. Panknin, Tel. 0351 260 3613 d.panknin@fz-rossendorf.de

04/2001 - 03/2004 Bundesministerium für Bildung und Forschung BMBF
Zusammenhang zwischen Plasmaparametern und Schichteigenschaften beim MF-Puls-Magnetronsputtern
Dr. A. Kolitsch, Tel. 0351 260 3348 a.kolitsch@fz-rossendorf.de

04/2001 - 12/2001 Sächsisches Staatsministerium für Wissenschaft und Kunst SMWK
Positron Annihilation Spectroscopy of nanocluster-rich SiO_2-layers
Dr. G. Brauer, Tel.: 0351 260 2117 g.brauer@fz-rossendorf.de

04/2001 – 03/2004 Sächsisches Staatsministerium für Wirtschaft und Arbeit SMWA
Erhöhung der Funktionssicherheit dünner Barrieren auf Ta-Basis für Kupfer-

Metallisierungssysteme, Teilthema: Plasma-Immersions-Ionenimplantation
Dr. E. Richter, Tel.: 0351 260 3326 e.richter@fz-rossendorf.de

04/2001 - 03/2004 Bundesministerium für Bildung und Forschung BMBF
Synthese und Charakterisierung vergrabener, optisch transparenter Übergangsmetalloxid-Schichten
Dr. F. Prokert, Tel.: 0351 260 3389 f.prokert@fz-rossendorf.de

07/2001 - 06/2003 Bundesministerium für Bildung und Forschung BMBF
Ionenstrahlmodifizierung und Synthese von Halbleiter-Nanoclustern in dünnen Gatedielektrika für Flash- und EEPROM- Anwendungen
Dr. J. von Borany, Tel.: 0351 260 3378 j.v.borany@fz-rossendorf.de

10/2001 - 9/2003 Bundesministerium für Bildung und Forschung BMBF
Hochenergie-Ionenimplantation in Si-Wafer für Bauelemente der Leistungselektronik
Dr. J. von Borany, Tel.: 0351 260 3378 j.v.borany@fz-rossendorf.de

Experimental Equipment

1. Accelerators, Ion Implanters and Ion-Assisted-Deposition

⇒	van de Graaf accelerator	1,8 MeV	
⇒	Tandem accelerator	5 MV	Russian
⇒	Tandetron accelerator	3 MV	*HIGH VOLTAGE, NL*
⇒	Ion implanter	80 kV	Own construction
⇒	Ion implanter	180 kV, medium current	*SCANIBAL, FL*
⇒	High current ion implanter	200 kV, high current	*DANFYSIK, DK*
⇒	High energy ion implanter	500 kV	*HIGH VOLTAGE, NL*
⇒	Plasma-immersion ion implantation	5-60 keV	
⇒	Fine focused ion beam	50 keV, 100 nm, 10 A/cm^2	
⇒	Ion beam assisted deposition		
⇒	Plasma enhanced chemical vapour deposition		

2. Particle Based Analytical Techniques

⇒	RBS	Rutherford backscattering	p,a: 1-6 MeV	
⇒	ERDA	Elastic recoil detection analysis	35 MeV, ^{35}Cl	
⇒	PIXE	Proton induced X-ray analysis	+ PIGE-option, external beam	
⇒		Nuclear microprobe	MeV, > 2 µm	
⇒	NRA	Nuclear reaction analysis	^{1}H (^{15}N,αγ) ^{12}C	
⇒	TEM	Transmission electron microscope	300 kV	*PHILIPS, NL*
⇒	AES	Auger electron spectroscopy	+ XPS-option	*FISIONS, GB*
⇒	CEMS	Mössbauer spectroscopy	^{57}Fe source	

3. Photon Based Analytical Techniques

⇒	XRD/XRR	X-ray diffraction / X-ray reflexion	8.04 keV (Cu-K$_{\alpha}$)	*BRUKER AXS, D*
		XRD/XRR with Synchrotron radiation	5 – 35 keV	*ROBL-CRG at ESRF, F*
⇒	SE	Spectroscopic ellipsometry	250 - 1700 nm	*WOOLLAM, USA*
⇒	FTIR	Fourier transform infrared spectrometry	600 - 7000 cm^{-1}	*NICOLET, USA*
⇒	FTIR	Fourier transform infrared spectrometry with infrared microscope	50 – 15000 cm^{-1}	*BRUKER, D*
⇒		Ti:Sapphire femtosecond laser		*SPECTRA PHYSICS, USA*
⇒	Raman	Raman spectroscopy (532 nm, 633 nm)	> 45 cm^{-1} shift	*JOBIN-YVON-HORIBA, F.*
⇒	PL	Photoluminescence	300 – 1500 nm	*JOBIN-YVON-HORIBA, F.*
⇒	EL	Electroluminescence (10-300 K)	300 – 1500 nm	*JOBIN-YVON-HORIBA, F*
⇒		Optical split-coil supercond. magnet	7 T	*OXFORD INSTRUM., UK*

3. Other Analytical and Measuring Techniques

⇒	Scanning tunneling microscope (with AFM-option)	*DME, DK*
⇒	Dektak surface profilometer	*VEECO, USA*
⇒	Micro indenter	*SHIMATSU, J*
⇒	Scratch tester	*SHIMATSU, J*
⇒	Spreading resistance profiling	*SENTECH, D*
⇒	Hall-effect equipment	*BIO-RAD, GB*
⇒	I-U and C-U- analyzer	*KEITHLEY, USA*

4. Preparation Techniques

⇒	Wet chemical etching and cleaning	including anisotropic selective KOH-etching
⇒	Photolithographic patterning	5 µm-level
⇒	Thermal treatment	Room Temperature - 2000°C • Furnace, Flash lamp unit, • Rapid thermal annealing, RF-Heating (Vacuum)
⇒	Physical deposition	Sputtering DC / RF, Evaporation
⇒	Dry etching	Plasma and RIE mode
⇒	Bonding techniques	Anodic, Si-Si and Wire Bonding

Forschungszentrum Rossendorf

Institute of Ion Beam Physics and Materials Research (IIM)

Postfach 51 01 19
D-01314 Dresden
Tel.: 0351 260 2245
Fax: 0351 260 3285
www.fz-rossendorf.de

DIRECTORS

Prof. Dr. W. Möller 2245

Prof. Dr. M. Helm 2260

Deputy: **Prof. Dr. E. Wieser** 3096

INDUSTRIAL CONTACTS (FWIK)
Dr. J. von Borany 3378

ION IMPLANTATION (FWII)
Dr. E. Richter 3326
- Ion Beam Assisted Deposition
- Biotechnological Materials
- Plasma Immersion Ion Implantation
- Ion Implanter Operation

ION BEAM ANALYSIS (FWIA)
Dr. R. Grötzschel 2802
- High-Energy Ion Beam Analysis
- Energy Loss and Charge Exchange Processes

ACCELERATOR TECHNOLOGY (FWIB)
Dr. M. Friedrich 3284
- MeV Accelerator Operation
- Accelerator Mass Spectrometry

THEORY (FWIT)
Dr. M. Posselt 3279
- Computer Simulations
- Reaction-Diffusion Models
- Ion Beam Synthesis and Defects

NEW MATERIALS (FWIM)
Dr. W. Skorupa 3612
- Semiconductors
- Optoelectronics
- Defect Engineering
- Focused Ion Beam

SEMICOND. SPECTROSCOPY (FWIH)
Dr. T. Dekorsy 2880
- Semiconductor Quantum Structures
- Infrared Spectroscopy
- Femtosecond Spectroscopy
- Free Electron Laser at ELBE

STRUCTURAL DIAGNOSTICS (FWIS)
Dr. W. Matz 3122
- Electron Microscopy
- X-ray Diagnostics
- Electron Spectroscopies

PREPARATION (FWIP)
Dr. B. Schmidt 2726
- Semiconductor Technology
- Nanostructures
- Clean Room Operation

List of Personnel

Directors: Prof. W. Möller, Prof. M. Helm
Deputy Director: Prof. E. Wieser
Office: I. Heidel, S. Kirch

Scientific Staff:

Permanent:

Dr. L. Bischoff
Dr. J. von Borany
Dr. W. Bürger
Dr. T. Dekorsy
Dr. F. Eichhorn
Dr. M. Friedrich
Dr. D. Grambole
Dr. R. Grötzschel
Dr. R. Günzel
Dr. V. Heera
F. Herrmann
Dr. K.-H. Heinig
Dr. H.-U. Jäger
Dr. R. Kögler
Dr. A. Kolitsch
Dr. U. Kreißig
Dr. W. Matz
Dr. A. Mücklich
Dr. C. Neelmeijer
Dr. D. Panknin
Dr. M.T. Pham
Dr. M. Posselt
Dr. F. Prokert
Dr. H. Reuther
Dr. E. Richter
Dr. B. Schmidt
Dr. W. Skorupa
Dr. H. Tyrroff
Dr. M. Voelskow

Post Docs:

Dr. T. Chevolleau
Dr. N. Georgiev
Dr. M. Klimenkov
Dr. M. Maitz
Dr. N. Shevshenko
Dr. J. Sun

Projects:

W. Anwand
Dr. A. Belov
V. Beyer
Dr. G. Brauer
Dr. R. Gago
Dr. A. Lebedev
M. Mäder
M. Peikert
Dr. W. Pilz
Dr. L. Rebohle
Dr. A. Rogozin
Dr. M. Seidel
Dr. H. Weishart

PhD Students:

C. Akhmadaliev
F. Berberich
C. Fitz
T. Fitz
B. Fritsche
T. Gebel
U. Hornauer
C. Klein
T. Müller
A. Peeva
J. Schmidt
S. Sinning

Diploma Students:

D. Kost
G. Laudien

Technical Staff:

Permanent:

R. Aniol
G. Anwand
I. Beatus
W. Boede
K.-D. Butter
E. Christalle
H. Felsmann
K. Fukarek
W. Gäßner
B. Gebauer
H.-J. Grahl
G. Grunert
P. Hartmann
G. Hofmann
S. Klare
R. Kliemann
J. Kreher
A. Kunz
G. Küster
D. Maul
M. Mißbach
K. Müller
U. Neupert
E. Quaritsch
B. Richter
M. Roch
B. Scheumann
H. Schluttig
G. Schnabel
J. Schneider
A. Scholz
K. Thiemig
S. Turuc
A. Vetter
A. Weise
I. Winkler

Projects:

H. Hohlfeld
F. Ludewig
W. Probst
A. Reichel
A. Schneider
H. Seifert
G. Winkler